Athens Journal of Sciences

Quarterly Academic Periodical, Volume 12, Issue 4
Published by the Athens Institute
URL: https://www.athensjournals.gr/ajs Email: journals@atiner.gr
e-ISSN: 2241-8466 DOI: 10.30958/ajs

December 2025

Athens Journal of Sciences

Quarterly Academic Periodical, Volume 12, Issue 4, December 2025

Published by the Athens Institute

URL: https://www.athensjournals.gr/ajs Email: journals@atiner.gr

e-ISSN: 2241-8466 DOI: 10.30958/ajs

Front Pages

Athens Journal of Sciences

Published by the Athens Institute

Athens Institute is an Athens-based World Association of Academics and Researchers based in Athens. Athens Institute is an independent and non-profit Association with a Mission to become a forum where Academics and Researchers from all over the world can meet in Athens, exchange ideas on their research and discuss future developments in their disciplines, as well as engage with professionals from other fields. Athens was chosen because of its long history of academic gatherings, which go back thousands of years to Plato's Academy and Aristotle's Lyceum. Both these historic places are within walking distance from Athens Institute's downtown offices. Since antiquity, Athens was an open city. In the words of Pericles, Athens"…is open to the world, we never expel a foreigner from learning or seeing". ("Pericles' Funeral Oration", in Thucydides, The History of the Peloponnesian War). It is Athens Institute's mission to revive the glory of Ancient Athens by inviting the World Academic Community to the city, to learn from each other in an environment of freedom and respect for other people's opinions and beliefs. After all, the free expression of one's opinion formed the basis for the development of democracy, and Athens was its cradle. As it turned out, the Golden Age of Athens was in fact, the Golden Age of the Western Civilization. Education and (Re)searching for the 'truth' are the pillars of any free (democratic) society. This is the reason why Education and Research are the two core words in Athens Institute's name.

The Athens Journal of Sciences (AJS) is an Open Access quarterly double-blind peer reviewed journal and considers papers from all areas of Natural & Formal Sciences, including papers on agriculture, computer science, environmental science, materials science, transportation science, chemistry, physics, mathematics and statistics, biology, geography, and earth science (geology, oceanography, astronomy, meteorology). Many of the papers published in this journal have been presented at the various conferences sponsored by the Natural & Formal Sciences Division of the Athens Institute. All papers are subject to Athens Institute's Publication Ethical Policy and Statement.

Athens Journal of Sciences
ISSN NUMBER: 2241-8466 - DOI: 10.30958/ajs
Volume 12, Issue 4, December 2025
Download the entire issue (PDF)

Athens Journal of Sciences
Editorial and Reviewers' Board

President's Message

All Athens Institute's publications including its e-journals are open access without any costs (submission, processing, publishing, open access paid by authors, open access paid by readers etc.) and is independent of presentations at any of the many small events (conferences, symposiums, forums, colloquiums, courses, roundtable discussions) organized by Athens Institute throughout the year and entail significant costs of participating. The intellectual property rights of the submitting papers remain with the author. Before you submit, please make sure your paper meets the basic academic standards, which includes proper English. Some articles will be selected from the numerous papers that have been presented at the various annual international academic conferences organized by the different divisions and units of the Athens Institute for Education and Research. The plethora of papers presented every year will enable the editorial board of each journal to select the best, and in so doing produce a top-quality academic journal. In addition to papers presented, Athens Institute will encourage the independent submission of papers to be evaluated for publication.

The current issue is the fourth of the twelfth volume of the *Athens Journal of Sciences (AJS)*, published by Natural & Formal Sciences Division of Athens Institute.

Gregory T. Papanikos
President
Athens Institute

14th Annual International Conference on Chemistry
20-24 July 2026, Athens, Greece

The Natural Sciences Unit of Athens Institute, will hold its **14th Annual International Conference on Chemistry, 20-24 July 2026, Athens, Greece** sponsored by the Athens Journal of Sciences. The aim of the conference is to bring together academics and researchers of all areas of chemistry and other related disciplines. You may participate as stream organizer, presenter of one paper, chair a session or observer. Please submit a proposal using the form available (https://www.atiner.gr/2026/FORM-CHE.doc).

Academic Members Responsible for the Conference

- **Dr. Haiduke Sarafian**, Head, Natural Sciences Unit, ATINER & Professor of Physics and Endowed Chair of John T. and Paige S. Smith Professor of Science, Pennsylvania State University, USA.

Important Dates

- Abstract Submission: **16 December 2025**
- Acceptance of Abstract: 4 Weeks after Submission
- Submission of Paper: **22 June 2026**

Social and Educational Program

The Social Program Emphasizes the Educational Aspect of the Academic Meetings of Athens Institute.

- Greek Night Entertainment (This is the official dinner of the conference)
- Athens Sightseeing: Old and New-An Educational Urban Walk
- Social Dinner
- Mycenae Visit
- Exploration of the Aegean Islands
- Delphi Visit

Conference Fees

Conference fees vary from 400€ to 2000€
Details can be found at: https://www.atiner.gr/fees

14th Annual International Conference on Physics
20-24 July 2026, Athens, Greece

The Natural Sciences Unit of Athens Institute, will hold its **14th Annual International Conference on Physics, 20-24 July 2026, Athens, Greece** sponsored by the Athens Journal of Sciences. The aim of the conference is to bring together academics and researchers of all areas of physics and other related disciplines. Please submit a proposal using the form available (https://www.atiner.gr/2026/FORM-PHY.doc).

Important Dates

- Abstract Submission: **16 December 2025**
- Acceptance of Abstract: 4 Weeks after Submission
- Submission of Paper: **22 June 2026**

Academic Member Responsible for the Conference

- **Dr. Haiduke Sarafian**, Head, Natural Sciences Unit, ATINER & Professor of Physics and Endowed Chair of John T. and Paige S. Smith Professor of Science, Pennsylvania State University, USA.

Social and Educational Program

The Social Program Emphasizes the Educational Aspect of the Academic Meetings of Athens Institute.

- Greek Night Entertainment (This is the official dinner of the conference)
- Athens Sightseeing: Old and New-An Educational Urban Walk
- Social Dinner
- Mycenae Visit
- Exploration of the Aegean Islands
- Delphi Visit
- Ancient Corinth and Cape Sounion

More information can be found here: https://www.atiner.gr/social-program

Conference Fees

Conference fees vary from 400€ to 2000€
Details can be found at: https://www.atiner.gr/fees

Athens Journal of Sciences - Volume 12, Issue 4, December 2025 – Pages 235-250

Study on the feasibility DLC coatings doped with Transition Metal Cu or Ag as Biosensing Electrode for Glucose

*By Jihua Peng**

Researching biosensing electrodes for glucose measurement is crucial for human health. These electrodes need to be accurate, reliable, and long-lasting. In this study, diamond-like carbon amorphous coatings were fabricated to contain nano-crystal Cu or Ag (a-C:Cu, a-C:Ag) by the complex deposition of the filtered cathode vacuum arc of graphite and magnetron sputtering of copper or silver. All electrodes showed good conductivity. The a-C:Cu electrodes had sp^3C fraction 29~45 %, while a-C:Ag had 26–42 at.%. The morphologies, microstructures, and the carbon hybridization structure, and the resistance of the specimens were characterized using SEM, XRD, Raman, XPS spectroscopy, and the four-point-probe. It is found that the catalytic activity of nano-crystal Cu particles (np-Cu) for glucose oxidation is not affected by a carbon layer on their surface, and this is different from nano-crystal Ag particles (np-Ag), which are sensitive to surface conditions. Thus, a-C:Cu, made by one-step vacuum deposition, is suitable for sensing glucose in an alkaline solution. The anodic peak current at 0.21 V vs. Hg/HgO increased in two log-linear regions with glucose content. However, in the 1M KCl+50 Mm $K_3Fe(CN)_6$, a-C:Cu and a-C:Ag cannot be used as glucose-sensing electrodes. The a-C:Ag coatings present challenges for glucose sensing due to difficulties in controlling the surface conditions of np-Ag.

Keywords: *Transition metal doping; Diamond-like carbon; Electrochemical performance; Glucose; Biosensing.*

Introduction

Diamond-like carbon (DLC) is a special form of amorphous carbon, which has a lot of sp^3 bonding and sp^2 bonding and offers excellent mechanical, physical, and chemical properties (Robertson 2000; Peng et al. 2021). These properties can be adjusted by doping and controlling layer structure during vapor deposition. DLCs are used on devices to enhance sealing, anti-corrosion, and anti-wear performance (Vetter 2014, Peng et al. 2022, Zhao et al. 2020). Adding transition metals like Cu or Ag to DLCs improves chemical bonding, adhesion, and overall performance (Markwitz et al. 2015, Yan C et al. 2023, Yan F et al. 2023). This makes coated devices operate well in ocean environments (Wei et al. 2020, Liu et al. 2016) and human body environment (Jastrzebski et al.2021, Birket et al. 2023, Towobola et al. 2025). In the energy sector, DLCs doped with Cu or Ag are strong candidates for metal bipolar plates and future supercapacitors (Tian et al. 2024, Buathong et al. 2025). In electrochemistry, DLCs are widely used as electrodes (Zeng et al. 2014). Transition metals Cu and Ag are key catalysts (Zhu et al. 2012, Jing et al. 2022, Dayakar et al. 2018). Combining the catalysis of Cu or Ag with the broad electrochemical window of DLCs shows great

*Associate Professor, School of Materials Science and Engineering, South China University of Technology, China.

promise for sensing biological and medical substances.

In recent years, there has been growing interest in creating sensors for blood glucose monitoring. These sensors aim to be selective, sensitive, responsive, and cost-effective for managing diabetes. Electrochemical biosensing has become the main approach. There are two main types: enzyme-based testing (Patolsky et al. 2004, Maalouf et al. 2007) and non-enzyme testing (Triroj et al.2020, Hwang et al. 2018). The latter has gained significant attention. For enzyme-free glucose-sensing electrodes, a catalytic substance is needed on the surface for glucose oxidation. Transition metals like copper, nickel, platinum, palladium, and silver have been suggested (Nagy et al. 2001, Naikoo et al. 2020, Usman et al. 2019). Some studies indicate that OH^- functional groups on the electrode can oxidize glucose without catalysts (Honda et al. 2013, Barragan et al. 2018). Currently, electrochemical deposition of catalytic species onto conductive substrates is the main method for creating enzyme-free electrodes (Wu et al. 2015, Dai et al. 2018, Aun et al. 2023). For DLC-based electrodes, a two-step fabrication process is used. First, DLCs are vapor deposited, then electrochemical deposition of the transition metal or compounds occurs. While these electrodes perform well in glucose sensing, they face issues like high costs and poor adhesion between the catalytic layer and substrate. Therefore, there is a need to explore a one-step fabrication method for DLC electrodes with transition metals and investigate their glucose biosensing potential.

The goal of this study is to create Cu or Ag doped DLC electrodes using a one-step method. We will examine their electrochemical performance in glucose electrolytes. For fabrication, we use a magnetically filtered cathode arc of graphite as the carbon source. We also use a direct current magnetron cathode of pure transition metal for the Cu or Ag source. This process embeds nano-crystal particles of Cu or Ag into the amorphous carbon matrix. We will explore the states of the doped Cu or Ag and their impact on bonding structure, surface morphology, and electrochemical performance. This study will help assess how well Cu/Ag doped DLC electrodes can measure glucose content in electrolytes.

After this introduction, we will present a section called "Literature Review." This will cover the catalysis of glucose oxidation by Cu and Ag, along with the status of transition metal-doped DLCs for glucose measurement. In the "Methodology" section, we will detail how to prepare DLC doped with Cu or Ag. We will also discuss the morphology, bonding structure, and electrochemical performance. The "Results and Discussion" section will showcase the main findings and provide insightful analysis. Finally, we will outline clear conclusion points.

Literature Review

Many studies show that in alkaline electrolytes, Cu or Cu-oxides can oxidize glucose (Nagy et al. 2001, Yang et al. 2010, Ma et al. 2019). The presence of Cu^{2+} in the solution also helps oxidize glucose (Zheng et al. 2019). When using the ferrocene derivative (FcCO-Glu-Cys-Gly-OH) to oxidize glucose, doped nanocrystal particles (np-) of Cu or Co act as electrocatalysts (Zhan et al. 2022). Similarly, np-Ag can promote glucose oxidation (Chen et al. 2012, Smikhovskaia et al.2019, Usman et al. 2019). However, the oxidation of np-Ag in alkaline solutions depends on its fabrication method. When np-Ag is made with carbon secured from the extraction process (Dayakar et al. 2018) and through electrochemical deposition (Buathong et al.

2025), its oxidation is reduced. This indicates that np-Cu or Ag can enhance glucose oxidation in alkaline electrolytes. DLC-based electrodes with np-Cu or Ag are promising for measuring glucose concentration. Additionally, the state of np-Cu or Ag affects the surface morphology and electrochemical performance of the electrode.

Using one-step vapor deposition to create transition metal-doped DLC-based electrodes builds a composite structure. This structure includes np-transition metal and an amorphous carbon matrix. This method adjusts bonding and adhesion. As a result, it offers better conductivity and electrochemical performance than traditional glassy carbon electrodes (Maalouf et al. 2006, Kim et al. 2009). Additionally, low-temperature fabrication of DLC electrodes supports semiconductor integration. The electrochemical performance can be fine-tuned using appropriate dopants during vapor deposition (McCreery 2008). These dopants can include metal elements that enhance electro-catalysis for bio-compounds.

A layer of nanocrystal Au, Ag, or Cu can be deposited onto DLCs using post-electrochemical methods. This process helps catalyze glucose oxidation (Liu et al. 2010, Jin et al.2 012). However, there is less research on Cu/Ag-doped DLCs as glucose biosensors. It has been shown that Ni-doped DLC electrodes improve sensitivity to H_2O_2 in the electrolyte by controlling Ni content (Liu et al. 2018). TDLC electrodes doped with Cu or Cu-Ni demonstrate fast reaction rates for the inner-sphere redox couple $(Fe(CN)_6)^{3-/4-}$ (Wang et al. 2022). Ag-doped DLC electrodes show quasi-reversibility of the $Fe^{2+/3+}$ redox couple in KOH solution (Buathong et al. 2025). These DLCs with Cu or Ag dopants are expected to be good electrodes for glucose sensing. However, both their ability to measure glucose content and their electrochemical performance require further investigation.

Methodology

Sample Preparation and Post-treatment

Commercial single-crystal Si wafers (20.00 mm × 10.00 mm × 0.63 mm) and polished stainless-steel coupons were cleaned with ethanol and deionized water. This removed the surface contaminants. Then, they were dried under N_2 gas. The a-C coatings were deposited using a filtered cathode vapor arc (FCVA) system (Peng et al. 2024). In this system, a Ti target (99.99% purity), Ag target (99.99% purity), and Cu target (99.99% purity) were powered by direct current magnetron sputtering. The graphite cathode arc target (99.99% purity) used a pulsed direct current source. After placing the substrate samples in the vacuum chamber, the base pressure dropped below 2×10^{-3} Pa. An Ar gas flow (99.99% purity, 30 sccm) was supplied through the inlet. The chamber was heated to 150 °C during the entire deposition process.

First, a –1200 V direct current pulse bias voltage (V_b) was applied to the samples. They were etched for 30 minutes with Ar ions. Next, a Ti-interlayer of about 150–300 nm thickness was deposited using the Ti magnetron sputtering target at 3 kW. After turning off the Ti target, the graphite target was activated. This prepared an a-C sub-layer for 45 minutes with a V_b of –1200 V. Finally, the a-C:Cu top layer was deposited for 90 minutes. Alternatively, a-C:Ag was deposited for 30–60 minutes, using a V_b of –650 V. This followed the Cu or Ag magnetron

sputtering target conditions in Table 1. In total, four batches of a-C:Cu and six batches of a-C:Ag samples were prepared.

Table 1. *Process Parameters during Deposition and Metal Content in the Top Layer*

Batch No.	Cu target power /W	Ar flow /sccm	Cu-target shield	Cu content /at.%	Ag content /at.%
T1	100	28	Fully closed	1.1	-
T2	200	28	Fully closed	5.2	-
T3	400	25	Fully closed	13.5	-
T4	400	23	Half opened	23.6	-
Ag1#	10	28	Fully open	-	0.5
Ag2#	100	28	Fully closed	-	5.0
Ag3#	200	20	Fully closed	-	12.1
Ag4#	400	28	Fully closed	-	45.0
Ag5#	300	20	Fully closed	-	52.1
Ag6#	100	48	Fully open	-	79.9

Morphological and Chemical Bonding Structure Characterization

The coatings were analyzed using an X-ray diffraction (XRD) diffractometer (PANalytical, USA) with Cu Kα irradiation (40 kV, 40 mA, wavelength 0.15418 nm). We scanned 2θ from 30° to 60° and used a 2° grazing angle to reduce substrate signal intensity. We observed the composition, top surface images, and fractured cross-section of the coated Si wafers using field-emission scanning electron microscopy (FE-SEM) with EDS (SU5000, Japan; or Nova NANOSEM430, USA) at a 15 kV voltage. The hybridization states of the carbon atoms were determined with micro-Raman spectroscopy, using an Ar-ion laser with a 532 nm excitation wavelength and 5 mW power (LabRAM Arami, France). The scanning range was 100–4000 cm^{-1} for 300 seconds. We characterized chemical bond shifts using X-ray photoelectron spectroscopy (XPS; Axis Supra^{+}, Japan) at an incident photon energy of 1486.6 eV. The X-ray gun operated at a 5 mA emission current and 15 kV accelerating voltage. The XPS instrument was calibrated using the Au $4f^{7/2}$ core-level electron binding energy (84.00 eV) as a standard. Before each measurement, we etched the sample surface for 120 seconds with Ar ions at 2 keV and a 1 mA mm^{-2} current density to remove contaminants. We used the Shirley method for background subtraction, and analyzed the data with XPS Peak 4.1 software. For peak fitting, a Gaussian–Lorentzian function with a Lorentzian fraction of 20% was applied, and the full-width at half maximum for C 1s, Cu 2p, and Ag 3d was fixed.

Conductivity and Electrochemical Performance Characterization

The resistivity of the coatings on the Si wafers was measured using a four-point sheet resistance probe (RTS9, Shenzheng Jundashidai Instrument Ltd., China). We analyzed the electrochemical properties of the DLC films using a three-electrode system on an electrochemical workstation (CompactStat.h, IVIUM, Netherlands) at room temperature. The cyclic voltammetry (CV) and differential pulse voltammetry (DPV) for this analysis was employed. During CV tests, we used scanning rates of 50, 100, 150, 200, 250, and 300 mVs^{-1}. The reference electrode was Ag/AgCl electrode when using a KCl-based electrolyte and an Hg/HgO electrode for NaOH-based electrolyte. A platinum foil (10 mm × 10 mm × 0.1 mm) served as the counter electrode. The working electrodes were a-C:Cu or A-C:Ag coated 316L substrates, each with an effective area of 1 cm^2. Compared to the normal hydrogen electrode (NHE), the zero-electrode potential of the Ag/AgCl is +0.244 V and that of the Hg/HgO electrode is +0.198 V.

All reagents in this work were analytical grade. They were dissolved in deionized water. This included potassium chloride, potassium ferricyanide, D-glucose, and nitric acid, all from Sigma-Aldrich®. Before use as working electrodes, the Cu or Ag-doped DLC films were cleaned. They were rinsed with acetone and double-distilled water for 10 minutes. To remove surface cotton-like particles that affect glucose sensing in an alkaline electrolyte, some a-C:Cu samples from a different batch were etched. This was done using a 1 M HNO_3 solution. The samples were immersed in the 1 M HNO_3 solution for 1 minute. After that, they were washed with tap water and then with deionized water. Finally, they were rubbed and dried with a cleanroom wiper. During the HNO_3 etching, a reaction likely occurred involving copper and Cu-oxides.

$$3Cu+8HNO_3\ (light) = 3Cu(NO_3)_2+2NO\uparrow+4H_2O \quad (1)$$

$$CuO+2HNO_3 \rightarrow Cu(NO_3)_2+H_2O \quad (2)$$

$$3Cu_2O+14HNO_3 = 6Cu(NO_3)_2+2NO\uparrow+7H_2O \quad (3)$$

Results and Discussion

Coating Surface Morphology

The SEM images of as-deposited a-C:Cu coatings are in Figures 1a–1d, with cross-section images as insets. Figure 1e shows Cu-free a-C coatings, made when the magnetron sputtering Cu-target was off during the final step. The a-C coating has a total thickness of 1.53 μm and a smooth surface with small droplets under 500 nm. From previous EDS study, the small size droplets were carbon-enriched particles, which was emitted from the graphite arc target during evaporation. Three sublayers exist in the a-C:Cu coatings: the Ti-interlayer is about 320 nm thick, and the a-C sublayer, made at V_b of –1200 V, ranges from 300 to 309 nm thick. The top a-C:Cu layer thicknesses of samples T1–T4 are about 629, 520, 978, and 1051 nm, respectively. The XRD pattern of these a-C:Cu samples are in Figure 1f, with their Cu contents in Table 1. Increasing Cu content in the DLCs led to more nanocrystalline Cu grains in the coatings (Liu et al.2016). The SEM images of as-deposited a-C:Ag coatings are in Figures 2a–2e, also with cross-section insets. Unlike the a-C:Cu

samples, the a-C:Ag coatings have a smooth surface with fewer droplets. As Ag content increases, the fraction of Ag-crystal grains also rises, as shown in Figure 2f.

Droplets are unavoidable when using the graphite arc to deposit DLCs (Peng et al. 2023), like the a-C coating in Figure 1e. In this study, cotton-like particles on the surface may affect the shield's sealing in front of the metal-target. These particles ignite after the a-C sub-layer deposition at –1200 V. Carbon ash sticks to the metal-target surface and gets sputtered out when the target ignites. This carbon ash forms more easily on the Cu-target than on the Ag-target.

Coating Composition, and the Bonding Microstructure

The Raman spectra provide key insights into carbon atom hybridization, hydrogen content, and residual stress in DLCs (Robertson 2000, Vetter 2014). Figures 3a and 4a show the spectra for as-deposited a-C:Cu and a-C:Ag coatings, respectively. These spectra were fitted using the double Gaussian method. The G peak at about 1555 cm^{-1} reflects the in-plane breathing vibration of sp^2C sites. In contrast, the D peak at 1370 cm^{-1} indicates the out-plane bending vibration of aromatic ring-like sp^2C and disordering (Liu et al. 2016, Peng et al. 2021). Typically, the intensity ratio of the D peak to the G peak (I_D/I_G) is inversely related to the sp^3C fraction in DLCs. It is also positively correlated to the size of ring-like sp^2C clusters when they are under 2 nm. Many factors affect the G peak position (G_{peak}), including the sp^2C fraction and residual stress in the coating. More disordering in the coating leads to a larger full width at half maximum of the G peak ($FWHM_G$). Table 2 shows the fitted parameters for the a-C:Cu and a-C:Ag coatings, along with their resistivity and the ratio of sp^2C=C/sp^3C–C bonds from XPS fitting. According to previous studies (Zhou 2016, Jing et al. 2022, Yan Cet al. 2023), increasing the Cu or Ag content in the coating enhances the sp^2C fraction, ordering extent, and sp^2C cluster size, while reducing residual stress.

Figure 1. *SEM Images (a–e) of the Top Surface and Cross-section of the Coatings with different Cu Content, as well as their XRD Pattern (f)*

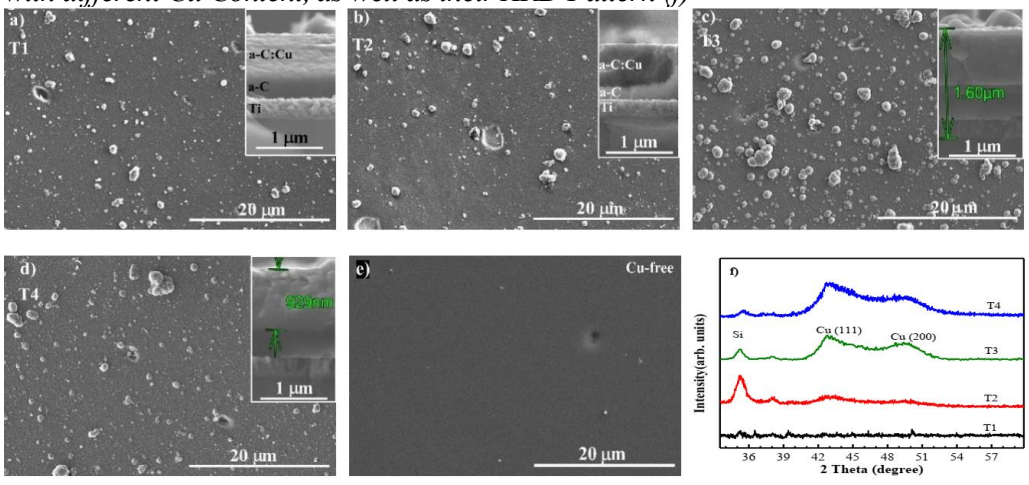

Figure 2. *SEM Images (a–e) of the Top Surface and Cross-section of the Coatings with different Ag Content, as well as their XRD Pattern (f)*

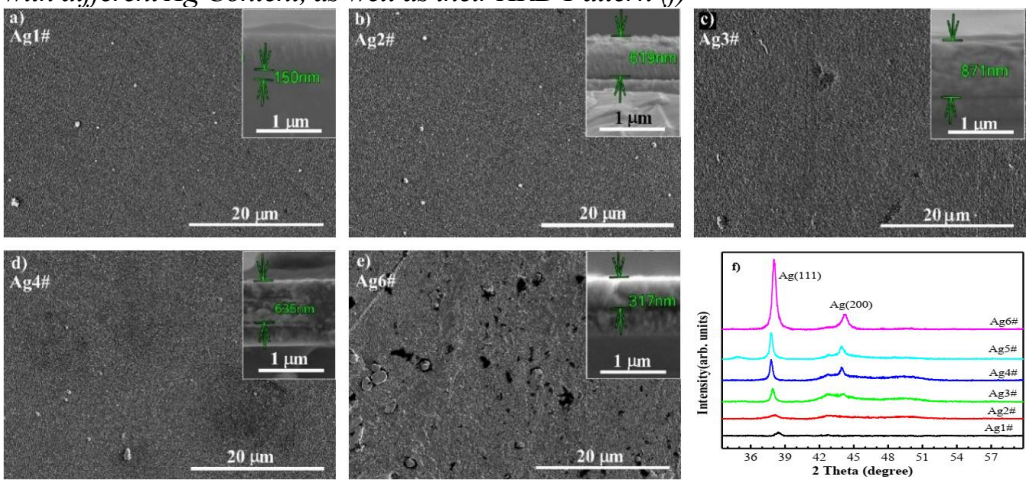

XPS is useful for characterizing the hybrid structure of carbon atoms at the surface. Its resolution is less than 5 nm. The C 1s and Cu 2p XPS spectra of the Cu-doped coatings are shown in Figures. 3b and 3c. Previous studies (Robertson 2000, Jin et al. 2012, Peng et al. 2024) report four peaks in the XPS spectra. These peaks correspond to different core orbital binding energies: sp^2C=C (284.4 ± 0.2 eV), sp^3C–C (285.1 ± 0.2 eV), C–O (286.4 ± 0.2 eV), and C=O (288.2 ± 0.2 eV). Cu atoms in the DLCs mostly exist in metallic states. They bond poorly with carbon (Khan et al. 2019, Wang et al. 2022). Some Cu–O bonds likely form as CuO or Cu_2O due to reactions with the atmosphere (Aun et al. 2023). The sp^2C=C/sp^3C–C ratio from XPS fitting matches the Raman analysis results. It is hard to differentiate the Cu $2p^{3/2}$ and Cu $2p^{1/2}$ peaks from metallic Cu or Cu-oxides. Thus, we assume Cu mainly exists in the metallic state, which aligns with the XRD pattern in Figure 1f. The C 1s and Ag 3d XPS spectra of the Ag-doped coatings are shown in Figures. 4b and 4c. Like the a-C:Cu coatings, carbon atoms in a-C:Ag coatings mainly take the form of sp^2C and sp3C sites. The Ag $3d^{3/2}$ (374.4 eV) and Ag $3d^{5/2}$ (368.4 eV) peaks were seen in the Ag-doped DLC (Liu et al. 2018, Yan et al. 2023). This indicates Ag atoms in the coatings form metallic Ag-clusters or Ag-crystals.

The conventional glassy carbon electrode shows that Cu solid-solution in sp^2C clusters likely caused more disorder. At higher Cu content, the cotton-like particles grew in size and density, which hindered electron transport. This led to an increase in resistivity (ρ) as Cu content rose. This finding contrasts with results in Ref (Khan et al. 2019). The doping of metallic Ag particles gives a-C:Ag better conductivity (Yan et al .2023).

Figure 3. *Raman Spectra (a) and XPS Spectra of C 1s (b) and Cu 2p (c) from different a-C:Cu Coatings*

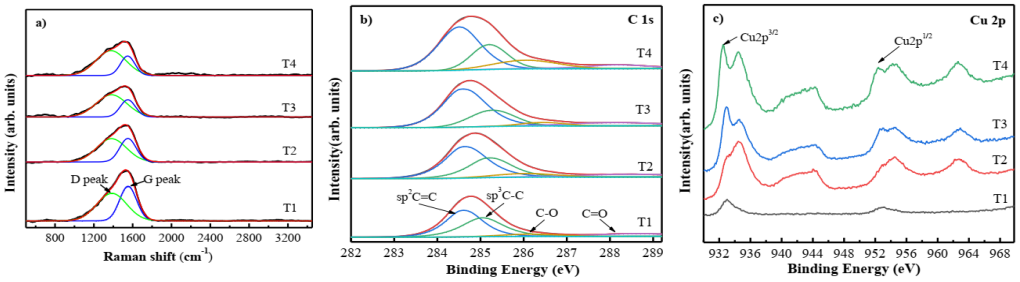

Figure 4. *Raman Spectra (a) and XPS Spectra of C 1s (b) and Ag 3d (c) from different a-C:Ag Coatings*

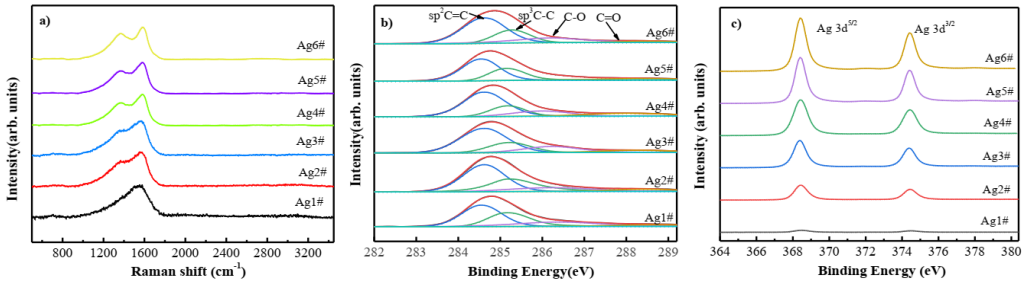

Table 2. *Resistivity and Peak Fitting Results from Raman/XPS Spectra of DLCs Coatings*

Specimen	I_D/I_G	G_{peak}/cm^{-1}	$FWHM_G$ cm^{-1}	sp^2/sp^3	ρ/Ω·m
T1	0.80	1552	205.2	1.19	4.76E-6
T2	0.99	1551	198.7	1.28	5.43E-6
T3	1.29	1550	182.4	2.50	6.26E-6
T4	1.28	1548	173.9	2.08	6.79E-6
Ag1#	0.72	1560	208.5	1.37	4.74E-8
Ag2#	1.09	1570	139.4	1.61	4.56E-8
Ag3#	1.15	1569	140.1	2.77	1.27E-7
Ag4#	1.03	1582	114.4	2.60	6.41E-8
Ag5#	1.19	1586	107.2	1.90	4.92E-8
Ag6#	1.06	1589	106.5	2.47	1.25E-8

Electrochemical Performance of DLCs Electrode in 1 M KCl with 50 mM $K_3Fe(CN)_6$ Electrolyte

* T2 Electrodes

The T2 coating had many nanocrystalline Cu and good conductivity. Thus, it was chosen as a suitable electrode for electrochemical experiments. Using Ag/AgCl as the reference electrode, setting scanning rates as 50, 100, 250, 200, 250, and 300 mV s^{-1}, Figure 5a presents the CV curves in 1 M KCl + 50 mM $K_3Fe(CN)_6$ electrolyte at different scanning rates. A pair of peaks appeared, indicating the redox of the $(Fe(CN)_6)^{3-/4-}$ couple. As the scanning rate climbed from 50 to 300 mV s^{-1}, the potential difference between the anodic and cathodic peaks (ΔE_p) grew from 142 to 420 mV. The peak current ratio (I_a/I_c) reached 1.09, 2.01, 2.07, 2.22, 2.50, and 2.41,

respectively. The quasi-reversibility of the $(Fe(CN)_6)^{3-/4-}$ couple was maintained at a slow scanning rate of 50 mV s^{-1} but worsened at higher rates. An anodic peak appeared at 0.71 V at 50 mV s^{-1}. This could be due to either the passivation of the carbon film (Turyan 2015) or the transformation of $Cu^{2+/3+}$ (Nagy et al. 2001, Aun et al. 2023). Compared to electrodes like B/N doped ta-C (Weber et al. 2024) and (Nb:N)-DLC (Liu et al. 2017), the T2 electrode in this study showed poorer quasi-reversibility for the $(Fe(CN)_6)^{3-/4-}$ couple. This is likely due to cotton-like particles on the T2 electrode. These particles may have affected the density of electron states, electron transfer, and the availability of active sites for reagent absorption (McCreery 2008, Markwitz et al. 2017).

Adding glucose concentration of 450 to 1170 mg L^{-1} into the electrolyte of 1M KCl+50 Mm $K_3Fe(CN)_6$, and setting the scanning rate at 50 mV s^{-1}, we analyzed the CV curves from the T2 electrode in Figure 5b. These curves show that the redox current pairs with glucose differ significantly from those without it. In the presence of glucose, the anodic peak potential varied widely, from 0.461 to 1.344 V. The anodic current peak ranged from 3.864 to 11.562 mA cm^{-2}. This suggests that multiple surface reactions control the anodic and cathodic peaks, not just the redox of the $(Fe(CN)_6)^{-3/-4}$ couple. Potential reactions include: 1) oxidation of OH^- radicals on the electrode surface (Honda et al. 2013); and 2) glucose oxidation catalyzed by $Cu^{2+/3+}$ reactions, along with the transformation of Cu itself (Yang et al. 2010, Zheng et al. 2019). Thus, the a-C:Cu electrode is unsuitable as a glucose biosensor in the KCl–$K_3Fe(CN)_6$ electrolyte system. Excessive reactions on the electrode surface complicate the differentiation of effects.

* Ag2# Electrodes

We selected Ag2# as the electrodes to study their electrochemical behavior based on conductivity and np-Ag content. Figure 6a shows the CV curves from the Ag2# electrode in a 1 M KCl + 50 mM $K_3Fe(CN)_6$ electrolyte at different scanning rates. An obvious redox peak from the $(Fe(CN)_6)^{3-/4-}$ couple appeared. However, the redox reaction was not fully reversible, even at a slow scanning rate of 50 $mV.s^{-1}$. At scanning rates of 50, 200, and 300 m $mV.s^{-1}$, the anodic peak current increased from 3.90 $mA.cm^{-2}$ to 7.02 $mA.cm^{-2}$. This suggests that the surface electrochemical reaction is limited by diffusion (Dayakar et al. 2018, Smikhovskaia et al. 2019). For these rates, the I_a/I_c ratios were 0.90, 0.96, and 0.98, while the ΔE_p values were 500, 770, and 860 mV, respectively. In comparison, the electrochemically deposited np-Ag electrode (Zhao et al. 2021) showed better reversibility for the $(Fe(CN)_6)^{3-/4-}$ couple. The lower reversibility in Ag2# may result from the np-Ag being wrapped by the amorphous carbon matrix.

Adding glucose concentration from 270 to 1170 mg L^{-1} to the electrolyte of 1M KCl+50 mM $K_3Fe(CN)_6$, and setting the scanning rate at 50 mV. s^{-1}, the CV curves from the Ag2# electrode are shown in Figure 6b. The curves with and without glucose are similar. The anodic and cathodic peak currents mainly show the redox reaction of the $(Fe(CN)_6)^{3-/4-}$ couple. However, the anodic peak current changes non-linearly with the glucose concentration. The density and size of np-Ag influence the electron transfer resistance (R_{ct}) of $(Fe(CN)_6)^{3-/4-}$ reaction on the graphene@Ag electrodes (Zhao 2021). Additionally, glucose adsorbs onto active silver sites, reducing the current. Meanwhile, Ag ions dissolve into the solution, promoting glucose oxidation and increasing anodic current. Although these effects on the current are small, they create a nonlinear relationship with glucose content. Thus, the a-C:Ag electrode is also

unsuitable as a glucose biosensor in the in the KCl–$K_3Fe(CN)_6$ electrolyte system.

Figure 5. *CV Curves of T2 Electrode in the 1 M KCl + 50 mM $K_3Fe(CN)_6$ Electrolyte: a) with and b) without Glucose*

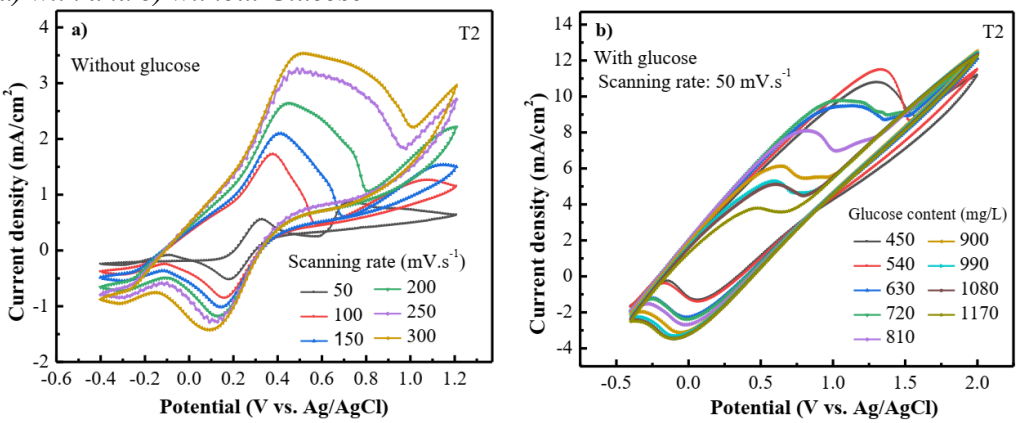

Figure 6. *CV Curves of Ag2# Electrode in the 1 M KCl + 50 mM $K_3Fe(CN)_6$ Electrolyte: a) with and b) without Glucose*

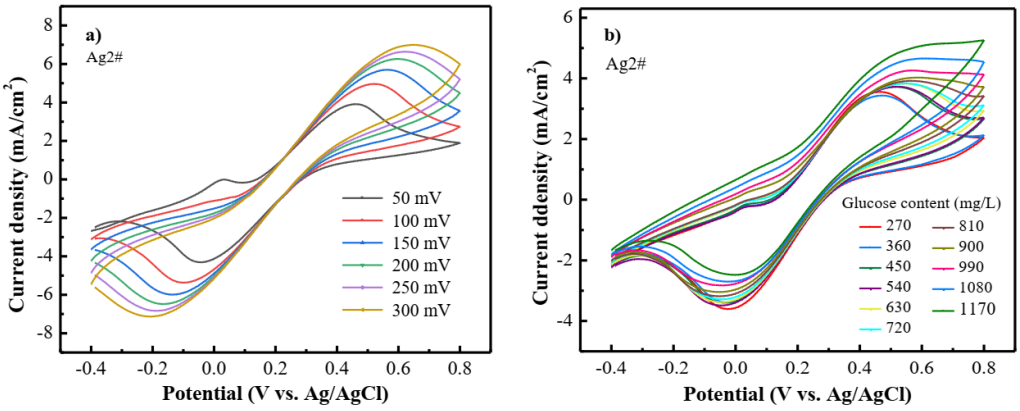

Electrochemical Performance of DLCs Electrode in 1 M NaOH Electrolyte

* T2 Electrodes

The oxidation reactions $Cu^{0/+}$, $Cu^{+/2+}$, and $Cu^{2+/3+}$ occur in alkaline electrolyte. Notably, $Cu^{2+/3+}$ boosts glucose oxidation (Nagy et al. 2001, Barragan et al. 2018, Zheng et al. 2019). With a scanning rate of 50 mV s^{-1} and a Hg/HgO reference electrode, Figure 7a shows the CV curves of the a-C:Cu electrodes in 1 M NaOH. The oxidation potentials for $Cu^{0/+}$, $Cu^{+/2+}$, and $Cu^{2+/3+}$ were marked. At about 900 mV, the anodic currents for T1–T4 electrodes were 73, 58, 70, and 97 µA cm^{-2}, respectively. These values are much higher than that of the pure Cu electrode (Nagy et al. 2001). This suggests that a-C:Cu electrodes have high reactivity due to the coatings, which include nanocrystalline Cu, metallic Cu clusters, and Cu–O bonds, either within the coating matrix or in the cotton-like particles. Thus, a-C:Cu-coated electrodes are promising for glucose biosensing in alkaline electrolytes.

Many studies have explored glucose's electrocatalytic oxidation using copper and Cu-oxide electrodes in alkaline electrolyte. The potential for glucose oxidation by $Cu^{2+/3+}$ is around 0.3–0.65 V vs. Ag/AgCl (Dai et al. 2018, Ma et al. 2019, Zhan et al. 2022). Some reports indicate it is below 0 V vs. Ag/AgCl (Wu et al. 2015, Barragan et al. 2018). This varies based on electrode surface, solution pH, and Cu's form. The oxygen evolution reaction occurs at 0.23 V vs. Hg/HgO on the pure copper electrode in pH 14 electrolyte, according to the Pourbaix E–pH diagram for copper. In a 1 M NaOH + 0.1 M glucose electrolyte, Figure 7b shows the CV curves of T1–T4 electrodes at a 50 mV s^{-1} scanning rate. T1–T3 show an anodic current peak around 0.21 V vs. Hg/HgO, with current densities from 92 to 217 µA cm^{-2}. This suggests $Cu^{2+/3+}$ catalyzes glucose oxidation. As Cu content in the coatings increases, the oxidation current also rises. Examining the surface morphology in Figure 1, the catalytic activity of the Cu particles appears unaffected by the carbon layer covering. However, glucose readily adheres to the cotton-like particles, which weakly attach to the surface. This forms a dense glucose film barrier on T4 electrodes with high particle density. It protects the electrode surface from the electrolyte, leading to nearly zero reaction current. This is due to gluconolactone, the reaction product, being hard to desorb (Zheng et al. 2019) and diffuse into the solution. Overall, the current peaks above 0.21 V vs. Hg/HgO for T1–T3 electrodes result from glucose oxidation aided by copper ions in the electrolyte and absorbed OH^- groups. Therefore, the anodic current above 0.2 V vs. Hg/HgO directly relates to the glucose content.

Figure 7. *CV Curves of the a-C:Cu Electrodes in 1 M NaOH Electrolyte without (a) and with Glucose*

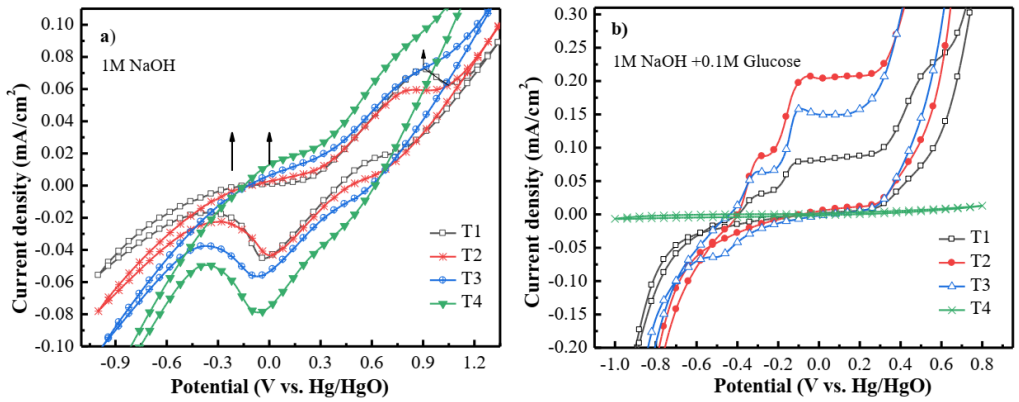

* Ag2# Electrodes

In this subsection, the scanning rate was set at 50 mV s–1. The voltage range was from –1.0 to 1.0 V, using Hg/HgO as the reference electrode. Figure 8a shows the CV curves of a-C:Ag electrodes with varying Ag content in 1 M NaOH. The current density remained below 10 µA.cm^{-2}, indicating that Ag, whether as Ag-cluster or np-Ag, is difficult to oxidize. Recent studies noted that np-Ag electrodes oxidize at specific voltages: Ag→AgOH at 0.34 V and Ag→Ag_2O at 0.73 V vs. Ag/AgCl (Usman et al. 2019). However, many reports state that np-Ag can catalyze glucose oxidation in alkaline solutions at potentials between 0.4–0.6 V vs. Ag/AgCl (Dayakar et al. 2018, Smikhovskaia et al. 2019), provided that the np-Ag has direct contact with the electrolyte. In this study, silver and carbon were co-deposited. The np-Ag was either wrapped in an amorphous carbon matrix or covered by a carbon layer on the

surface. This reduced the amount of np-Ag that directly contacted the solution, hindering its oxidation during potential scanning. After adding 0.1 M glucose to the 1 M NaOH electrolyte, the CV curves for all a-C:Ag electrodes are shown in Figure 8b. At 0.4 V vs. Hg/HgO, the Ag5# electrode displayed an anodic current of about 200 $\mu A.cm^{-2}$, indicating glucose oxidation by the silver catalyst. In contrast, other a-C:Ag electrodes showed only slight catalytic activity for glucose oxidation. This suggests that the catalytic activity of np-Ag depends on the area that directly contacts the solution. A similar observation was made with coated electrodes where Ag and carbon were deposited together (Dayakar et al. 2018, Buathong et al. 2025). Due to this sensitivity in catalytic activity, a-C:Ag electrodes face significant challenges as sensors for measuring glucose in alkaline electrolytes.

Feasibility of the a-C:Cu Electrode as a Glucose Sensor in an Alkaline Electrolyte

The weak adhesion of cotton-like particles on the surface can affect measurement reproducibility. To address this, we selected the T2 electrode for this section. We modified its surface using nitric acid etching (Formula (1–3)) to remove the particles, leaving craters behind. We recorded the CV curves in Figure 9a using a scanning rate of 50 mV s^{-1}, within a range of –1.0 to 1.0 V, in 1 M NaOH-based electrolytes with varying glucose concentrations. The anodic current peak appeared at 0.2–0.4 V vs. Hg/HgO, mainly due to glucose oxidation. To improve measurement precision, we employed the DPV method (Zhan et al. 2022) at a scanning rate of 4 mV s^{-1}, in the range of –0.2 to 0.6 V. The DPV curves are shown in Figure 9b. As glucose concentration increased, the peak current at 0.25 V vs. Hg/HgO rose steadily. Figure 9c illustrates the relationship between peak current and glucose content. We observed two linear regions with different slopes: one from 270 to 720 mg L^{-1} glucose, and another from 720 to 1080 mg L^{-1} glucose.

This finding slightly differs from reports by Yang et al. (2010) and Ma et al. (2029), which noted only one linear region in the measurement range. This difference stems from the surface condition of the etched T2 electrode, which had craters. The size of the glucose molecule is too large to enter the small craters. Thus, it gets absorbed by the active sites on the flat surface when glucose concentration is low. At high glucose concentrations, the active sites on the flat area become fully covered. Some glucose then "squeezes" into the craters, where copper ion concentration is high. Therefore, ensuring a smooth and uniform a-C:Cu electrode surface is crucial for the ongoing study.

Figure 8. *CV Curves of the a-C:Ag Electrodes in 1 M NaOH Electrolyte without (a) and with Glucose*

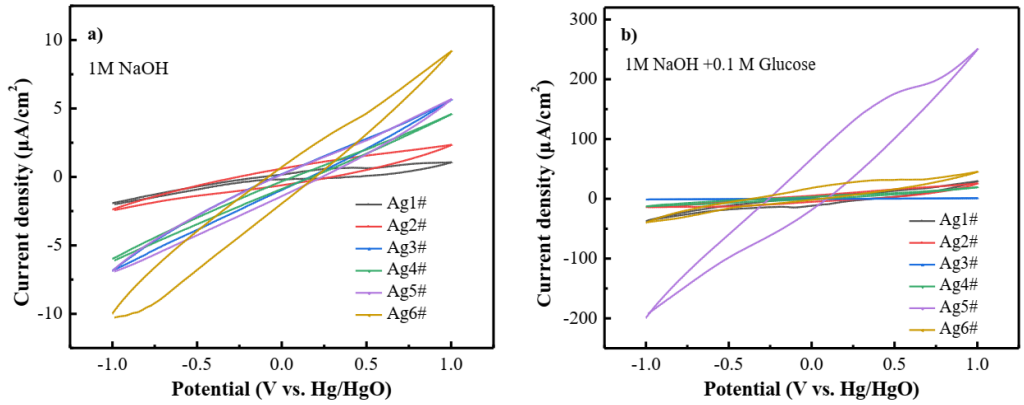

Figure 9. *CV Curves (a), DPV curves (b) from the etched T2 Electrode in 1 M NaOH Electrolyte with different Glucose Content, together with the Dependence between Glucose and Peak Anodic Current (c)*

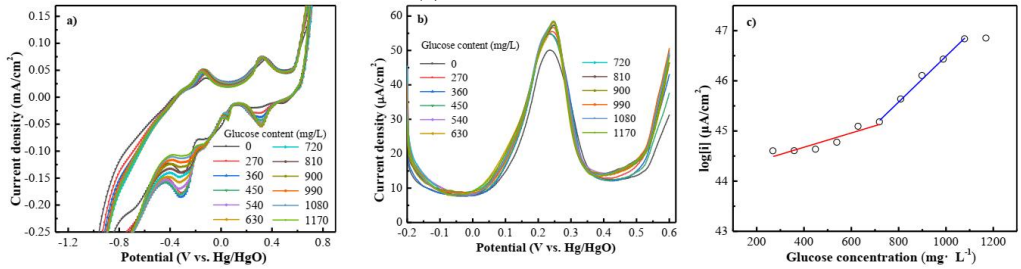

Conclusion

1) This study shows that a-C:Cu or a-C:Ag electrodes with nano-crystal particles (np-) can be made in one step. This uses a complex method that combines filtered cathode arc and magnetron sputtering deposition. The nps-Cu or Ag particles are wrapped in a carbon matrix. Those on the surface have a layer of carbon. As the Cu/Ag content increases, the sp^2C fraction and np-metal content also increase. During the a-C:Cu deposition, many cotton-like particles appeared on the surface. This was linked to the shield condition in front of the Cu target.

2) In the 1M KCl + 50 mM $K_3Fe(CN)_6$ electrolyte, the as-deposited T2 electrode with 5.2 at.% Cu showed a quasi-reversible behavior for the $(Fe(CN)_6)^{-3/-4}$ redox couple at a slow scanning rate. However, it degraded at higher rates. When 450 – 1170 mg/L glucose was added, reactions on the electrode surface included the $(Fe(CN)_6)^{-3/-4}$ redox, oxidation of OH^- groups and Cu, and oxidation driven by $Cu^{2+/3+}$. Therefore, the a-C:Cu electrode was not suitable as a glucose biosensor in this electrolyte system.

3) In the same electrolyte, the as-deposited Ag5# electrode with 5.0 at.% Ag showed poor reversibility for the $(Fe(CN)_6)^{-3/-4}$ redox couple at scanning rates from 50 to 300 $mV.s^{-1}$. After adding 450 – 1170 mg/L glucose, the anodic peak current was mainly due to the $(Fe(CN)_6)^{-4/-3}$ oxidation. Only a small amount of current came from silver-catalyzed glucose oxidation, which did not correlate linearly with glucose content. In a 1 M NaOH electrolyte, the metallic Ag particles in the a-C:Ag electrodes

remained unoxidized. The catalytic oxidation of glucose by np-Ag was highly affected by its surface condition, which was difficult to control. Thus, the a-C:Ag electrode was also unsuitable as a glucose biosensor in both electrolyte systems.

4) In alkaline electrolyte, the catalytic oxidation activity of np-Cu for glucose was not sensitive to its surface condition, whether covered by a carbon layer or not. However, the carbon layer significantly reduced the catalytic activity of np-Ag. The $Cu^{2+/3+}$ reaction promoted glucose oxidation at a potential of 0.2 – 0.3 V vs. Hg/HgO. The relationship between anodic peak current and glucose content showed two log-linear regions. This likely relates to the surface condition of the studied T2 electrode.

Acknowledgment

This study was financially supported by Guangzhou Grandtech Co., Ltd. (grant numbers 2023440002002575 and 2024440002002824).

Reference

Barragan J, Kogikoski S Jr, da Silva ET, Kubota L (2018) Insight into the electro-oxidation mechanism of glucose and other carbohydrates by CuO-based electrodes. *Analytical Chemistry* 90: 3357–3365.

Birkett M, Zia A, Devarajan D, Soni M, Panayiotidis M, Joyce T, *et al.* (2023) Multi-functional bioactive silver- and copper-doped diamond-like carbon coatings for medical implants. *Acta Biomaterialia* 167: 54–68.

Buathong S, Harnchana V, Pimsawat A, Jarernboon W, Pimanpang S, Amornkitbamrung V (2025) Electrodeposition of Ag-doped diamond-like carbon films on stainless steel for supercapacitor applications. *Journal of Alloys and Compounds* 1010: 177942.

Dayakar T, Rao K, Parb J, Sadasivuni K, Rao K, Rambabu N (2018) Non-enzymatic biosensing of glucose based on silver nanoparticles synthesized from *Ocimum tenuiflorum* leaf extract and silver nitrate. *Materials Chemistry and Physics* 216: 502–507.

Dai Y, Molazemhosseini A, Abbasi K, Liu C (2018) A cuprous oxide thin film non-enzymatic glucose sensor using differential pulse voltammetry and other voltammetry methods and a comparison to different thin film electrodes on the detection of glucose in an alkaline solution. *Biosensors* 8: 4.

Hwang D, Lee S, Seo M, Chung T (2018) Recent advances in electrochemical non-enzymatic glucose sensors—A review. *Analytica Chimica Acta* 1033: 1–34.

Jastrzebski K, Białecki J, Jastrebska A, Kaczmarek A, Para M, Niedzielski P, *et al.* (2021) Induced biological response in contact with Ag- and Cu-doped carbon coatings for potential orthopedic applications. *Materials* 14: 1861.

Jin C, Zeng A, Cho S, Boo J (2012) Investigation of copper and silver nanoparticles deposited on a nitrogen-doped diamond-like carbon (N-DLC) film electrode for biosensing. *Journal of the Korean Physical Society* 60: 912–915.

Khan M, Adil F, Majeed S, Farooq W, Hasan M, Jabeen R, *et al.* (2019) Structural, morphological, electrical and optical properties of Cu-doped DLC thin films. *Materials Research Express* 6: 126420.

Liu Y, Guo P, He X, Li L, Wang A, Li H (2016) Developing transparent copper-doped diamond-like carbon films for marine antifouling applications. *Diamond and Related Materials* 69: 144–151.

Liu C, Chen W, Sun Y, Lin C (2018) Fabrication and electrochemistry characteristics of nickel-

doped diamond-like carbon film toward applications in non-enzymatic glucose detection. *Applied Surface Science* 436: 967–973.

Liu N, Zhu H, Wei Q, Long H, Deng Z, Yu Z, *et al.* (2017) A niobium and nitrogen co-doped DLC film electrode and its electrochemical properties. *Journal of the Electrochemical Society* 164: H1091–H1098.

Maalouf R, Chebib H, Saikali Y, Vittori O, Sigaud M, Garrelie F, *et al.* (2007) Characterization of different diamond-like carbon electrodes for biosensor design. *Talanta* 72: 310–314.

Markwitz A, Leveneur J, Gupta P, Suschke K, Futter J, Rondeau M (2015) Transition metal ion implantation into diamond-like carbon coatings: Development of a base material for gas sensing applications. *Journal of Nanomaterials* 2015: 706417.

Naikoo G, Salim H, Hassan I, Awan T, Arshad F, Pedram M, *et al.* (2021) Recent advances in non-enzymatic glucose sensors based on metal and metal oxide nanostructures for diabetes management—A review. *Frontiers in Chemistry* 9: 748957.

Nagy L, Nagy G, Hajos P (2001) Copper electrode-based amperometric detector cell for sugar and organic acid measurements. *Sensors and Actuators B* 76: 494–499.

Patolsky F, Weizmann Y, Willner I (2004) Long-range electrical contacting of redox enzymes by SWCNT connectors. *Angewandte Chemie International Edition* 43: 2113–2117.

Peng J, Liao J, Zhang G, Huang J, Qiu X (2023) Microstructure evolution and mechanical performance of tetrahedral amorphous carbon coatings with dense droplets during annealing. *Materials Chemistry and Physics* 301: 127697.

Peng J, Li X, Li B, Liao J (2024) Controlling adhesion and thermal stability of tetrahedral amorphous carbon coatings with intermediate sp^3C fraction. *Thin Solid Films* 788: 140151.

Peng J, Xiao Y, Yang M, Liao J (2021) Effect of nitrogen doping on the microstructure and thermal stability of diamond-like carbon coatings silicon and oxygen. *Surface and Coatings Technology* 432: 127479–127488.

Peng Y, Peng J, Wang Z, Xiao Y, Qiu X (2022) Diamond-like carbon coatings in the biomedical field: Properties, applications and future development. *Coatings* 12: 1088.

Robertson J (2002) Diamond-like amorphous carbon. *Materials Science and Engineering R* 37: 129–281.

Tian F, Tao X, Wang J, Huang Z, Tian W, Chen J (2024) Investigation of Cu-doped amorphous carbon film in improving corrosion resistance and interfacial conductivity of proton exchange membrane fuel cell. *Surface and Coatings Technology* 485: 130926.

Towobola A, Jack T, Hosseini V, Yang Q (2025) Synthesis and characterization of Ag-doped DLC films for biomedical implants. *Diamond and Related Materials* 152: 111884.

Vetter J (2014) 60 years of DLC coatings: Historical highlights and technical review of cathodic arc processes to synthesize various DLC types, and their evolution for industrial applications. *Surface and Coatings Technology* 257: 213–240.

Wei J, Guo P, Liu L, Li H, Li H, Wang S, *et al.* (2020) Corrosion resistance of amorphous carbon film in 3.5 wt% NaCl solution for marine application. *Electrochimica Acta* 346: 136282.

Wu W, Periasamy A, Lin G, Shih Z, Chang H (2015) Palladium copper nanosponges for electrocatalytic reduction of oxygen and glucose detection. *Journal of Materials Chemistry A* 3: 9675–9681.

Yan C, Guo P, Zhou J, Chen R, Wang A (2023) Dependence of piezoresistive behavior upon Cu content in Cu-DLC nanocomposite films. *Diamond and Related Materials* 136: 109935.

Yan F, Jiang B, Liu B, Yang C, Dong D, Shi J (2023) Retention mechanism and conductivity corrosion resistance performance of Ag-doped GLC and TiN films for metal bipolar plates. *Vacuum* 208: 111702.

Zeng A, Neto V, Gracio J, Fan Q (2014) Diamond-like carbon (DLC) films as electrochemical electrodes. *Diamond and Related Materials* 43: 12–22.

Zhan T, Feng X, An Q, Li S, Xue M, Chen Z, *et al.* (2022) Enzyme-free glucose sensors with efficient synergistic electrocatalysis based on a ferrocene derivative and two metal nanoparticles. *RSC Advances* 12: 5072–5079.

Zhao Z, Yu X, Zhang Z, Shu W, Li J (2020) Attempting Ag-doped diamond-like carbon film to improve seal performance of hydraulic servo-actuator. *Materials* 13: 2618.

Zhou B, Liu Z, Piliptsou D, Yu S, Wang Z, Rogachev A, *et al.* (2016) Structure and optical properties of Cu-DLC composite films deposited by cathode arc with double-excitation source. *Diamond and Related Materials* 69: 191–197.

Zhu Z, Garcia-Gancedo L, Flewitt A, Xie H, Moussy F, Milne W (2012) A critical review of glucose biosensors based on carbon nanomaterials: carbon nanotubes and graphene. *Sensors* 12: 5996–6022.

Athens Journal of Sciences - Volume 12, Issue 4, December 2025 – Pages 251-284

Evaluating the Multi-Functional Benefits of Urban Green Infrastructure for Climate Adaptation: A Nature-Based Approach in Konak District, Izmir

By Birsu Kambur[*] & Stefano Salata[±]

Climate change is a reality, and the entire world is experiencing its effects. Coastal areas are highly affected by climate change. In addition to effects such as heat waves, floods, droughts, and decreased biodiversity, coastal areas are threatened by sea level rise and erosion. Türkiye, one of the most exposed countries, has struggled with an average temperature increase of 1 °C in the last decade. The coastal city of Izmir, Türkiye's third largest city, has become vulnerable under increasing population pressure, causing massive urbanization of the fringe. This research investigates the feasibility and effectiveness of implementing Nature-Based Solutions (NBS) in the Konak district, which represents one of the city's most ecologically vulnerable urban areas due to limited green space and high density. Within Konak, Alsancak, being one of its most historical neighborhoods, is used as a pilot site to test spatial interventions. The study aims to enhance coastal resilience and reduce vulnerability to climate change impacts. To achieve this, Geographic Information System (GIS) and InVEST tools were employed to evaluate key ecosystem services including carbon sequestration, urban heat island mitigation, air quality, and habitat quality. The vulnerability of Izmir, particularly Konak, to sea level rise, storm surges, and erosion was analyzed. Potential NBS suitable for adaptation were identified through parametric analysis. The socio-economic and environmental benefits of NBS were compared with traditional engineering-based solutions under two scenarios. Based on the findings, a comprehensive design proposal was developed to integrate NBS into the urban context. The reuse of post-industrial sites, such as the Sümerbank Factory, is proposed to enhance ecosystem connectivity and resilience. This research aims to serve as a roadmap for other coastal cities facing similar climate challenges.

Keywords: *climate change, nature-based solutions, ecosystem services, coastal resilience, urban heat island effect*

Introduction

Climate change poses serious global threats, including heatwaves, floods, droughts, biodiversity loss, sea-level rise, and coastal erosion. The Intergovernmental Panel on Climate Change (IPCC) notes that limiting warming to 1.5°C instead of 2°C could prevent millions from losing their homes due to sea-level rise (IPCC 2022). Climate change affects not only the environment but also ecosystems and human communities.

The Mediterranean is amongst the world's most climate-exposed areas, likely to undergo systemic breakdown in the face of rising temperatures, water scarcity, and

[*]Graduate Student, Polytechnic of Milan, Italy.
[±]Associate Professor, Polytechnic of Milan, Italy.

degradation of ecosystems (UN Environment 2017). Reducing exposure and enhancing the resilience of the marine and coastal environment using ecosystem-based and Nature-Based Solutions (NBS) is important.

NBS have gained more support globally due to being eco-friendly, low-cost interventions with many benefits, including urban cooling, flood control, and biodiversity improvement (McPhearson et al. 2023).

Izmir, the third-largest city in Türkiye, is most exposed to climate change due to the fact that it is coastal, urbanized, and expanding rapidly. The Konak district, for instance, has a low runoff retention capacity (46%) and not enough green infrastructure, increasing such vulnerabilities as urban heat and flash flooding. Alsancak, being an old district of Konak, is most exposed due to lower adaptive capacity and protection constraints. This study was developed within the MSc thesis work of the first author in the Sustainable Architecture and Landscape Design program at Politecnico di Milano. The research builds upon the strategic urban resilience vision outlined in İzmir's Green Infrastructure Strategy (2017) and İzmir Sustainable Energy and Climate Action Plan (2020), further extending their framework through spatial analysis and ecosystem modeling (using InVEST and GIS tools) to evaluate the climate adaptation potential of green infrastructure in Konak District. Even though the above policy reports present a broad outline for enhancing urban resilience and ecological integrity, this paper completes their vision through spatially rich and model-based research based on ecosystem service evaluation tools, e.g., InVEST. The focus is placed on the Konak District, being a model representative for the application of nature-based solutions towards mitigating climate-related urban vulnerabilities.

However, Alsancak provides a location to test NBS integration in urban development, particularly for services like water harvesting, carbon sequestration, and cooling. The main purpose of this study is to evaluate the multifunctional ecosystem services of existing and proposed green infrastructure elements in the Konak District of Izmir, including carbon sequestration, urban heat island mitigation, habitat quality, and air purification. Using GIS-based spatial analysis and InVEST modeling tools, the research aims to assess the environmental performance of nature-based solutions and inform integrative design strategies that enhance urban climate resilience, ecological connectivity, and public well-being in Mediterranean coastal cities.

Literature Review

Climate change is a pressing global issue, with warming of 1.1°C above pre-industrial levels already observed (IPCC 2022). The Mediterranean is particularly vulnerable, experiencing rising temperatures, droughts, and more extreme events (MedECC 2020, UN Environment 2017).

Coastal cities like Izmir are exposed to sea-level rise, storm surges, and heat stress. Rapid urbanization and weak green infrastructure exacerbate these risks, especially in historic neighborhoods such as Alsancak within Konak (İzmir SEİEP 2020, Salata et al. 2022).

Nature-Based Solutions (NBS) are increasingly used to enhance urban resilience. Defined by the IUCN (2016) as actions to restore and manage ecosystems to address societal challenges, NBS provide co-benefits such as climate regulation, improved air quality, and enhanced community well-being (McPhearson et al. 2023, Epelde et al. 2021). Green roofs, permeable surfaces, and urban forests are examples applied in urban contexts (Coutts et al. 2013, Manso et al. 2021).

Ecosystem services, classified as provisioning, regulating, cultural, and supporting, play a central role in NBS planning. Including them in urban decision-making enables better outcomes (Eggermont et al. 2015, Palta et al. 2017). In this study, InVEST was used to quantify key services, including habitat quality, carbon storage, and urban cooling, in Alsancak, highlighting weaknesses in Izmir's current strategy.

However, NBS performance depends on local socio-ecological factors such as governance, density, and participation (Dorst et al. 2019, Haase 2017). Therefore, integrating NBS into İzmir's planning framework is crucial for achieving long-term success.

Methodology

Climate change vulnerability is here quantified for Izmir and NBS capacity to build resilience is experimented with for the Konak municipality, focusing specifically on the Alsancak quarter. Spatial analysis and ecosystem modeling platform was used through GIS and InVEST platforms (Kambur 2025).

Study Area and Data Sources

Izmir, located on the Aegean coast, is Türkiye's third largest city. The historical heart of the city is Konak (which includes Alsancak), which has high-density development and a low amount of green space (6%) but significant heritage value, and faces significant ecological challenges associated with urbanization (i.e. pressures on biophysical systems).

The datasets used are:

- **LULC**: Landsat 9 imagery (July 2024) via EarthExplorer
- **Tree Cover**: Copernicus (2018 raster)
- **Building Height**: Urban Atlas (2012)
- **Air Quality (PM10)**: Stations in Bayraklı, Alsancak, Güzelyalı (Oct 2023–2024)
- **Carbon Values per LULC Class**: Natural Capital Project

All spatial data were projected in UTM Zone 35S (Datum: WGS84).

Green Infrastructure Analysis

Green infrastructure within Konak was evaluated based on Izmir Municipality's 2017 strategy document (İzmir Yeşil Altyapı Stratejisi 2017). GIS analysis identified key green spaces, such as Kültürpark and Kadifekale, as well as the presence of proposed green corridors along the Meles River. Tree cover density statistics were used to calculate spatial distribution and vegetation gaps. The results show that there is very little green space, and the existing green spaces are fragmented, therefore, do not adequately support climate adaptation efforts and require concurrent planning of integrated ecological approaches to urbanism.

Ecosystem Service Models Using InVEST

Four ecosystem services were modeled using InVEST software (v3.14.2):

- Carbon Sequestration
- Habitat Quality
- Urban Heat Island Mitigation
- Air Pollution Mapping (via ArcGIS)

Carbon Sequestration

The InVEST Carbon Sequestration model (v3.14.2) calculates carbon storage using LULC data and four values of carbon pools: aboveground, belowground, soil, and dead organic matter. A Landsat 9 image (July 2024) was utilized to produce a LULC map using ArcGIS software and grouped into six classes: water, artificial, bare land, forest, agriculture, and shrubland.

Accuracy was validated by 300 random points and ground truthing. Classification was 0.856 kappa coefficient, verifying sufficient reliability to use in carbon calculations.

Habitat Quality

The InVEST Habitat Quality model assesses biodiversity via threats, sensitivities, and LULC. The data needed include LULC maps, sensitivity tables, raster of relevant threats, and information on protected areas. We selected data for threats and sensitivity from Salata et al. (2022). We also used the same LULC data as in our carbon modeling. We used the type of threat and sensitivity data together with threat intensity and adjusted intensity of threat depending of distance from threats and habitat type. Our output captured habitat vulnerability and quality.

Urban Heat Island Mitigation

To assess urban heat mitigation, the InVEST Urban Cooling Model was used. It estimates the cooling effect of land uses via evapotranspiration, shade, albedo, and proximity to green areas.

The input data included LULC, reference temperature, UHI values, and biophysical parameters. This model helped evaluate how nature-based interventions reduce heat vulnerability in urban areas.

Air Pollution Mapping

Annual PM10 concentrations (October 2023–2024) for the survey area were interpolated using ArcGIS IDW at the 3 monitoring stations in Alsancak, Güzelyalı, and Bayraklı into a single map based on monitoring data. Due to their ability to penetrate the deep tissues of the lungs, PM10 is one of the most hazardous air pollution components (Türkmen 2019). The developed map reflects the spatial variability of air quality throughout Konak.

Model Validation and Processing

All InVEST outputs were validated against peer-reviewed data and local records. Reclassification, normalization, and raster overlays were made in ArcGIS Pro 3.4.2 for the data's integration and visualization.

Environmental Impact Assessment and Analytical Tools

Environmental performance of tree-planting strategies at the Sümerbank site was assessed using species-specific ecological coefficients.

- **Carbon Sequestration:** 1,036,678 kg CO_2 projected lifetime storage.
- **Annual CO_2 Assimilation:** 83,647 kg/year.
- **Pollutant Removal:** 91.5 kg O_3, 80.82 kg NO_2, 72.4 kg SO_2, 48.22 kg PM10 annually.

Species like *Celtis australis* and *Quercus ilex* were key contributors. Results were contextualized through equivalents such as flight emissions and diesel usage. Google Earth imagery was also utilized to confirm land-use changes in the Meles Delta (2002–2025) and validate design strategies, such as wetland creation and riparian restoration.

Results

Green Infrastructure

These were also validated against peer-reviewed data and local records for the InVEST results. Reclassification, normalization, and overlay inspection through raster were performed in ArcGIS Pro 3.4.2 to be incorporated and visualized.

Konak, which is one of İzmir's older districts, has been urbanized to a great extent, and green space expansion was behind. Inner green areas such as Kültürpark and Kadifekale are unused, with green space coverage at only ~6%, which is considerably below the recommended 10 m^2 per capita (Türker & Gül 2022) (Figure 1).

In response, İzmir Green Infrastructure Strategy (2017) proposed holistic ecological measures like transitional spaces, recovery of ecosystem services, and corridor planning, especially along the Meles River for connecting fragmented locations and balancing urban growth with ecological requirements.

Key measures include:

- Large-canopy trees to reduce urban heat.
- Buffer zones and height regulations.
- Tiered conservation in biodiversity hotspots.
- Conversion of idle lands into green infrastructure.

Figure 1. *Izmir Municipality Green Infrastructure Strategies*

Source: İzmir Büyükşehir Belediyesi 2017.

Tree Cover Density

The tree cover is scant in Konak, having emerged in patches surrounding Kültürpark and on parts of the Meles River. Urban environments, such as Alsancak, lack vegetation with occasional street trees scattered outside the Akdeniz and Konak regions (Figure 2). The urban forest canopy needs to be improved to improve ecological resilience. There would also be benefits from integrating the Meles corridor into a connected urban green network, reducing spatial fragmentation, and encouraging the sustainability of the city.

Figure 2. *Tree Cover Density 2018 (raster 10 m) of the Konak District*

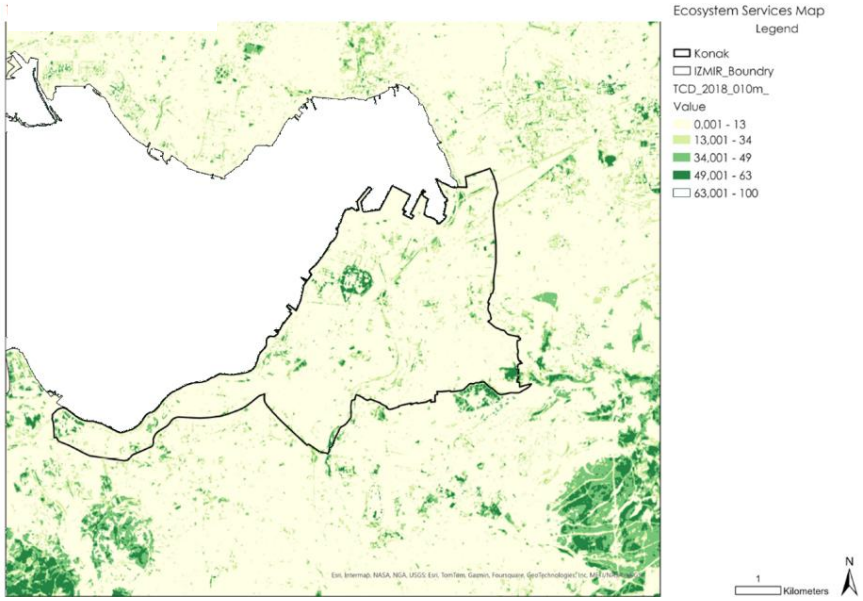

Source: author's elaboration using Tree Cover Density 2018 raster file, UTM Zone 35S, Datum WGS 84.

Land Use/Land Cover (LULC)

Over 80% of Konak's land is covered by urban uses, reflecting dense residential, commercial, and administrative development (Figure 3). Alsancak Port further intensifies industrial land use nearby. While the historical fabric contributes cultural value, the dominance of impermeable surfaces reduces green coverage and climate resilience.

Figure 3. *Urban Atlas 2018 LULC Data of the Konak District*

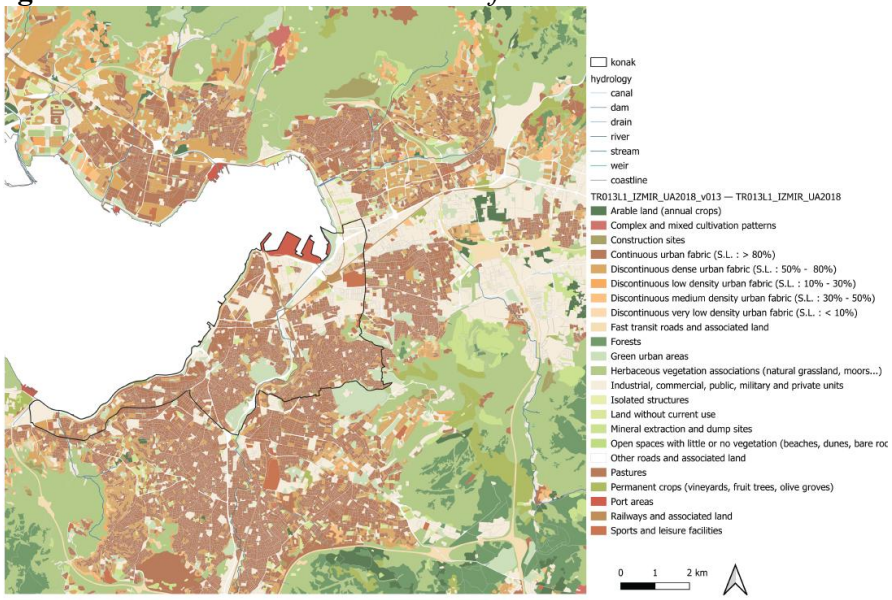

Source: author's elaboration using Urban Atlas 2018 vector file, UTM Zone 35S, Datum WGS 84).

Building Height

Konak building heights range from 3 to 76 meters (Figure 4). Alsancak and Mimar Sinan districts are represented with higher buildings (20–30 m), indicating densification, but conserved areas like Kemeraltı maintain low-rise buildings due to cultural heritage constraints. These are spatial distinctions emphasizing various urban pressures and needs for conservation.

Figure 4. *Urban Atlas Building Height 2012 of the Konak District*

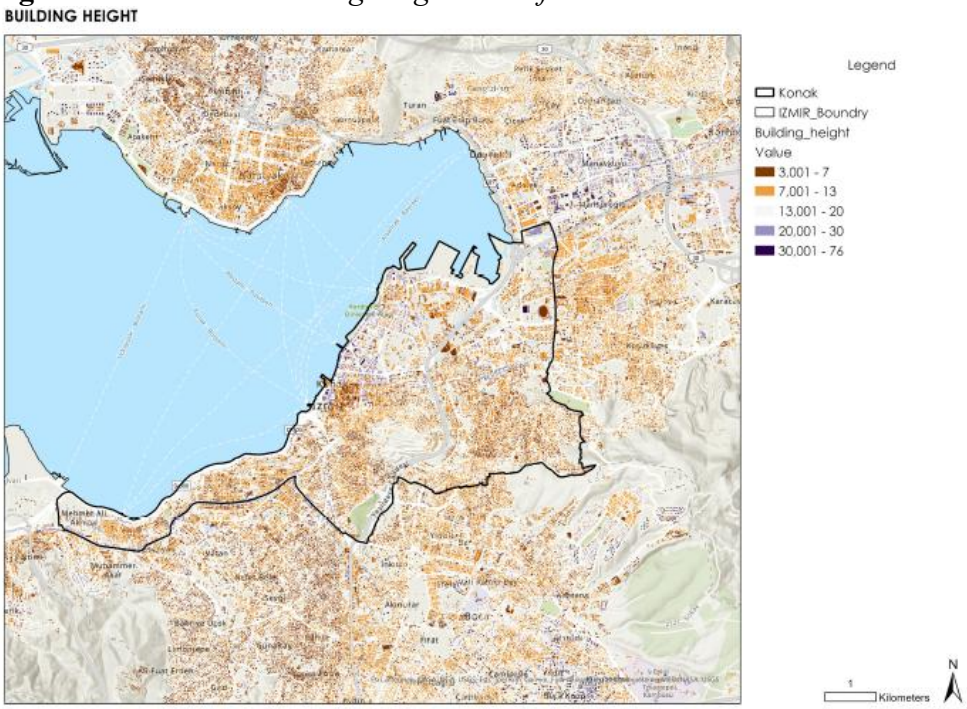

Source: author's elaboration using Urban Atlas 2012 vector file, UTM Zone 35S, Datum WGS 84.

Ecosystem Service Modeling

Carbon Sequestration

Carbon stock is critically low in urbanized areas of Konak, with only green zones like Kültürpark and Kadifekale retaining moderate values (~64.8Mg C/ha) (Figure 5). This emphasizes the need for NBS to be implemented (e.g., green roofs and vertical gardens). The opportunity to turn abandoned plots into vegetated areas, as well as supporting green mobility (e.g., bike lanes through Kültürpark into Alsancak), adds to the sequestration potential.

Figure 5. *Carbon Sequestration Map of Konak*

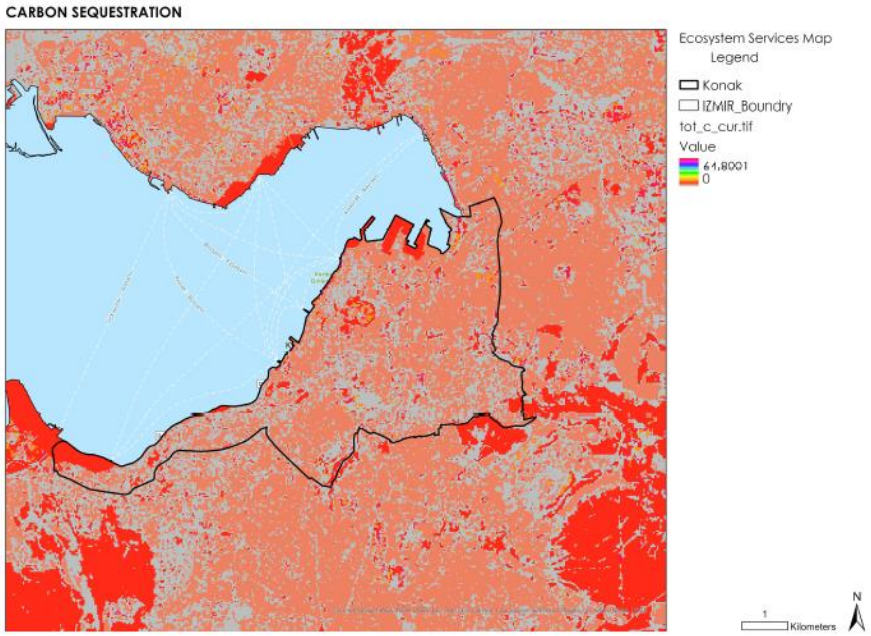

Source: author's elaboration with InVEST.

Habitat Quality

Over 90% of Konak exhibits low habitat quality (below 0.3 on a 0–1 scale) as a result of urban and agricultural expansion, and only a small number of patches above 0.6, indicating medium or high ecological value (Figure 6). Habitat fragmentation threatens biodiversity across the globe, and is reducing climate resilience (Admasu et al. 2023).

Figure 6. *Habitat Quality Map of Konak*

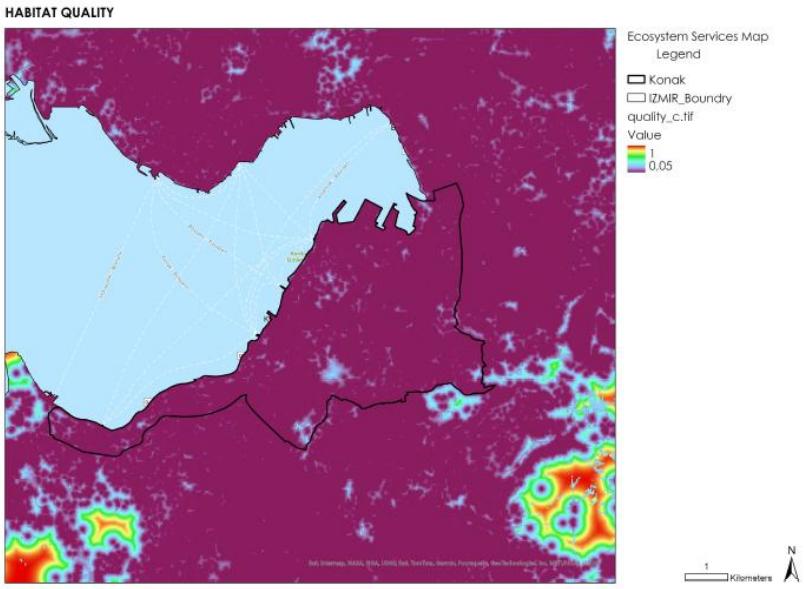

Source: author's elaboration with InVEST.

Urban Heat Island Mitigation

Konak is at high risk from UHI effects, and some areas are only showing substantial cooling values such as dense vegetation in areas like Mehmet Ali Akman, Güzelyalı, Göztepe, and Kültürpark which produced cooling values of 0.803 (on a normalized scale) (Figure 7). It will be especially critical to implement NbS such as green roofs and tree planting- especially in high-density areas. Increasing tree coverage by 10% can reduce local UHI intensity by (55) in the summer (Rogers et al. 2020).

Figure 7. *Heat Island Mitigation Map of Konak*

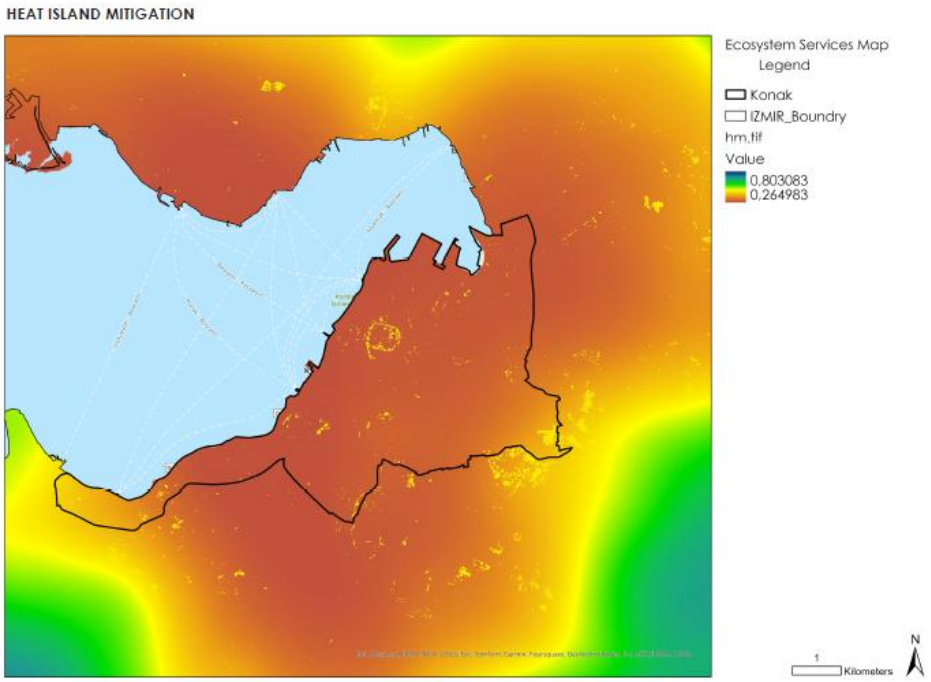

Source: author's elaboration with InVEST.

Environmental Vulnerabilities in Konak

The spatial analysis showed some significant environmental gaps. The area south of Alsancak Harbour shows the extent of flood vulnerabilities and the subsequent risks posed by climate exacerbation. The fragmented green infrastructure greatly deterrents mobility has been central to UHI, low habitat and carbon sequestration and pollutant exposures, which suggests that there is significant health risks related to populations exposed in areas like the Meles Stream corridor given the poor biodiversity and lack of vegetated barriers to pollution allergies. These vulnerabilities are spatially visualized in Figure 8, which highlights the key environmental weaknesses of Konak district, including flood risk, fragmentation, and low biodiversity.

Design interventions must focus on areas identified as most vulnerable, and think holistically to integrate NBS and planning for a regional scale for long-term climate adaptation.

Figure 8. *Weakness Map of Konak*

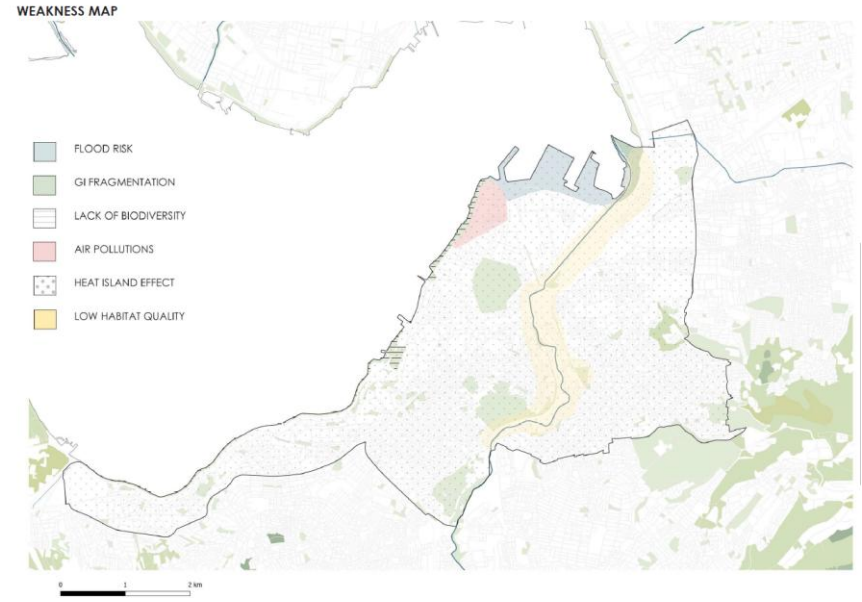

Design Proposal: Integrating Nature-Based Strategies for Urban Resilience in Alsancak, Izmir

Green and Blue Infrastructure Integration

The ecological integrity of Izmir increasingly depends on the agricultural basins and sustainability of its green corridors. In the context of a Blue Growth Strategy for the sustainability of the Gulf of Izmir, a reformed green network system has an increased importance to the Central Green Belt. The long-term vision of the municipality of Izmir (Izmir Sustainable Energy and Climate Action Plan 2020) proposes a continuous green corridor that follows the Meles Stream. This would be enterprising that can re-establish some ecological connectivity around the urban core (see Figure 9). The proposal to connect some of the fragmented green areas (e.g., Kültürpark and the coastal edge) with green infrastructure and street trees will provide connectivity solutions. In support of this, the proposed Green Infrastructure Strategy contains specific urban interventions based on the mapping of ecosystem services (Figure 10). The order is sequential and prioritized:

- **Ecological Bridge in Tabakhane Area:** Reconfigured a road to convert a highway into an underpass that is topped with a green bridge to reconnect disjointed green and facilitate wildlife movement.
- **Vegetation at Highway Intersections:** Taking usually neglected intersections and using them as a way to create more public green spaces to mitigated urban heat islands and increase biodiversity.
- **Green Corridor Expansion**: A new corridor is proposed along the Melta Stream, extending the existing green framework.

- **Urban Terraces**: Designed to improve vertical and functional connectivity between **Kadifekale** and the urban core.
- **Air Quality Enhancements**: Green façades, roofs, and permeable pavements are introduced in **Alsancak** and **Kordon Promenade** to mitigate air pollution.

These interventions constitute a multifunctional ecological network that enhances climate adaptation while promoting biodiversity and human well-being (Figure 11).

Figure 9. *Green Network Proposal*

Figure 10. *Green Infrastructure Strategy*

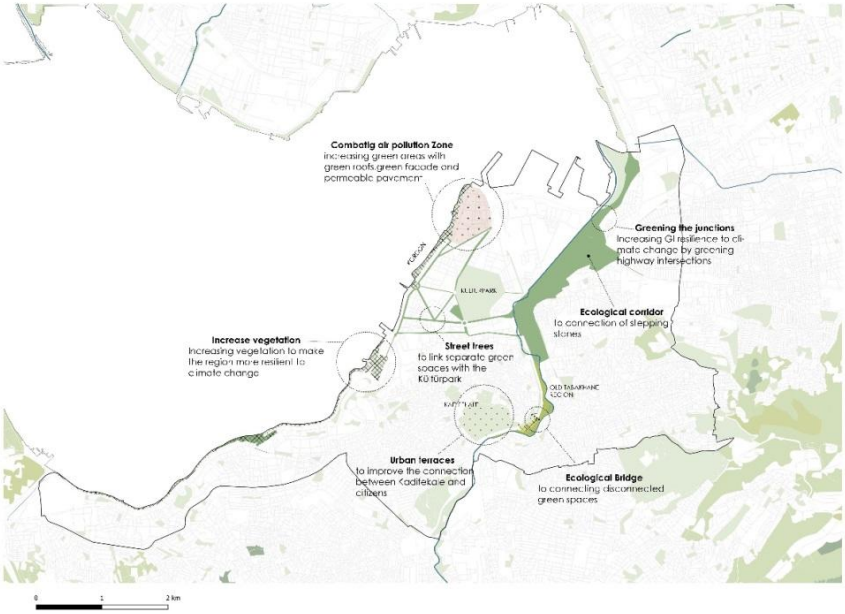

Figure 11. *Air Pollution Mitigation Strategy Map*

Blue Infrastructure and Coastal Adaptation

The Meles Delta is an ecologically sensitive and flood-prone area. Examination through Google Earth reveals that incredible changes are occurring (e.g., urbanization, altered river discharge, drought) from 2002 to 2025 (Figure 12). To restore hydrological balance and ecological integrity, a **Blue Infrastructure Strategy** (Figure 13) has been integrated, including:

- **Floodplain Wetlands**: Designed to store excess water during peak flows, enhancing resilience and biodiversity.
- **Wetland Restoration in Former Industrial Zones**: The vacated site near **Mandra Stream** is repurposed to restore natural water filtration.
- **Floating Wetlands & Filtration Ponds**: Improve water quality using phytoremediation.
- **Fish Passages and Buffer Zones**: Address flow interruptions and enhance aquatic biodiversity.
- **Groundwater Recharge Surfaces**: Along the **Meles Stream**, green and permeable surfaces improve infiltration and reduce runoff.

Together with the green strategy, this approach forms a hybrid urban ecosystem resilient to both climate and anthropogenic pressures.

Figure 12. *Evolution of the Coastal Area and the Meles Delta*

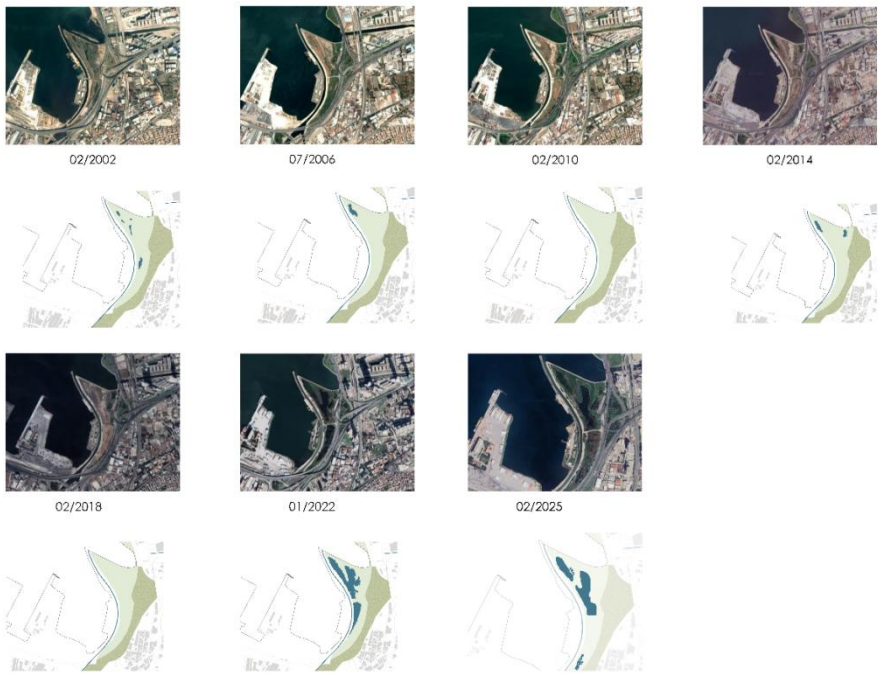

Source: Author's elaboration based on satellite imagery analysis (Google Earth, 2002–2025).

Figure 13. *Blue Infrastructure Strategy Map*

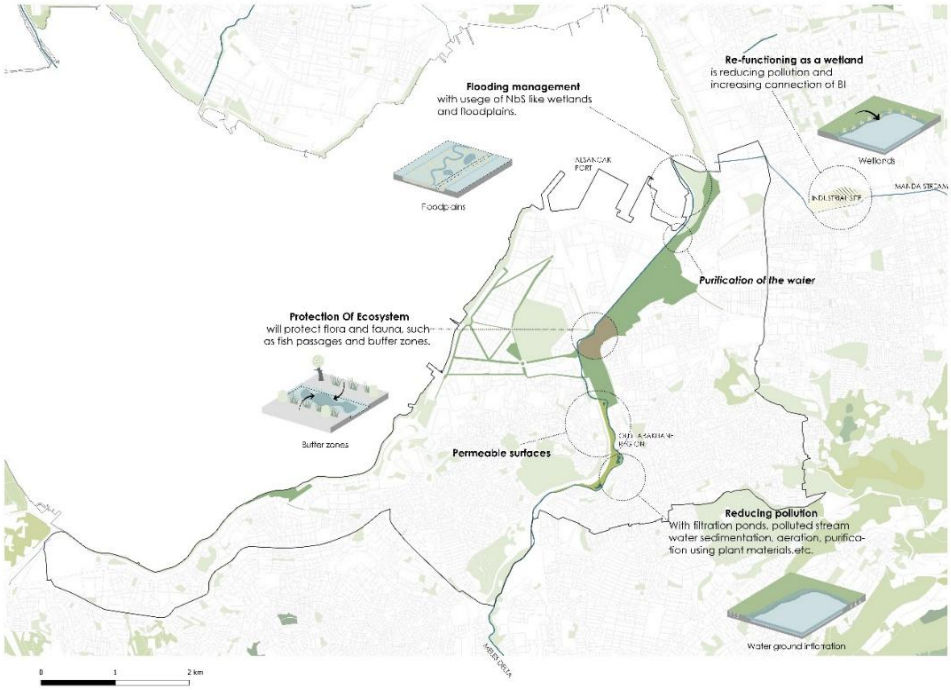

Mobility and Climate-Compatible Transport

The purpose of transportation redesign is to connect urban energy and mobility with the ecological system (Figure 14). It includes: - Bicycle and Pedestrian Paths: New bicycle and pedestrian paths are proposed along the Meles Stream and Kadifekale providing public space that is also linked to the ecological systems. - Permeable Surfaces on Tramway: In particular, a redesigned tramway with permeable surfaces proposed for the Kordon waterfront reduces run-off: These mechanisms indicated a strong link between humans and natural corridors and improved environmental quality.

Figure 14. *Transportation Strategy Map*

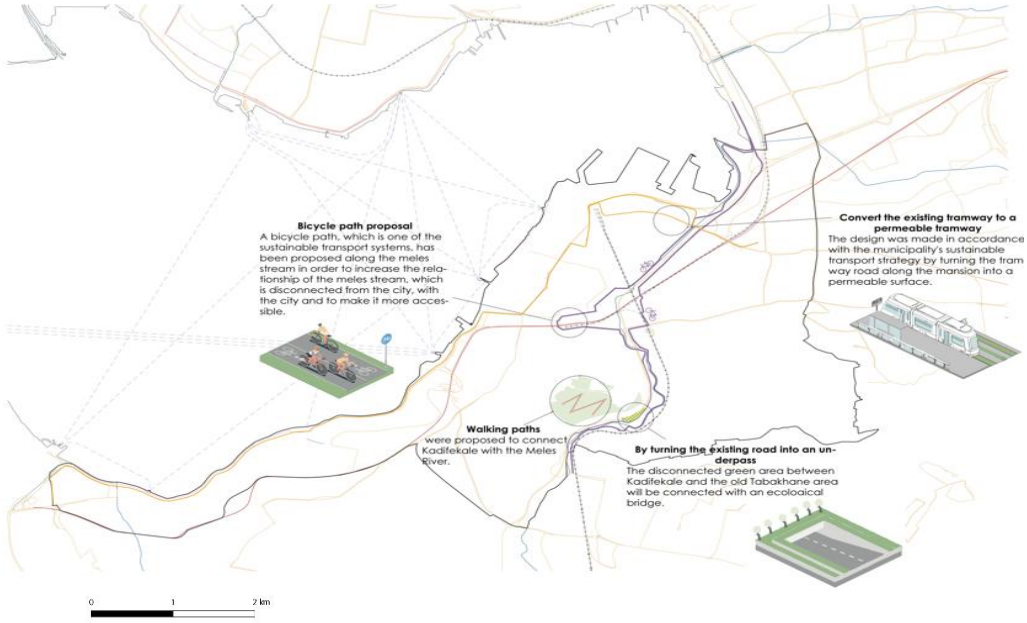

Strategic Vision and Master Planning for the Ecological City

Conceptual Framework: The Ecological City Model

Through thorough spatial, environmental, and vulnerability assessment, a strategic mechanism was created before the whole master plan was finalized (Figures 15-16). This strategic mechanism integrates green, blue, and transport systems into one unified planning vision, featuring the Ecological City Concept as the philosophical and spatial foundation of design. The concept has three pillars:

- **Climate Resilience:** enhancing the city's capacity to adapt to extreme weather, floods, and heat waves.
- **Social Equity**, ensuring that green and blue infrastructure benefits all populations, particularly vulnerable groups.
- **Ecological Integrity** conserves biodiversity and restores degraded ecosystems through green networks and sensitive land use.

The Meles Delta was identified as a priority zone due to its ecological value and vulnerability to climate impacts. In this regard, protecting the habitats is essential for the endemic fauna and urban biodiversity. Being one of Izmir's climate-threatened provinces and districts, Fazil Konak emphasizes the importance of Nature-Based Solutions as primary tools for adaptation and mitigation.

Other determining factors for this model's success would include awareness of civil society and the stakeholders.

Understanding how urban ecosystems operate helps a community build support, strengthen stewardship, and promote long-term viability.

Figure 15. *Concept Diagram*

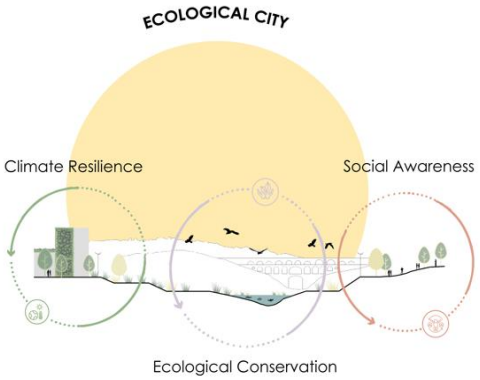

Figure 16. *Strategy Map*

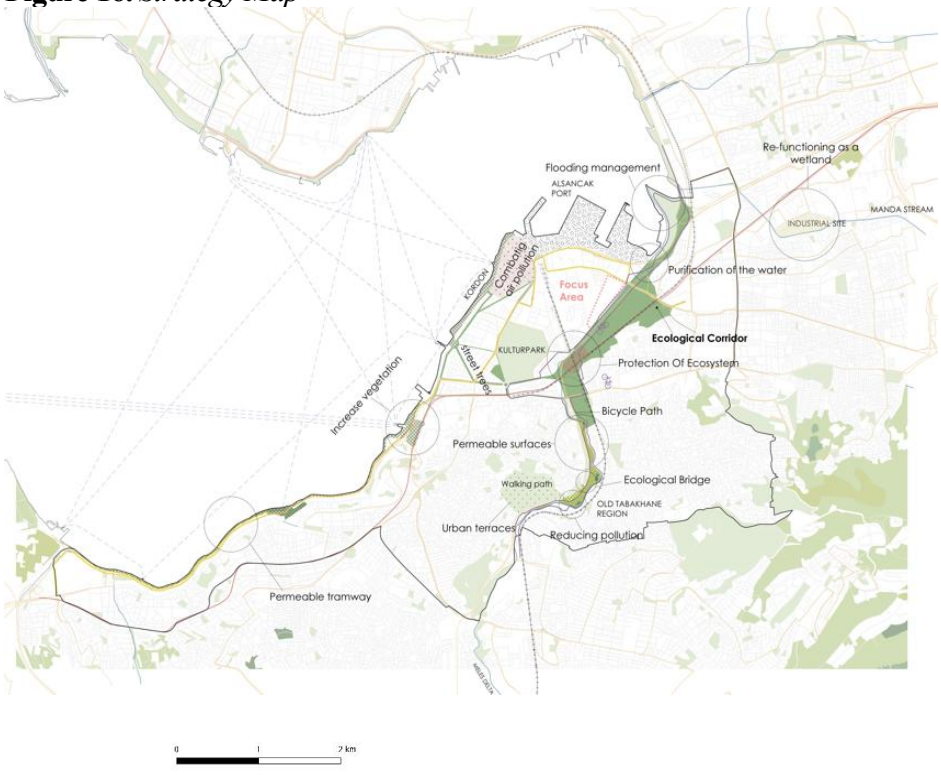

Master Plan: Integrating Green-Blue Networks in Alsancak

Building on the strategic concept, the Master Plan (Figure 17) integrates site-specific interventions across green, blue, and transportation domains, especially within Alsancak Port, where the Meles Stream meets the Gulf of Izmir. Seasonal analyses (Figure 12) revealed that parts of this area exhibit wetland characteristics during rainy periods, offering an opportunity for ecological enhancement and water-sensitive design.

The site is reimagined as a functional wetland system that respects natural hydrology. Enhanced green and tree-canopied spaces are introduced to capture stormwater, reduce flooding, and cool the local urban microclimate. A continuous boardwalk connects the spine of the intervention's three:

- Observation decks for environmental education and recreation.
- Pedestrian walkways and bike paths to promote sustainable mobility.

This structural intervention provides an ecological and circulation opportunity to connect the Meles Stream corridor to Kültürpark while connecting the community with the waterfront. The three land-use changes derive the transformation from:

- Vacant lands to green spine.
- Parking lots are redesigned as permeable green areas.
- New street trees reinforce ecological corridors along highways.

The green corridor from Kültürpark to the coast is divided into four landscape typologies:

1. Public Areas – for cultural events and civic gatherings.
2. Ecological Protection Areas – with restricted access to conserve sensitive habitats like the Meles Delta.
3. Recreation Areas – for walking, nature viewing, and low-impact leisure.
4. Sport Areas – with jogging and cycling routes and fitness equipment, surfaced with permeable materials to manage runoff and reduce heat.

This typology, based on ecological sensitivity and spatial analysis, ensures a balanced landscape that supports climate adaptation, strengthens ecological connectivity, and harmonizes urban development with environmental stewardship.

Figure 17. *Master Plan*

Ecological Conservation and Biodiversity Enhancement

The ecological conservation plan supports a sustainable, urban vision for the overall planning of Konak by enhancing protected areas, buffer zones, ecological corridors, permeable networks, and publicly available participatory spaces. This multiservice platform provides biodiversity benefits while supporting Konak's climate resilience. Although the Meles Delta has many kinds of flora and fauna, the previous industrialization and riverbed alteration has led to widespread habitat degradation. The plan proposed a master ecological plan based on local biodiversity, which aimed to restore ecological integrity through select interventions. The design proposes:

- **Protected Zones** to restrict access and allow natural regeneration.
- **Buffer Zones** to mitigate urban disturbances and prevent habitat fragmentation.
- **Observation Areas** for education and research, maintaining ecological integrity with controlled access through walkways and decks.

Species-focused strategies include the planting of **Olea europaea** (olive tree) to provide food and shelter, and habitat enhancements for birds like **Halcyon smyrnensis** (White-throated Kingfisher) and **Carduelis carduelis** (European Goldfinch).

Water quality restoration in the Meles River is a significant objective. For this, phytoremediation is introduced using aquatic plants with pollutant-removal capabilities (Figure 18):

- *Lemna minor* (duckweed): absorbs nutrients and heavy metals.
- *Trapa natans* (water chestnut): reduces pollutants and provides habitat.

- *Scirpus lacustris* (bulrush): stabilizes sediment and filters water.
- *Eichhornia crassipes* (water hyacinth): removes organics and heavy metals.
- *Phragmites australis* (common reed): improves oxygenation and filtration.

These nature-based solutions promote habitat recovery, improve water quality, and strengthen the coexistence of urban and natural systems in the Meles Delta. Importantly, this combined approach also coincides with international frameworks that promote climate-resilient approaches integrating natural ecosystems with built heritage, enhancing the ecological and cultural value of the Sümer Bank Factory and its environment, in accordance with ICOMOS (2019).

Figure 18. *Water Quality Improvement Strategy*

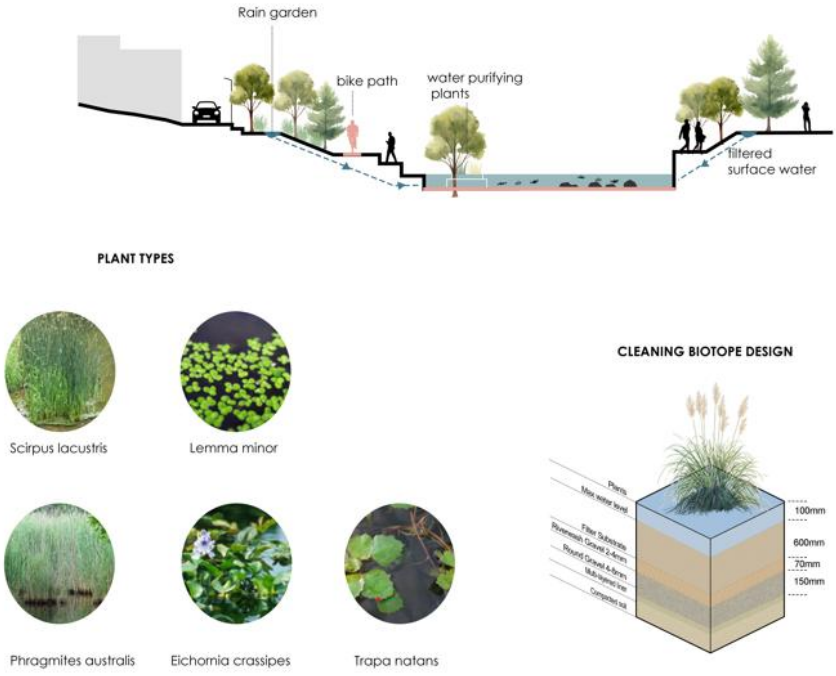

Focus Area: Sümerbank Factory as a Catalyst for Urban Regeneration

Rationale for Selection and Urban Context

The Sümerbank Factory was selected as the primary focus area within the Alsancak green corridor project due to its historical, spatial, and ecological significance (Figure 19). The tradition of early Turkish industrialization follows another that carries the collective memory of Izmir's heritage of manufacturing. Its current abandonment brings about urban fragmentation, in turn disrupting the ecological and cultural continuum of the city. Integrating the site along the green corridor will allow the project to rehabilitate it as a multifunctional ecological and social node, enhancing biodiversity as well as public interest.

Situated adjacent to green spaces and transportation axes, Sümerbank could serve as a spatial anchor, strengthening ecological connectivity for the Meles River. The adaptive reuse supports sustainable renewal by way of heritage conservation and

climate resilience. Allowing the site to return to a natural state reclaims a disused industrial site and creates living infrastructure that fuses-built heritage with eco-system restoration.

Figure 19. *Focus Area*

Historical Trajectory of Sümerbank Factory

Founded in 1933, Sümerbank emerged as both a **state-owned industrial and financial institution**, inheriting the functions of the earlier Industrial and Mining Bank, established in 1925. It was established to manage textile factories, support local industry through credit, and regulate the Turkish economy during its period of modernization (Toprak 1988). Following the closure of the State Industry Office and the Industry and Credit Bank due to structural inefficiencies, Sümerbank unified these roles and became instrumental in constructing major textile, chemical, and mining facilities under the First and Second Five-Year Industrial Plans (Arıtan 2004).

The Sümerbank Factory was chosen as the leading focal point of the Alsancak green corridor project because of its significant importance historically, spatially, and ecologically (See Figure 19). Sümerbank's influence extended all across Turkey with factories located in Kayseri, Nazilli, and other cities dependent upon raw materials, development emphasis, and military potentiality (Uğrasal 2011). Although it was fully privatized by 1993 and operations ceased by the early 2000s, Sümerbank's factories remain critical to the history of Turkey's industrial architecture and socio-economic development (Köksal & Ahunbay 2006).

Site Analysis and Design Approach

The spatial organization of the İzmir Sümerbank Basma Sanayi Complex, which is organized in spaces effective for operation as a place with separate areas for production, administration, housing, and public facets (See Figure 20). The entrance on Şehitler Street marked the starting point of a well-defined circulation axis (Axis 1), which connected all primary functions of the site, facilitating both secure factory operations and public access to social areas.

Today, although some buildings are used for educational purposes (e.g., Nevvar Salih İşgören Campus), many original industrial structures have fallen into disrepair. Despite the conservation decisions made in 1998 and 2001 by İzmir's Cultural Heritage Board, which registered the steam power plant, social facility, and other elements as second-degree cultural assets (Uğrasal 2011), much of the complex remains underutilized. The present-day disjointed state of the site represents the need for a design-based type of intervention to reinstate the operational and ecological functioning of the site. As seen in Figure 21, the Sümerbank Factory is physically disjointed, decayed, abandoned, and lacks any sort of maintenance. This ground-level photograph highlights the site's vulnerability and reinforces the necessity of nature-based strategies to rehabilitate its cultural and ecological assets.

Figure 20. *The Functional Zoning of the Sümerbank with Entrances*

Source: Uğrasal, 2011.

Figure 21. *Current State of the Sümerbank Factory Site Showing Structural Decay and Abandonment*

Source: GerçekİzmIr 2018.

Understanding the place's historical importance, a series of analyses was conducted before engaging in the process of design. Flooding, as well as studies on air pollution, revealed that the area is critically prone to floods, and notably, the area with the five schools is most at risk. The rate of air pollution was also observed to be quite intense along 1525 Street. Therefore, the design process addresses these environmental conditions so that development will be environmentally friendly and responsive.

Figure 22. *Air Pollution and Flooding Risk Maps*

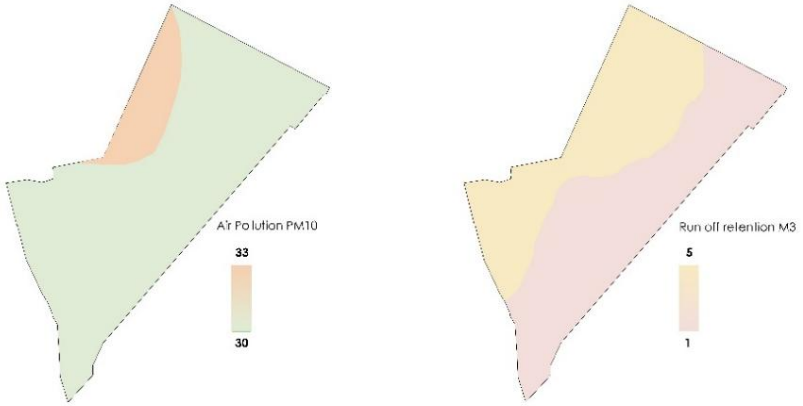

Sümerbank Factory Design Proposal

The Sümerbank Factory site, located near the Meles River, is designed as part of the river's green corridor with a focus on expanding green areas. The aim is to develop a network of contiguous green spaces to enhance flood resilience, improve water absorption, and establish ecological continuity between natural and urban environments.

Flood Risk and Educational Facilities

As earlier analyses revealed (Figure 22), five schools on-site face flood risks. Their position will be shifted into a safer zone, and in place of various scattered schools, an integrated educational complex shall be developed.

Wetlands for Flood Mitigation and Biodiversity

Wetlands are proposed to be established in flood-prone areas for the temporary storage of excess water and for mitigating the effects of water. The location of the site near the Meles River supports the wetlands in increasing biodiversity and habitat functions.

Reconnecting the City to the River

Viewpoints and recreational areas are integrated along the riverbank to reconnect the public with the Meles River, thereby enabling new social and environmental interactions.

Heritage Conservation and Adaptive Reuse

To conserve the heritage of the area, the important buildings are retained and converted for further use. While 80% of the Printing Processing Factory was demolished, the remaining structures will become an open museum. The Yam Weaving Building will serve as social facilities, and the original factory entrances are retained to preserve spatial identity.

Integrated Mobility and Green Transportation

A bicycle route along the Meles River passes through the area, promoting access and sustainable transport. Cycling infrastructure supports urban mobility and environmentally friendly commuting.

As shown in Figure 23, the design process followed a series of ecological assessments, conceptual zoning strategies, and interventions informed by a variety of stakeholders to achieve a climate-responsive transformation of this industrial site.

Figure 23. *Sümerbank Factory Site Design Process*

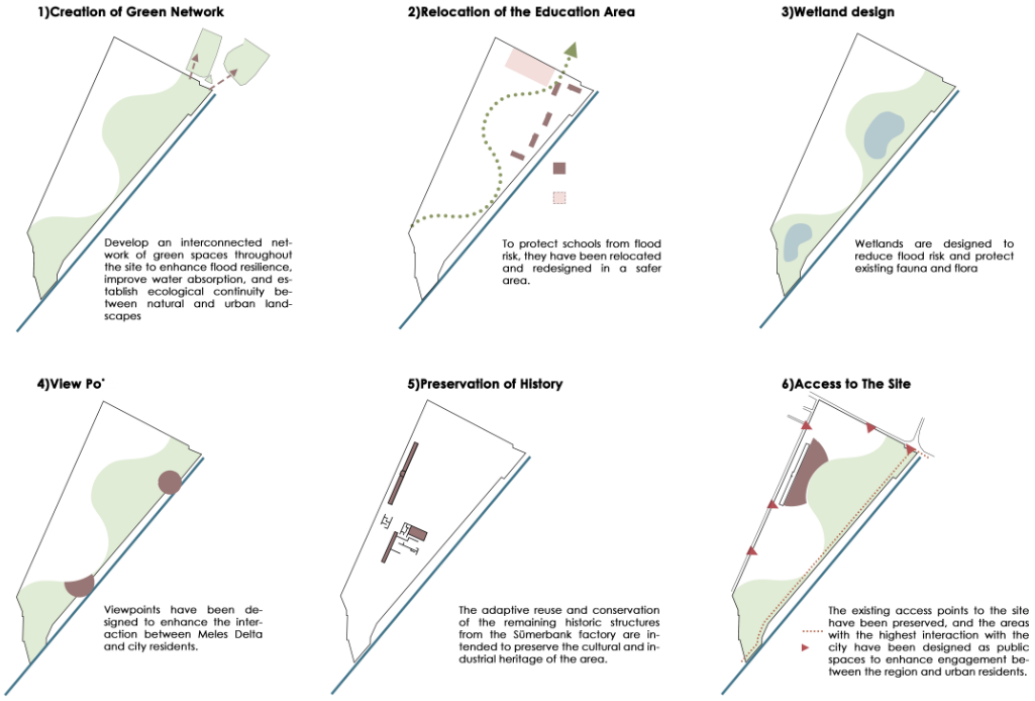

Circulation Strategy

The circulation system constructed for the Sümerbank Factory site provides a full-fledged experience by merging architecture and nature. Prioritizing pedestrian access, walkers enjoy views over the wetlands, heritage buildings, or public spaces, and their path elevates their experience and environmental consciousness. Protected bird zones are distinguished by observation points to the extent that visitors can observe wildlife without detracting too much from the ecosystems. The network also interlinks cultural and ecological facets, such as museums, social hubs, and bioswales, to unite sustainable environments alongside constructed ones. The bicycle path ushers connectivity to the larger Meles River green corridor, while sunlit pathways and their adjoining public facilities promote entrance, sustainability, and continuity. Figure 24 demonstrates the comprehensive master plan that serves this integrated vision and illustrates how blue-green infrastructure, adaptive reuse strategies and pedestrian connectivity combine to create a climate-resilient cultural landscape.

Figure 24. *Master Plan*

Ecological Restoration

To support the wider initiative for urban regeneration of the site, Sümerbank will also employ ecological restoration to reverse the previous and significant forms of environmental damage resulting from industrial activity in relation to soils, vegetation, and habitats. The principle of restoration here incorporates notions of biodiversity, habitat diversity and complexity, and ecological resilience using nature-based and adaptable landscape design approaches. Approaches will include:

- Protection/translocation of mature trees
- Seed banking for grassland recovery
- Faunal-assisted seed dispersal
- Shaded microclimates with targeted planting
- Accelerated succession through diverse planting
- Native species use, in-situ tree conservation, and reuse of removed vegetation (e.g., logs for insects/seating)

These strategies support a self-sustaining, biodiverse, and climate-resilient ecosystem.

Vegetation is selected for mitigating air/noise pollution, reducing UHI, and supporting biodiversity. Species are urban-adapted and ecologically functional (Figure 25).

Tree species include: Celtis australis, Acer campestre, Fraxinus excelsior, Tilia platyphyllos, Platanus × acer folia, Quercus ilex – chosen for drought resistance, pollution absorption, and shade.

Shrub species include: Lavandula, Rosmarinus, Pittosporum, Phillyrea, Juniperus, Sambucus – selected for air purification, adaptability, and habitat support.

Planting locations are based on vulnerability, including road proximity, flood-prone zones, and solar exposure.

Figure 25. *Climate Resilience Intervention Map*

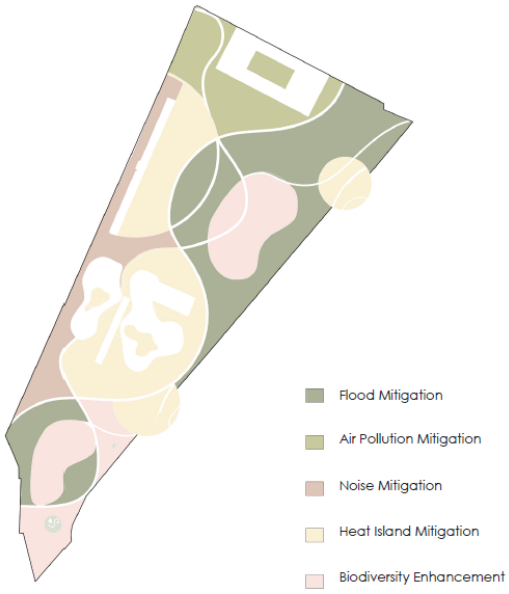

Zoning for Ecological Processes and Education Three ecological zones support functioning with minimal intervention:

- Protected Zones –limit human access for natural regeneration
- Buffer Zones – shield core areas and support edge species
- Observation Areas – allow public learning without disturbing ecosystems.

This structure ensures a balance between preservation, education, and recreation.

Enhancing Urban Biodiversity and Habitat Suitability Bird habitat creation is prioritized. Tilia platyphyllos and Fraxinus excelsior offer shelter and food for birds and pollinators. Juniperus and Nerium oleander provide additional food sources and cover. Wetlands provide fresh water and nesting grounds (Figure 26). These create year-round microhabitats for ecosystem continuity.

Figure 26. *Biodiversity Enhancement Strategy*

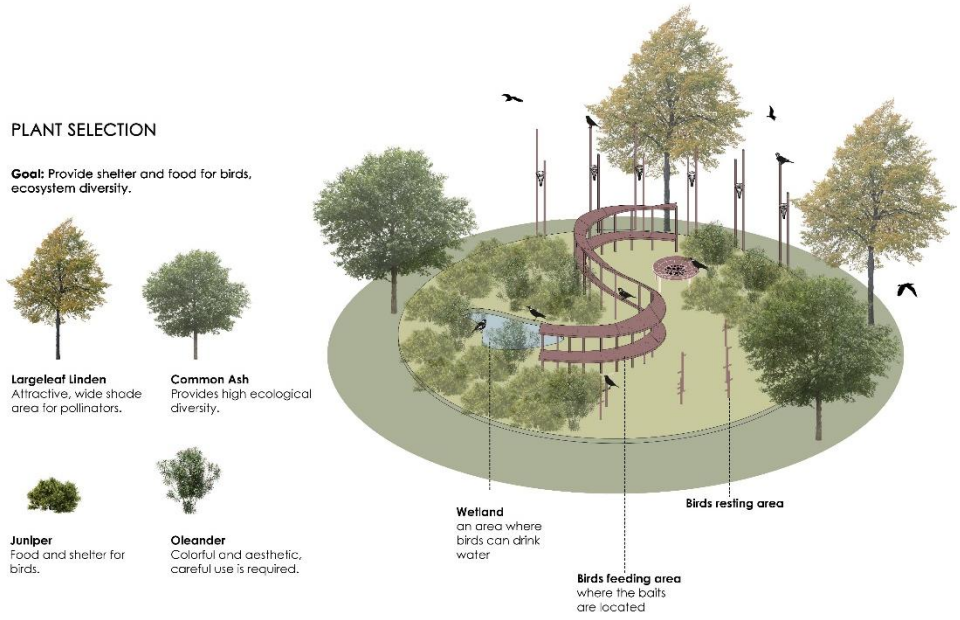

Mitigating Urban Heat Island Effect

The proposed biodiversity strategy includes key zones for habitat, pollinator plantings, and the reinstatement of native species. With summer temperatures exceeding 40°C in İzmir, key strategies will include planting shade trees and trees that transpire large amounts of water i.e. Platanus × acerifolia, Tilia platyphyllos and Fraxinus excelsior. Cooling at ground level will be provided by reflective species i.e., Pittosporum tobira and Phillyrea latifolia to ensure climatic comfort and resilience.

Air and Noise Pollution Mitigation Strategies

Pollution levels along the busy 1525 Street are very high, and intervention is desperately needed. For example, tree species as Platanus × acer folia, Celtis australis, and Acer campestre will help capture pollutants.

Noise is reduced with multi-layer vegetation. Carpinus betulus acts as a sound buffer, especially along roads. Acer campestre and Viburnum tinus support year-round acoustic absorption.

This ecological restoration approach transforms Sümerbank into a resilient urban ecosystem. Strategic planning, functional zoning, and nature-based mitigation enhance biodiversity, reduce environmental stress, and build a climate-adaptive landscape.

Water Management Strategy

The Sümerbank site faced growing challenges associated with flooding given its proximity to the Meles River; consequently, it needed a water management plan that considered Nature-Based Solutions (NBS) to address hydrological vulnerabilities, restore ecological function, and enable better quality public space with nature-based elements. NBS interventions include rain gardens, bioreactors, wetlands, riparian

buffers, rainwater harvesting, and greywater reuse systems. Figure 27 shows these interventions across the site and with the potential for green infrastructure capturing stormwater, reducing flooding, and improving ecosystem connections. Rain gardens, are vegetated basins that temporarily intercept shallow stormwater, filter surface contaminants, improve infiltration, and increase biodiversity. Constructed wetlands, located in low-lying zones, store floodwater and purify it through phytoremediation. Species like *Phragmites australis*, *Typha latifolia*, and *Juncus effusus* stabilize soils and support aquatic life.

Figure 27. *Water Management Strategy*

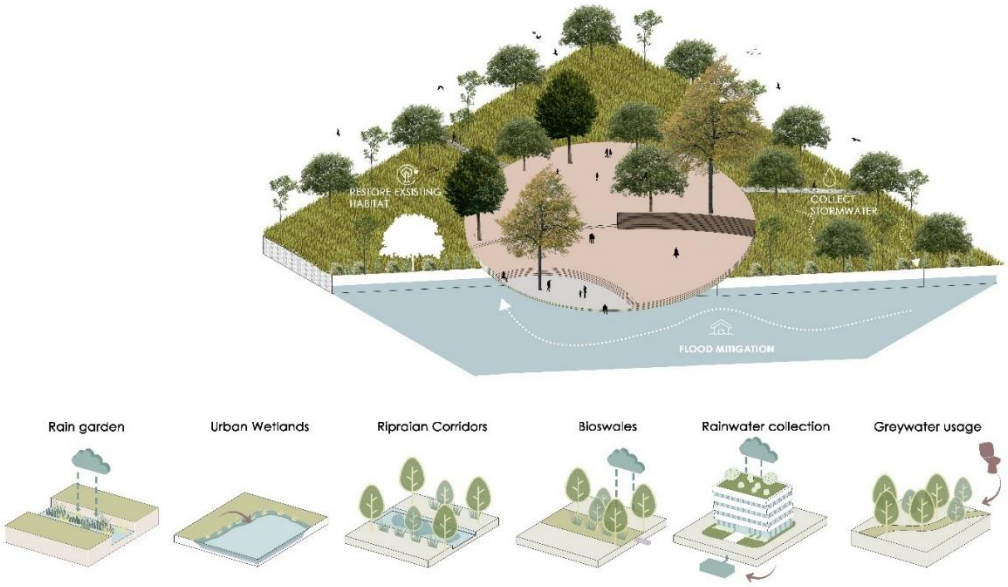

Bioswales, vegetated linear channels, guide runoff through open spaces along a corridor, allowing sediments and pollutants to filter through gravel base layers and bio-retention layers. As depicted in Figure 28, they are located to filter runoff, facilitate groundwater recharge, and create microhabitats as part of the activities on the Sümerbank green corridor. Plantings include *Acer campestre* and *Fraxinus excelsior* for shade and evapotranspiration, while *Rosmarinus*, *Juniperus*, and *Lavandula* spp. Contribute to both purification processes and the visual character of the green infrastructure system.

The rainwater harvesting system on the educational campus collects runoff via green roofs and permeable surfaces, channeling it to underground tanks for irrigation and non-potable reuse. The surface doubles as a public plaza with sculpted topography for recreation and cultural events. As illustrated in Figure 29, the multifunctional design integrates water-sensitive urban design (WSUD) with landscape architecture, where form, slope, and paving patterns facilitate runoff collection while also creating vibrant, community-oriented public spaces.

Greywater reuse systems are proposed, particularly in green zones, to maximize water efficiency. Riparian buffers along the Meles River are restored with native vegetation to stabilize banks, reduce erosion, and connect the river with interior green spaces.

Together, these water-sensitive urban strategies make the Sümerbank site climate-adaptive, ecologically functional, and socially vibrant, demonstrating how post-industrial areas can evolve into resilient ecological infrastructure for future cities.

Figure 28. *Bioswale Design*

Figure 29. *Rainwater Collection*

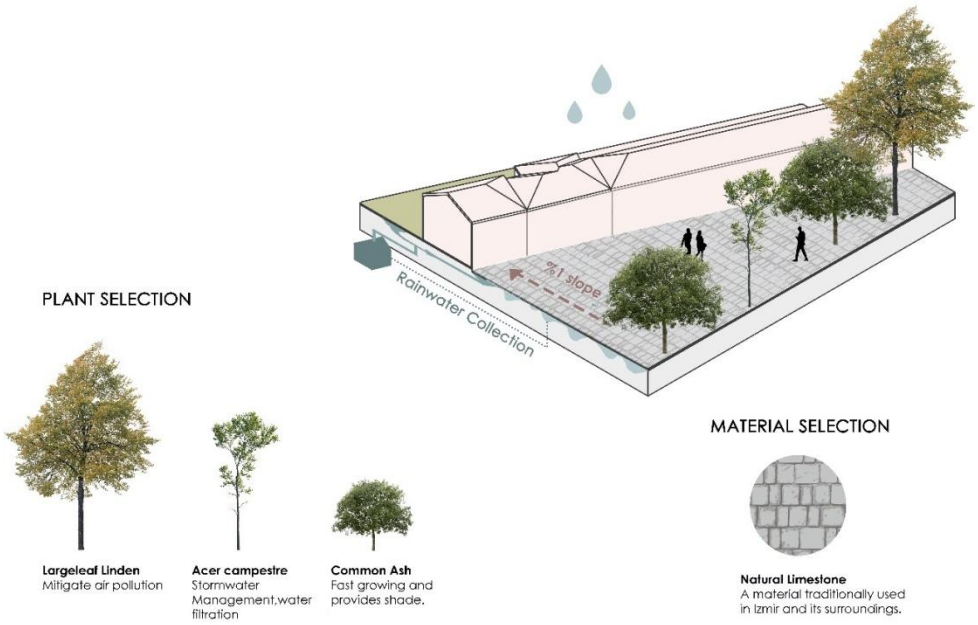

Adaptive Reuse and Environmental Performance of Urban Greening

The Sümerbank regeneration project is based on adaptive reuse and circular design principles. The elements were designed for reuse, from the abandoned building structures and relocated schools, all aimed at reducing construction waste and embodied carbon. Crushed aggregates from demolished buildings were incorporated

into the museum plaza elements, while providing a means for stormwater to permeate and contribute to management. Corten steel was applied to museum walls for its low maintenance and visual continuity between past and present. Permeable paving supports both water management and climate resilience.

Environmental Impact Assessment of Urban Tree Planting

To evaluate these approaches, a performance assessment of urban greening and tree planting was undertaken. The design added 342 new native trees and 64 784 m² of new vegetated area, preservation and increase of natural biota and overall connectivity and exchange between environments, ecosystem functions and ecology were improved and ecological connectivity level was improved due to these new reintroduced and preserved biodiversity along with preservation and increase of urban vegetation. In addition to the trees, 21 faunal species and 15 native plant species were reintroduced.

The environmental benefits of the project were measured and modelled with respect to: carbon sequestration, CO_2 assimilation and pollution removal. The trees planted are expected to sequester 1,036,678 kg CO_2 by the natural life of the trees, equating to 83,647 kg annually. Our urban greening and tree planting will also remove: ozone (O_3) and nitrogen dioxide (NO_2), Sulphur dioxide (SO_2) and particle pollution (PM_{10}). Species-specific reductions were outlined as:
Celtis australis: 13.1 kg O_3 26.2 kg NO_2 and had the ability to intercept and retain 39.3 kg SO_2 annually. Quercus ilex: was shown to retain 5.2 kg PM_{10}. In terms of equivalent real-world amounts:

CO_2 = 237 short trips from Izmir –Milan
PM_{10} = 3.2 million km worth of car trips
SO_2 = amount from burning 3.8 tons of coal
NO_2 = amount from 84,188 liters of diesel
O_3 = amount filtered from 2,287 mature trees

These results provided tangible, measurable results for air quality, climate resilience, and environmental justice measures. The inclusion of native trees and plant species, as well as recycled materials and design thinking, transformed the Sümerbank design from an industrial area considered to be in "a state of anthropogenic vulnerability", into an estimated sustainable, resilient, low-carbon, ecologically and environmentally enriched urban ecosystem.

Discussion

This study highlights the critical role that Nature-Based Solutions (NbS) play in enhancing climate resilience, particularly in dense urban coastal cities like Izmir. Through the integration of NbS into ecological and socio-spatial contexts, the study illustrates how urban planning and ecosystem recovery can come together through adaptive, multifunctional methods.

The interventions proposed for Alsancak and Sümerbank are not only spatial compositions but also ecological infrastructures. The study discovers that fragmented

green spaces, historic forms, and vacant industrial lands can be redesigned as regenerative landscapes with measurable ecosystem values.

One of the notable observations is the potential for NbS stacking, such as combining rain gardens and open spaces, or leveraging adaptive reuse materials that allow both stormwater infiltration and thermal comfort. The Sümerbank Factory is a good example of how climate mitigation, historic preservation, and community use can all be integrated into a single location.

Quantifiable outcomes, such as sequestering 237 flights' worth of CO_2 or removing 3.8 tons of coal worth of SO_2, take intangible sustainability objectives and make them tangible results critical when making the case for NbS over traditional grey infrastructure.

There are, though, challenges. Success with NbS depends on political will, routine maintenance, and inclusive governance. Involvement by the government and multi-stakeholder cooperation are essential to preventing underuse or degradation in the long term.

Finally, tools such as GIS, InVEST, and Google Earth facilitated the development of a solid approach towards prioritization, ecosystem service modeling, and adjusting the design to site-specific conditions. This approach can be replicated in other Mediterranean cities along the coastline that face similar challenges.

In total, the research offers both a blueprint and proof for NbS as part of a larger urban resilience agenda. Situating climate action within landscape architecture and environmental simulation, it represents a replicable model for data-driven, community-based, and ecologically regenerative city change.

Conclusion

This article discusses the intensifying impacts of climate change on urban coastal cities, with a special focus on Izmir, Türkiye. As a Mediterranean city already experiencing heatwaves, droughts, floods, and sea-level rise, Izmir is exposed to intensifying environmental pressures. Qualitative assessment of exposure to the city indicates the need for adaptive measures to improve resilience.

Centered to this approach are Nature-Based Solutions (NbS), offering a means to address climate risk while generating ecosystem services like flood protection, air filtration, and carbon sequestration. The research recommends integrating NbS from the regional scale to site-level interventions with an emphasis on their role in contributing to systemic resilience.

Barcelona and Izmir case studies show NbS's capability in addressing both socio-economic and environmental issues in coastal regions. The green planning and infrastructure gaps in Konak were discovered by mapping ecosystem services, including low vegetation cover, poor air quality, and inadequate flood control, placing importance on ecologically based urban design.

The proposed NbS intervention for Konak, including its pilot site, Alsancak, consists of increasing tree cover, restoring river-edge ecosystems, creating permanent green and blue corridors, and adaptively reusing post-industrial sites, such as the Sümerbank Factory.

In addition to their environmental and physical benefits, the success of NbS also depends on governance, public participation, and facilitatory policy. Their participatory approach, which includes citizens, planners, and authorities, is crucial to long-term success.

Lastly, whereas climatic change is an ongoing challenge, in this case, it is clear that NbS offer a strong rationale for the marriage of climatic adaptation, urban regeneration, and nature protection. Using the natural processes to synergize with development, NbS can allow for the creation of healthier and more resilient cities if augmented by sustained policy and community support.

References

Admasu S, Yeshitela K, Argaw M, Bloor M (2023) Assessing habitat quality using the InVEST model in the Dire and Legedadi watersheds, central highland of Ethiopia: Implications for watershed management. *Sustainable Environment* 9(1).

Arıtan Ö (2004) *Kapitalist-sosyalist modernleşme modellerinin erken Cumhuriyet dönemi mimarlığının biçimlenişine etkileri – Sümerbank kit yerleşkeleri üzerinden yeni bir anlamlandırma*. (The effects of capitalist-socialist modernization models on the formation of early Republican architecture – A new interpretation through Sümerbank kit campuses). Doktora tezi. Dokuz Eylül Üniversitesi.

Babbar D, Areendran G, Sahana M, Sarma K, Raj K, Sivadas A (2020, August 5) Assessment and prediction of carbon sequestration using Markov chain and InVEST model in Sariska Tiger Reserve, India. *Journal of Cleaner Production* 278(Jan): 123333.

Balık Sanlı F, Kurucu Y, Esetlili MT (2009) Determining land use changes by radar-optic fused images and monitoring its environmental impacts in the Edremit region of western Turkey. *Environmental Monitoring and Assessment* 151(1–4): 45–58.

Berberoğlu S, Çilek A, Ünlükaplan Y (2019, Mart) Dirençli kentler için bir çerçeve: Yeşil odaklı uyarlama. (A framework for resilient cities: Green-focused adaptation). *Türkiye Sağlıklı Kentler Birliği*. https://www.skb.gov.tr/wp-content/uploads/2019/07/Izmir-Buyuksehir-Belediyesi-Yesil-Odakli-Uyarlama-Kilavuzu.pdf

Chen Y, Qiao F, Jiang L (2016) Effects of land use pattern change on regional-scale habitat quality based on the InVEST model: A case study in Beijing. *Acta Scientiarum Naturalium Universitatis Pekinensis* 52: 553–562.

Coutts AM, Tapper NJ, Beringer J, Loughnan M, Demuzere M (2013) Watering our cities: The capacity for water-sensitive urban design to support urban cooling and improve human thermal comfort in the Australian context. *Progress in Physical Geography: Earth and Environment* 37(1): 2–28.

Eggermont H, Balian E, Azevedo JMN, Beumer V, Brodin T, Claudet J, et al. (2015). Nature-based solutions: New influence for environmental management and research in Europe. *Gaia* 24(4): 243–248.

Epelde L, Mendizabal M, Gutiérrez L, Artetxe A, Garbisu C, Feliu E (2021) Quantification of the environmental effectiveness of nature-based solutions for increasing the resilience of cities under climate change. *Urban Forestry & Urban Greening* 67(Jan): 127433.

Gerçek İzmir (2018, March19) İzmir'in ve Cumhuriyet tarihinin simge fabrikası viraneye döndü (The iconic factory of Izmir and the history of the Republic has been reduced to rubble). [Fotoğraf]. *Gerçek İzmir*. https://www.gercekizmir.com/haber/Izmir-in-ve-Cumhuriyet-tarihinin-simge-fabrikasi-viraneye-dondu/42242.

Hu X, Cao J, Qian Y, Zhou W, Zheng Z (2024) Extreme heat events in mainland China from 1981 to 2015: Spatial patterns, temporal trends, and impacts of urbanization. *Sustainable Cities and Society* 100: Article 104999.

ICLEI (2017) *IUCN European Regional Office in Brussels*. ICLEI.

ICOMOS (2019) *The future of our pasts: Engaging cultural heritage in climate action*. International Council on Monuments and Sites. https://www.icomos.org/en/what-we-do/focus/climate-action.

IPCC (2022) *Climate change 2022: Impacts, adaptation, and vulnerability. Contribution of Working Group II to the Sixth Assessment Report of the Intergovernmental Panel on Climate Change*. Edited by H Pörtner, D Roberts, M Tignor, et al. Cambridge University Press.

İzmir Büyükşehir Belediyesi (2017) *İzmir Yeşil Altyapı Stratejisi*. (Izmir Green Infrastructure Strategy). https://izmirdoga.izmir.bel.tr/CKYuklenen/İzmirYeşilAltYapıStratejisi.pdf.

İzmir Büyükşehir Belediyesi (2020) *İzmir Sürdürülebilir Enerji ve İklim Eylem Planı*. (Izmir Sustainable Energy and Climate Action Plan). http://skpo.izmir.bel.tr/content.aspx?MID=112.

Kambur B (2025) *How Cities Adapt to Climate Change? The Example of Izmir, Türkiye.* Master's Thesis. Politecnico di Milano, MSc in Sustainable Architecture and Landscape Design.

Köksal TG, Ahunbay Z (2006) İstanbul'daki endüstri mirası için koruma ve yeniden kullanım önerileri. *TÜ Dergisi* 5(2): 125–136.

Lau TK, Lin TP (2024) Investigating the relationship between air temperature and the intensity of urban development using on-site measurements, satellite imagery, and machine learning. *Sustainable Cities and Society* 100: Article 104982.

Manso M, Teotónio I, Silva CM, Cruz CO (2021) Green roof and green wall benefits and costs: A review of the quantitative evidence. *Renewable and Sustainable Energy Reviews* 135: 110111.

McPhearson T, Frantzeskaki N, Kabisch N, Seto KC (2023) Foreword II. In *Nature-Based Solutions for Cities*, 13. Edward Elgar Publishing.

McPhearson T, Kabisch N, Frantzeskaki N (2023, August 15) *Nature-based solutions for cities*. Elgar Online. https://www.elgaronline.com/edcollbook-oa/book/9781800376762/9781800376762.xml.

MedECC (2020) *Climate and environmental change in the Mediterranean Basin – Current situation and risks for the future*. Edited by W Cramer, J Guiot, K Marini.. Union for the Mediterranean, Plan Bleu, UNEP/MAP.

Natural Capital Project (n.d.) *Carbon storage and sequestration model*. Stanford University. https://naturalcapitalproject.stanford.edu/invest/carbon.

Oke TR (1982) The energetic basis of the urban heat island. *Quarterly Journal of the Royal Meteorological Society* 108: 1–24.

Ossola A, Lin BB (2021) *Making nature-based solutions climate-ready for a 50°C world*. ResearchGate.

Oukawa GY, Krecl P, Targino AC, Batista LFA (2024) Advantages of modeling the urban heat island intensity: A tool for implementing nature-based solutions. *Sustainable Cities and Society* 102: Article 105204.

Palta MM, Grimm NB, Groffman PM (2017) "Accidental" urban wetlands: Ecosystem functions in unexpected places. *Ecology and the Environment* 15(5): 248–256.

Regional Climate Change Adaptation Framework for the Mediterranean Marine and Coastal Areas (2017) *UN Environment/MAP*. Athens, Greece.

Salata S, Velibeyoğlu K, Baba A, Saygın N, Couch VT, Uzelli T (2022) Adapting cities to pluvial flooding: The case of İzmir (Turkey). *Sustainability* 14(24): 16418.

Sharp R, Douglass J, Wolny S, Arkema K, Bernhardt J, Bierbower W, et al. (2020) *InVEST User's Guide*. Natural Capital Project: Stanford University, University of Minnesota, The Nature Conservancy, and World Wildlife Fund.

Toprak Z (1988) *Sümerbank*. İstanbul: Creative Yayıncılık.

Türker BH, Gül A (2022) Kentsel açık ve yeşil alanlarının niceliksel analizi ve irdelenmesi: Uşak kent merkezi örneği. (Quantitative analysis and examination of urban open and green spaces: Uşak city center example). *Kent Akademisi Dergisi* 15(4): 2088–2109.

Türkmen Ü (2019) Temiz hava solumak tüm vatandaşların temel hakkıdır. (Breathing clean air is the fundamental right of all citizens). *TMMOB Kimya Mühendisleri Odası*. https://www.kmo.org.tr/genel/bizden_detay.php?kod=4557&tipi=3&sube=6.

Uğrasal S (2011) *Tarihi yapıların yeniden işlevlendirilmesi: İzmir Sümerbank Basma Sanayi Yerleşkesi örneği*. (Re-functioning of historical buildings: The example of the Izmir Sümerbank Printing Industrial Campus). Yüksek lisans tezi. Dokuz Eylül Üniversitesi.

Athens Journal of Sciences - Volume 12, Issue 4, December 2025 – Pages 285-298

Identifying Strengths and Weaknesses in Mathematics Learning: An Analysis of Exam Preparation Course Outcomes

*By Annika Paltsepp**

In Estonia, upper secondary school students are required to take national examinations in Estonian, mathematics, and a foreign language. To support exam readiness, a free 20-week mathematics preparatory course was offered to all interested students. The course concluded with a final test covering key curriculum topics. This study analyzes the test results to identify strengths and weaknesses in students' mathematical knowledge. Quantitative analysis was used to assess accuracy across topic areas, and qualitative examples illustrate frequent and critical errors. Topics such as algebraic manipulation and basic functions were generally well understood, whereas geometry proofs and word problems presented greater challenges. Common errors included misinterpreting problem statements, calculation mistakes, and incomplete reasoning in open-ended tasks. Results are compared with patterns from previous years' national exam statistics to evaluate the course's alignment with exam expectations. While individual exam data are confidential, aggregate comparisons help highlight consistent learning challenges. The study provides practical insights for improving future preparatory programs. It also supports broader educational goals promoted by the Estonian Engineering Academy (INSA), which funded the course and works to increase university applicants and reduce dropout rates by strengthening foundational skills in STEM education.

Keywords: *mathematics education, national exams, student performance analysis, error patterns, exam preparation*

Introduction

The mathematics national examination is one of the three compulsory final exams that upper secondary school students in Estonia must take. The aim of these exams is to assess students' knowledge and skills in accordance with the national curriculum and to provide feedback to students, schools, policymakers, and the general public on the effectiveness of teaching and learning. Over the years, mathematics exam results have shown considerable variation, and certain topic areas have consistently posed greater challenges for students.

To support students in preparing for the exam, a free 20-week preparatory course was organized and made available to all interested participants. The course aimed to offer systematic revision of key topics from the national curriculum and to help students better understand complex problems. At the end of the course, students completed a final test that included a variety of question types and closely mirrored the structure of the national examination.

*Lecturer, Estonian University of Life Sciences, Estonia.

The purpose of this study is to analyze the results of the final test to identify which mathematical topics were better mastered and which proved more challenging for students. Additionally, the study examines common errors and their possible causes. The results are compared to trends from previous years' national examination data, which are published annually in official overviews by Estonian education authorities (Ministry of Education and Research 2022, 2023, 2024). These yearly reports provide aggregated feedback on exam performance and common problem areas. This study draws on those reports to evaluate the alignment between course outcomes and broader national trends. While individual exam data are confidential and cannot be directly linked to course participants, aggregate patterns allow meaningful comparison.

This study was guided by the following research questions:

1. In which areas of mathematics did participants demonstrate the greatest proficiency, and which topics proved to be the most difficult?
2. What recurring error patterns were observed in participants' responses, and what do these suggest about underlying conceptual difficulties?
3. How do the results of the final test align with or differ from previous national exam trends, and what can be concluded from this comparison to improve the structure of future preparatory courses?

Previous research has explored various factors influencing mathematics exam performance. Scholars at the University of Tartu (Aaviste and Täht 2022) have examined how students' self-perceptions and attitudes relate to outcomes, while researchers at Tallinn University of Technology (TalTech 2025) have studied how mathematics exam results predict later success or dropout in higher education. Similar findings were reported by Kenosi et al. (2024), who found a statistically significant positive correlation between students' attitudes toward mathematics and their performance, based on a study among Form Three students in Botswana. This study complements those efforts by focusing on learning outcomes in the context of a preparatory course, helping to identify the most problematic content areas and typical mistakes.

Several international studies have helped to contextualize the present findings. Greefrath et al. (2017) examined preparatory courses in engineering and computer science education in Germany and concluded that structured participation, both in-person and online, was linked to significantly better academic performance. Fatawu et al. (2023) focused on secondary school students and used Newman's Error Analysis to identify frequent mistakes in solving word problems. Their findings pointed to difficulties in understanding problem statements and translating them into solvable equations, which closely match the patterns observed in this study. Most notably, Lin et al. (2024) conducted a systematic review of mathematical error patterns among students with learning difficulties. They categorized common mistakes into conceptual, procedural, and interpretive types, providing a valuable framework that aligns well with the types of errors identified here. Together, these studies show that the challenges observed in this preparatory course reflect wider issues found across different educational contexts.

Despite strong interest in national mathematics exam preparation, dropout rates from voluntary courses remain high, and it is unclear which content areas cause the most difficulty or what types of mistakes students most often make. There is also a lack of data on how such preparatory efforts align with national exam trends. This study addresses these gaps by analyzing student performance in a structured preparatory course and identifying both strengths and recurring challenges. The findings aim to inform future course design and contribute to broader discussions on how to improve mathematics readiness among upper secondary students.

In addition to its educational aims, the course also served broader strategic objectives aligned with national STEM priorities. It was supported by the Estonian Engineering Academy (INSA), a national cooperation initiative involving the government, universities, industry, and professional associations. INSA aims to enhance the quality of engineering education, ensure an adequate supply of qualified professionals, and raise interest in STEM fields. Its key goals include increasing the number of university applicants, improving the relevance of higher education to labor market needs, and reducing dropout rates. By providing evidence-based insights into how preparatory programs can strengthen foundational skills and improve exam readiness, this study contributes directly to those goals.

Materials and Methods

In November 2024, a free online preparatory course for the Estonian national mathematics examination was launched at the Estonian University of Life Sciences, supported by the Estonian Engineering Academy (INSA). The course was open to all individuals interested in strengthening their upper secondary school mathematics skills in preparation for the national exam. A total of 470 participants from across Estonia registered for the 20-week course, which was delivered once a week in an online format.

While registration numbers were high, the subsequent analysis in this study is based solely on the 78 participants (16.6%) who chose to complete the final test at the end of the course.

The course curriculum was designed to systematically cover all major topic areas included in the national upper secondary mathematics syllabus. These topics were: Expressions and number sets; Equations and systems of equations; Inequalities and Trigonometry I; Trigonometry II; Vectors in the plane and linear equations of curves; Probability and statistics; Functions and numerical sequences; Exponential and logarithmic functions; Trigonometric functions, limits and derivatives; Applications of derivatives; Integration and planar geometry; Lines and planes in space; Solid geometry; Applications of mathematics in real-world processes.

The final written test resembled the structure and content of the national examination and was completed on paper in person at the university. Tasks were selected to ensure coverage of the full curriculum. Of the 78 test-takers, 27 were male and 51 female; 66 were current upper secondary school students (abiturients), and 12 were graduates from previous years. The average score achieved was 37.3 out of a maximum of 100, with scores recorded in whole numbers. All test submissions were anonymized prior to analysis.

Descriptive statistics were used to assess performance across different topic areas. In addition, qualitative analysis was conducted to identify and categorize common errors, misconceptions, and incomplete reasoning. The results were compared with national trends based on summary reports of previous years' mathematics examinations published by the Estonian Education and Youth Board.

As participation in both the course and the final test was entirely voluntary, the results may reflect a self-selected group of more motivated or confident learners. Therefore, the findings may not be fully generalizable to the broader population of upper secondary students.

Results

A total of 470 individuals registered for the preparatory mathematics course, of whom 189 (40.2%) were male and 281 (59.8%) female. Among all registrants, 278 (59.2%) were final-year upper secondary school students (abiturients), while 114 (24.3%) were graduates from previous years. Demographic information was unavailable for 78 individuals, either due to incomplete registration data or because they did not provide their background details.

Table 1 presents the demographic composition of all 470 registered course participants.

Table 1. *Participant Distribution by Category and Gender*

	Male	Female	Total	Share of total (%)	Male (%)	Female (%)
Graduates	139	217	356	75.74%	39.04%	69.96%
Other	50	64	114	24.26%	43.86%	56.14%
Total	189	281	470	100.00%		

Of all registered participants, 78 individuals (16.6%) completed the final test. Among these test-takers, 27 were male (34.6%) and 51 were female (65.4%). To better understand performance variation, the results were analyzed by gender, year of birth, and student status. The overall average score for the 78 test-takers was 37.3 out of a maximum of 100. These comparisons, including mean values, standard deviations, score ranges, and confidence intervals, are summarized in Table 2.

Gender-based performance showed relatively similar mean values: males achieved an average score of 38.0 (SD = 24.1), while females had a slightly lower mean of 36.9 (SD = 23.6). The score range was wide in both groups, with minimum scores of 2 and maximums of 85 (male) and 90 (female), respectively.

Age-based analysis revealed that participants born between 2000 and 2010 (N = 70) performed better on average (M = 37.9) than older age groups. By contrast, those born between 1980 and 1989 (N = 4) had the lowest mean score (M = 19.0), but this result should be interpreted with caution due to the very small sample size and wide confidence interval.

Student status appeared to be a stronger differentiating factor. Current abiturients (N = 66) had a significantly higher average score (M = 39.3) than graduates

from previous years (N = 12, M = 26.3). This suggests that active school engagement may contribute positively to exam readiness.

Table 2. *Final Test Performance by Gender, Birth Year, and Student Status*

		N	Lower CI	Mean Score	Upper CI	Std. Dev.	Min	Median	Max
Gender	Male	27	28,50	38,04	47,58	24,11	2	35	85
	Female	51	30,25	36,88	43,51	23,58	2	31	90
Birth year	1980-1990	4	-10,20	19,00	48,20	18,35	2	14,5	45
	1990-2000	4	17,32	45,00	72,68	17,40	28	42	68
	2000-2010	70	32,22	37,91	43,61	23,90	2	31	90
Graduates	Graduates	66	33,41	39,27	45,13	23,84	4	33,5	90
	Others	12	13,75	26,33	38,92	19,81	2	21	68

As illustrated in Figure 1, the largest group of students (17 individuals) achieved only 11–20 points, followed by 13 students in the 21–30 range and 7 in the 0–10 range. In turn, very few students reached the higher intervals: for example, only two participants scored between 51–60 points, and no one achieved above 90. Although some participants did obtain moderately higher results (up to 85–90 points), the overall distribution shows that most students remained in the lower and middle ranges. This outcome highlights not only the considerable difficulty of the test tasks but also suggests that stronger preparation would be needed to help a larger proportion of learners move into the higher performance bands.

Figure 1. *Distribution of Participants by Score Ranges in the Final Test*

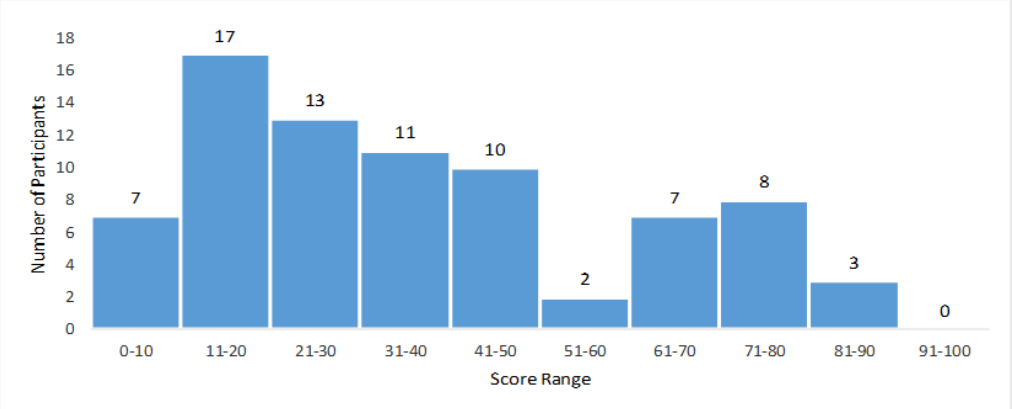

Table 3 presents summary statistics for each task in the final test, including the maximum score, average score, standard deviation, task content, and the percentage of students who did not attempt each task. The results reveal considerable variation in both task difficulty and student engagement, reflecting clear differences in how well participants mastered various mathematical topics. For instance, Task 1, which covered irrational and exponential expressions, had one of the strongest outcomes, with a relatively high average score of 5.8 out of 10 and a very low non-attempt rate of only 2.6%. This indicates that students felt more confident in basic algebraic manipulations compared with other areas.

In contrast, Tasks 8 and 9, involving planimetry, stereometry, derivative applications, and analytical geometry, were clearly the most difficult. They produced the lowest average scores (1.5 and 3.1, respectively) and the highest non-attempt rates

(53.9% and 50.0%). Task 2, which focused on word problems, percentages, and systems of equations, also showed weak performance (3.4 on average) and a high non-attempt rate of 44.9%. These figures suggest that many students lacked confidence in setting up equations from verbal statements and struggled to translate real-world contexts into solvable mathematical form.

Table 3. *Summary Statistics of Final Test Tasks, Including Average Scores, Standard Deviations, and Task Engagement Rates*

Task No.	Max Possible Points	Average Score (points)	Standard Deviation	Task Content (Course Topics)	Not Attempted
Task 1	10	5,8	3,6	Irrational expressions (I), exponential expressions (VIII)	2.56%
Task 2	10	3,4	4,2	Word problems (II, XIV), percentage (I), system of equations (II)	44.87%
Task 3	10	6,4	4,2	Inequalities (III), word problems (II), planimetry (XI)	16.67%
Task 4	10	4,8	3,5	Probability theory (VI)	6.41%
Task 5	10	4,8	3,7	Function analysis (VII, IX, X)	16.67%
Task 6	10	2,7	3,4	Arithmetic and geometric sequences (VII)	32.05%
Task 7	10	4,8	4,3	Integral (XI)	21.79%
Task 8	15	1,5	3,6	Planimetry (XI), stereometry (XIII, XVI), derivative applications (X)	53.85%
Task 9	15	3,1	4,8	Analytical geometry (V)	50.00%

Overall, the evidence from Table 3 highlights a consistent pattern: geometry-related and application-heavy tasks were among the most challenging for students, both in terms of performance and willingness to attempt them. This finding emphasizes the importance of strengthening instructional support in these content areas in order to improve exam readiness.

Table 4 provides a more detailed view of how students performed on each task, including average scores by gender, the most common mistakes, and the percentage of non-attempts. The results reveal marked contrasts between tasks, with geometry and multi-step problem-solving questions standing out as particularly difficult. Planimetry and analytical geometry, for instance, had some of the highest rates of skipped tasks, suggesting that these topics caused uncertainty or felt too demanding. In several cases, recurring mistakes pointed to deeper issues with understanding concepts or applying procedures correctly.

Task 1, which dealt with irrational and exponential expressions, had a moderate average score of 5.8 out of 10 (58%). Male students performed slightly better (60.7%) than female students (56.5%), and only 2.6% left the task unanswered. The most common mistakes included misusing product identities, struggling to simplify fractional expressions, confusing exponent base conversions, and losing track when moving from simplification to solving. These errors indicate that many students still have difficulties with basic algebraic skills.

Task 2, focusing on setting up and solving systems of equations, turned out to be one of the most difficult in the entire test. The average score was only 3.4 out of 10 (34%), and 44.9% of participants did not attempt it. This suggests that many either lacked confidence or found the task too complex to approach. Typical errors included difficulties in translating word problems into equations, trouble expressing ratio-based relationships, and incomplete solutions. These patterns highlight the need to strengthen skills in problem interpretation and system-solving strategies.

Slightly better performance was observed in Task 3, involving systems of inequalities, where the average score was 6.4 (64%) and 16.7% left it blank.

Nevertheless, frequent issues included unjustified variable selection, misinterpretation of the solution sets, and partial answers that failed to address all components.

Probability (Task 4) produced an average score of 4.8 (48%), and 6.4% of students skipped it. Mistakes often stemmed from confusion between multiplication and addition rules, as well as incorrect use of permutations and combinations, suggesting limited mastery of basic probability concepts.

Function analysis (Task 5) yielded a similar average score of 4.8 (48%), with 16.7% not attempting it. Frequent errors included omitting key steps such as identifying zeros, extrema, and intervals of positivity, as well as incomplete graphs and insufficient explanations. These issues reflect broader challenges in clearly communicating function properties.

Task 6, on arithmetic and geometric sequences, appeared particularly demanding. Students averaged only 2.7 points (27%), and 32.1% left it blank. Errors often included omitting multiplication steps, neglecting geometric sequences, or misapplying formulas, especially for decreasing series, indicating weak procedural fluency in numerical patterns.

Integration (Task 7) produced a moderate average score of 4.8 (48%), with 21.8% non-attempts. Common mistakes involved solving quadratic equations incorrectly when finding intersection points, plotting parabolas inaccurately, omitting parentheses in integrals or antiderivatives, and reversing limits of integration without explanation. These show that students struggled with both the mechanical and conceptual aspects of integration.

Task 8, covering planimetry, stereometry, and derivative applications, was the most difficult overall, with an average of 1.5 (10%) and more than half (53.9%) not attempting it. Errors included neglecting relevant geometric elements (e.g., a semicircle in axial sections) and failing to verify results against problem conditions, pointing to conceptual gaps in spatial reasoning and calculus.

Finally, Task 9, which focused on analytical geometry involving line and circle equations, had an average score of 3.1 (20.7%) and a 50% non-attempt rate. Students often struggled with formulating equations of parallel or perpendicular lines, calculating midpoints correctly, and recognizing the geometric meaning of segment lengths as radii of circles. These difficulties point to gaps in both procedural fluency and spatial understanding.

Table 4. *Task-wise Performance, Gender Differences, Common Errors, and Rates of Non-attempt in the Final Test*

Task no	Max points	Avg Points	Avg %	Gender		Not Attempted (%)	Task content
				Male	Female		
1	**10**	**5,8**	**58**	**60,7**	**56,5**	**2,6**	**Irrational expression, exponential expression.**
	Did not apply product identities correctly Simplifying a fractional expression involving a sum Did not know how to convert the base of an exponent Incorrectly shifted from simplifying an exponential expression to solving an equation						
2	**10**	**3,4**	**34**	**45,6**	**27,3**	**44,9**	**Setting up and solving systems of equations**
	Could not translate the word problem into equations Was unable to write a ratio equation between the unknowns Was unable to solve the system of equations						
3	**10**	**6,4**	**64**	**71,5**	**59,8**	**16,7**	**Formulating and solving a system of inequalities**
	The choice of unknowns was not justified Did not interpret the solution of the inequalities correctly The specific question was not addressed						
4	**10**	**4,8**	**48**	**44,8**	**49,4**	**6,4**	**Probability**
	Did not solve the subtask requiring the multiplication rule Used the addition rule instead of the multiplication rule Applied permutations instead of combinations						
5	**10**	**4,8**	**48**	**45,2**	**49,8**	**16,7**	**Analyzing functions**
	Did not write the conditions for identifying zeros, positivity intervals, and extrema Completely lacked explanations Graph was presented incompletely						
6	**10**	**2,7**	**27**	**34,1**	**23,9**	**32,1**	**Arithmetic and geometric sequences**
	The multiplication resulting in a^2 was omitted in the equation $5a_1 \cdot 11a_1 = 220$ Did not start solving the geometric sequence problem The formula for the sum of a decaying geometric series was not applied						
7	**10**	**4,8**	**48**	**35,9**	**54,5**	**21,8**	**Integral**
	Mistake made in finding the intersection points of the lines (error in solving the quadratic equation) Did not plot the parabola in the correct position Missing parentheses in the integrand and the antiderivative Integration limits were swapped and the resulting negative value was not explained						
8	**15**	**1,5**	**10**	**9,9**	**10,5**	**53,9**	**Planimetry, stereometry, and applications of derivatives**
	In the case of the axial section, the semicircle was not taken into account The result was not verified (the found value does not meet the problem conditions)						
9	**15**	**3,1**	**20,7**	**19**	**21,3**	**50**	**Analytical geometry (line in a plane, equation of a circle)**
	Formulating the equation of a line parallel or perpendicular to a given line Finding the midpoint of a segment Did not understand that the length of segment BC is the radius of the circle						

Tasks 8 and 9, taken together, yielded notably low average scores and were the most challenging items in the test. Positioned at the end of the paper, they required extensive problem-solving, which may have made them particularly vulnerable to time-related constraints. It is therefore plausible that many students did not attempt them because of time limitations rather than a complete lack of understanding. This interpretation is supported by years of teaching experience and by previous national exam analyses, which consistently show that optimization problems are perceived as highly demanding and are among the least favored tasks for students. For instance, in the 2024 national mathematics exam, the average completion rate for an optimization problem was only 4.9%. Similarly, performance on stereometry tasks has remained low across years, a trend once again confirmed by the present test results.

Overall, these findings highlight distinct strengths and weaknesses in students' mathematical abilities, as reflected in their performance across diverse topics aligned with the national curriculum. While algebraic manipulations and inequalities showed relatively higher success rates, substantial difficulties were evident in geometric reasoning, calculus applications, and multi-step problem solving. The considerable proportion of unattempted tasks in complex topics further emphasizes areas in need of targeted instructional support.

This comprehensive error analysis provides valuable insights for educators designing preparatory courses and instructional materials, underscoring the importance of enhanced focus on problem translation, conceptual clarity, and multi-step reasoning in mathematics education and exam preparation.

Summary of Results

The analysis of final test performance in the mathematics preparation course revealed clear differences in student achievement across topic areas. Students generally performed better in algebraic tasks, such as irrational expressions, while more complex topics like systems of equations, planimetry, stereometry, and analytical geometry proved more challenging. Average scores varied noticeably between tasks, with lower results and higher rates of non-attempts particularly common in mathematical analysis and sequence-related problems. Gender differences were minimal and seemed to relate more to task complexity and content than to any underlying ability.

Evaluator feedback highlighted frequent conceptual misunderstandings and procedural errors, especially in multi-step problem solving, optimization, and spatial reasoning. The fact that a large proportion of students left complex problems unanswered suggests not only conceptual gaps but also time management difficulties during test-taking. Student comments reinforced this interpretation, pointing to insufficient time for thorough engagement with challenging problems.

These findings emphasize the need to strengthen instructional strategies that focus on interpreting mathematical problems, applying step-by-step solutions, and developing spatial visualization skills. In particular, geometry, sequences, and calculus topics require greater emphasis in preparatory instruction. The results also confirm that teacher support plays a critical role in shaping students' confidence and attitudes, aligning with earlier studies that link supportive learning environments to improved performance and motivation.

From a curriculum development perspective, better alignment between preparatory course content and national examination formats is essential. This includes not only coverage of key topics but also pacing, familiarity with problem types, and practice with integrated tasks. Incorporating retrieval-based learning strategies and increasing opportunities for formative assessment may further enhance knowledge retention and conceptual understanding.

Overall, the results suggest that well-structured, supportive, and diagnostically informed preparatory programs can help bridge persistent gaps in mathematical proficiency and better equip students to succeed in high-stakes examinations. These insights are also valuable for national education policy efforts aimed at strengthening STEM readiness and reducing dropout rates in higher education.

Discussion

The analysis of the online preparatory mathematics course and its final test results offers important insights into student readiness for the Estonian national upper secondary mathematics examination. The data reveal several key themes related to participant engagement, performance variability, and specific content area challenges. Although 470 individuals initially registered, this study focuses solely on the 78 participants who completed the final test. All results, comparisons, and interpretations refer exclusively to this group of test-takers.

Firstly, the high initial interest in the course, with 470 registrants from across Estonia, reflects a clear demand for accessible preparatory resources. However, the relatively low proportion (16.6%) of participants who completed the final test suggests potential issues with sustained motivation, course difficulty, or external factors limiting full engagement. The predominance of female participants (59.8%) throughout the course and even more so among test-takers (65.4%) aligns with broader educational trends but may also warrant further exploration to understand gender-specific learning preferences and barriers.

Performance analysis showed that active engagement in school (current abiturients) was a strong predictor of better test outcomes, with abiturients scoring significantly higher than previous graduates. This finding underscores the importance of ongoing academic involvement and suggests that preparatory courses might benefit from closer integration with school curricula or additional support for adult learners.

The distribution of scores and task-specific results pointed to considerable variation in difficulty across topics. Algebraic areas, such as irrational expressions, generally yielded higher scores and greater attempt rates, indicating stronger student familiarity and procedural skills, whereas systems of equations remained among the more challenging topics. Conversely, geometry-related tasks (planimetry, stereometry) and advanced topics involving calculus and analytical geometry had notably lower success rates and higher non-attempt frequencies. This pattern is consistent with international research highlighting spatial reasoning and multi-step problem solving as persistent challenges in mathematics education.

Qualitative error analysis further elucidated common conceptual misunderstandings and procedural difficulties, especially in tasks requiring translation of word problems into mathematical models, stepwise reasoning, and geometric visualization. Errors such as confusion between permutation and combination rules, incorrect application of derivatives, and failure to fully articulate function properties point to gaps in both foundational knowledge and application skills. These findings are consistent with international research by Lin et al. (2024), who identified systematic error patterns among students with mathematical difficulties and grouped them into three main categories: conceptual misunderstandings, procedural errors, and misinterpretation of tasks. The same patterns appeared frequently in our results. For example, procedural errors were common in algebra tasks, while misinterpretation often occurred in geometry and optimization problems, and conceptual difficulties were evident when students misused formulas or misunderstood the properties of functions. Lin et al. also emphasized that meaningful error analysis should go beyond checking whether an answer is right or wrong, but instead explore the reasoning behind students' thinking.

This perspective matches the aim of the present study and highlights the importance of teaching strategies that help students understand not only how errors occur but also why they happen.

The similarity of performance between male and female participants suggests that gender is not a major factor influencing exam readiness, though subtle differences in task engagement and error types may exist. Age-related differences were less clear due to small sample sizes in older cohorts but generally showed younger participants performing better, possibly reflecting more recent exposure to the curriculum.

These findings have important implications for designing future preparatory courses and instructional strategies. Emphasis should be placed on reinforcing problem interpretation skills, providing scaffolded multi-step solution approaches, and enhancing spatial reasoning through targeted geometry exercises. Additionally, encouraging continuous engagement and providing differentiated support for diverse learner groups, including adult returnees, could improve overall effectiveness.

In conclusion, while the preparatory course successfully attracted a broad audience and covered the full national curriculum, student performance results indicate substantial room for improvement, particularly in complex, application-oriented topics. Addressing these challenges through refined course design, pedagogical focus on conceptual clarity, and ongoing evaluation will be crucial to better prepare students for the national mathematics examination and foster deeper mathematical competence.

Another noteworthy aspect concerns the role of learning strategies and psychological factors in students' performance. Prior research has shown that curiosity and perseverance (The Australian 2022), as well as active recall through retrieval-based learning (Chan et al. 2020), are positively associated with academic achievement in mathematics. While these aspects were not directly measured in the current study, the high dropout rate and frequent non-attempts on complex problems may indicate challenges in self-regulation, persistence, and strategy use. These are all factors worth addressing in future course design. Incorporating these elements could help students manage cognitive load and build deeper, transferable skills.

Furthermore, the importance of teacher support as a motivating and stabilizing factor was reflected in student feedback and aligns with findings by Ober et al. (2021), who emphasize the impact of perceived support on student engagement and attitude. Future preparatory courses should therefore prioritize clear communication, emotionally supportive learning environments, and access to instructor feedback, especially in online or asynchronous formats. These adjustments may not only improve participation but also foster greater confidence and resilience in approaching difficult mathematical content.

One limitation of the current study is that, although trigonometry was included in the course curriculum, it was not represented among the evaluated test tasks. This omission likely limited the comprehensiveness of the course evaluation and should be addressed in future iterations of the preparatory program. Including trigonometry is essential to ensure full alignment with curriculum requirements and to adequately prepare students for all components of the national exam.

Conclusions

Although 470 individuals registered for the free online preparatory course, this study is based solely on the 78 participants (16.6%) who completed the final test. All reported results, comparisons, and conclusions refer to this group of test-takers. The relatively low completion rate highlights challenges in sustaining motivation and ensuring full participation, even when the initial interest is high.

Most participants who completed the test were current upper secondary school students, and they performed better than previous graduates. This suggests that ongoing academic engagement positively influences exam readiness. In addition, female participants were more numerous both in registration and test-taking, which aligns with broader participation trends but may also warrant further exploration regarding learning preferences and engagement patterns.

The low completion rate raises valid questions about the long-term effectiveness and perceived value of voluntary preparatory courses. Similar concerns were addressed by Greefrath et al. (2017), who found that while preparatory course participation was only modestly linked to later academic success, these courses played a key role in identifying students who might need more support. Their study suggests that preparatory programs do more than just review content. They also help students build learning habits, identify weak areas early, and reduce the risk of falling behind, especially in STEM-related subjects.

With this in mind, future versions of the course could benefit from built-in progress checks, more personalized feedback, and closer ties to school curricula. Preparatory courses should not be seen simply as optional refreshers but as useful tools for early support and guidance.

Students in this study performed best in algebra-related tasks, particularly in working with irrational expressions. By contrast, tasks involving systems of equations, geometry, calculus, and analytical geometry proved more difficult, as seen in lower scores and a higher rate of unattempted questions. Students often struggled with interpreting complex instructions, completing multi-step solutions, and visualizing geometric relationships. These issues point to persistent gaps in both understanding and execution that call for more structured and focused instruction.

Gender did not seem to play a major role in performance, as male and female students scored similarly. While data on older participants was limited, younger students generally performed better. This may reflect their more recent exposure to the curriculum. Looking ahead, preparatory courses should place more emphasis on teaching students how to break down problems, build solutions in steps, and improve spatial reasoning. Chan et al. (2020) found that retrieval-based learning, where students actively recall information instead of passively reviewing it, can significantly strengthen long-term understanding. Adding such strategies may help students better retain and apply knowledge during exams. Motivation and ongoing encouragement also remain essential, especially for those who struggle with confidence or self-regulation.

Feedback from participants largely supported these findings. Many appreciated the clarity and encouraging tone of the instruction, which echoes research by Ober et al. (2021) showing that perceived teacher support improves attitudes and engagement

in mathematics. Several students mentioned that the course helped them organize their knowledge and feel more prepared.

At the same time, some students expressed a wish for more frequent sessions. One hour per week was often not enough to master complex topics. This matches the test data, which showed particular difficulties in stereometry, sequences, and trigonometry. These observations reflect wider international findings: low confidence and emotional stress, especially in difficult math tasks, can reduce performance. A report by *The Australian* (2022) also emphasized that qualities like curiosity and perseverance are closely associated with success in mathematics.

Overall, both the test data and student feedback point to the value of improving the course's structure. Increasing the number of sessions, offering more guidance for difficult content, and maintaining academic and emotional support would help students feel more confident and better prepared. A well-balanced focus on both knowledge and mindset is essential to help students succeed in national exams and develop lasting mathematical competence.

Acknowledgments

The author gratefully acknowledges the support of the Estonian Engineering Academy (INSA), whose funding made possible the development and implementation of the preparatory mathematics course. Special thanks are also extended to all participants who provided valuable feedback, as their reflections offer important insights that will contribute to the continued improvement and refinement of future course iterations.

References

Aaviste G, Täht K (2022) Relationships between mathematics state exam results and students' self-perceptions. Presentation at the *Estonian Mathematics Days 2022*. Available at: https://matemaatika.eu/wp-content/uploads/2022/11/Matemaatika-riigieksami-tulemus te-seosed-oppijate-enesekohaste-hoiakutega.pptx89.pdf.

Chan JCK, Meissner CA, Davis SD (2020) Retrieval potentiates new learning: A theoretical and meta-analytic review: Correction to Chan, Meissner, and Davis (2018). *Psychological Bulletin* 146(12): 1202.

Fatawu IA, Alhassan MN, Owusu-Darko I (2023) Analysis of senior high school students' errors in solving word problems using Newman's Error Analysis (NEA) procedure. *International Journal of Mathematics and Computer Research* 11(8): 3685–3693.

Greefrath G, Koepf W, Neugebauer C (2017) Is there a link between preparatory course attendance and academic success? A case study of degree programmes in Electrical Engineering and Computer Science. *International Journal of Research in Undergraduate Mathematics Education* 3(1): 143–167.

Kenosi K, Mutweleli SM, Wambua RM (2024) Relationship between attitudes towards mathematics and mathematics performance among Form Three students in the Southeast Sub-Region, Botswana. *International Journal of Research and Innovation in Social Science* 8(8): 1836–1845.

Lin TH, Riccomini PJ, Liang Z (2024) Mathematical error patterns of students with mathematics difficulty: A systematic review. *Journal of Learning Disabilities.* Advance online publication. https://doi.org/10.1177/07319487241310873.

Ministry of Education and Research (2022) *Data on state examinations and student academic progress*. Available at: https://projektid.edu.ee/pages/viewpage.action?page Id=142575079.

Ministry of Education and Research (2023) *Mathematics State Exam Report 2023*. Available at: https://projektid.edu.ee/display/THO/Matemaatika+riigieksami+aruanne+2023.

Ministry of Education and Research (2024) *Mathematics State Exam Report 2024*. Available at: https://projektid.edu.ee/display/THO/Matemaatika+riigieksami+aruanne+2024.

Ober TM, Coggins MR, Rebouças-Ju D, Suzuki H, Cheng Y (2021) Effect of teacher support on students' math attitudes: Measurement invariance and moderation of students' background characteristics. *Contemporary Educational Psychology* 66: 101988.

TalTech (2025) *Analysis of the relationship between university students' progress, state exam results, and mathematics course outcomes*. Tallinn University of Technology. Available at: https://haldus.taltech.ee/sites/default/files/2025-02/Üliõpilaste%20edasijõudmise%2C%20riigieksamite%20ja%20matemaatika%20ainete%20tulemuste%20seosed_analüüs2024_0.pdf.

The Australian (2022) *Curiosity and perseverance the key to high marks: new study reveals*. The Australian. Available at: https://www.theaustralian.com.au/nation/curiosity-and-perseverance-the-key-to-high-marks-new-study-reveals/news-story/be6464acf28356472573a0b1e2effab1.

Athens Journal of Sciences - Volume 12, Issue 4, December 2025 – Pages 299-314

Event-based Energy Modelling

*By Manuel Lehner**

Information technology is a major contributor to global energy consumption. This study estimates event-level energy usage through linear regression applied to synthetic signals generated from process event logs. These signals incorporate sine-modulated baselines, randomized noise, and event-specific energy costs. A custom framework supports signal generation, cost attribution, and performance evaluation. The model demonstrates high estimation accuracy for frequent and independent events, though performance declines with tightly sequenced process chains. R-squared values suggest a strong overall model fit, while percentage deviations vary depending on signal characteristics. The method assumes linearity, independence, and homoscedasticity—assumptions are largely satisfied in the synthetic dataset. Real-world applications, however, are limited by potential multicollinearity and require validation using actual event logs and measured energy data. Modular processes with stable event costs offer a promising testbed. Potential applications include process-level energy attribution, optimization, and client-specific billing. Although not yet deployable, this research lays the foundation for event-based energy modelling in complex IT environments.

Keywords: *process mining, energy efficiency, IT sustainability, data visualization, supply chain*

Introduction

As digital transformation accelerates across all sectors, the energy consumption of information technology (IT) systems has become a pressing environmental and economic concern. (Gelenbe 2023) Data centers, blockchain networks, and distributed computing infrastructures now account for a substantial share of global electricity usage. While aggregate energy consumption statistics are well documented, fine-grained insights into how individual computational events contribute to energy use remain limited. This knowledge gap hinders efforts to optimize energy efficiency at the process or service level and complicates attempts to assign energy costs to specific users or operations.

Recent advances in process mining and telemetry data collection have made it feasible to track detailed event logs of digital systems. However, directly linking these logs to energy consumption remains a challenge due to the noisy, high-dimensional, and often opaque nature of IT infrastructure. Traditional energy profiling methods either rely on coarse system-level measurements or require specialized hardware instrumentation, making them difficult to scale or integrate into live systems.

To address these limitations, this study explores an event-based modeling approach to estimate energy consumption using statistical inference from synthetic data. By combining process event logs with simulated energy signals that include deterministic (event-related) and stochastic (noise) components, the methodology

*Scientific Staff, Chair on distributed Information Systems, University of Passau, Germany.

aims to infer per-event energy costs using linear regression. This offers a scalable and potentially real-time mechanism to estimate energy footprints at a granularity compatible with process analysis and optimization.

Such a framework has promising applications: from attributing energy usage to specific business processes or users, to identifying inefficiencies in software workflows, and even enabling billing models based on actual resource consumption. However, the validity of this approach hinges on several key assumptions—including linearity, independence, and low multicollinearity—which may not hold in complex real-world systems. Therefore, this research provides a proof-of-concept using synthetic data and outlines the challenges and opportunities for applying the method to actual operational environments.

Literature Review

A look into the field of process mining reveals some trends with the view of adding sustainability to the field. Ma et al. (2020) proposes data driven optimizations on specific energy demanding industries with an elaborate collection of cloud-based monitoring, enabled by extensive hardware monitoring using RFID tags and smart sensors. While being a reasonable approach for the proposed industries, an extension towards regular businesses is unlikely due to lack of knowledge, personnel, funding or all the above. However, Delgado et al. (2023) shows a methodology to encompass sustainability data into process mining discovery, which are also securely shared using blockchain technology. While addressing the security needs for an enforceable mechanism sharing and trusting sustainability data, the way to retrieve the data to feed into such a reporting system is still not addressed. The new research of Fritsch (2024) gives a link of challenges between life cycle analysis (LCA) and Business Process Modelling (BPM) research projects. While creating a mapping between the fields, the methodologies of LCAs are notoriously difficult to adapt into real life applications, which can be seen by industries usually adapting statistical averages for their consumption data on non-financial reporting, instead of accurately measuring their values. This is done to a decrement as indications show an improvement in reporting when using actual measurements instead of statistical estimations (Tsalis et al. 2017).

Methodology

Energy Event Evaluation

The mathematical evaluation of the dataset is done using a multiple linear regression combined with an ordinary least squares estimation to distinguish event costs from background noise such as uncorrelated processes on a particular machine or manufacturing site. The basic evaluation equation and estimation formular can be seen in equation 1. The following equation 2 describes the estimation method used to arrive at the values. The methodology relies on the assumption that every event relevant to the specific enterprises is logged in the event log.

Equation 1: Basic formulation of the linear equation where: E_{total} is the total energy consumption observed during the measurement process (dependent variable), $E_1 \ldots E_n$ the energy consumption associated with individual events recorded (independent variables or predictors). β_0 the intercept term, representing baseline energy consumption that is independent of the specific events. $\beta_1 \ldots \beta_n$ the regression coefficients, indicating the magnitude of contribution each event makes to the total energy consumption.

$$E_{total} = \beta_0 + \sum_{i=1}^{n} \beta_i \, iE_i$$

Equation 2: the Ordinary Least Squares (OLS) method is employed. This approach minimizes the sum of squared residuals for each interval I, when looking at all the intervals in a matrix X, the second equation has to be solved:

$$S = \sum_{i=1}^{n} (E_{total,i} - (\beta_0 + \beta_1 E_{1,i} + \beta_2 E_{2,i} + \beta_3 E_{3,i}))2$$

$$(X^T X)\beta = X^T Y$$

To be able to distinguish between noise signal and actual consumption values from each event the estimation needs two inputs, an **event matrix** and an **energy signal**. The event matrix is provided that was derived from the dataset using the timestamp. In code this was accomplished by parsing the dataset file and counting each occurrence of an event type during one interval. Listing 1. gives a small example of such an event matrix to a fictitious event log.

Listing 1. *Example of an Event Matrix to a Fictitious Event Log*

Given an event log with mm:ss timestamps and the event types:
***read_data**, **process_data** and **write_data**:*
00:01 read_data, 10:15 process_data,
12:13 read_data, 17:12 process_data,
18:00 write_data
Given the interval length of 15 minutes the resulting matrix is: $\begin{bmatrix} 2 & 0 \\ 1 & 1 \\ 0 & 1 \end{bmatrix}$

The second input is ideally a combined real time energy measurement of all entities that consume energy to achieve the process goal. As such measurements contain a variety of unrelated consumption values, such as overhead processing power from computers, consumption data from other processes and many more, the methodology must be robust against noisy consumption signals. As the dataset provided does not contain such an energy measurement, a methodology to generate such an energy measurement was derived using simple assumptions on the way energy is consumed by each of those processes. These consumption values rely on a huge

number of factors, not limited to hardware used, virtualizations or even the programming language of an application (van Kempen et al. 2025). Due to this limitation, it is hard to justify specific values for a given process, if the implementation of the processes is unknown. However, the goal of this study is to evaluate the general applicability of this method to a variety of different costs and implementations. To accomplish this an energy data generation framework was developed that can create energy consumption signals with optional variations to process costs, amount of noise or fluctuations during regular daytime hours. When looking at the results in chapter 4 the usage of concrete values was minimized, as they in themselves do not have any significance. Rather it is to show that for any known amount of energy that a given process uses, can this estimation methodology be used to reconstruct the costs of different events when only given an event matrix and the sum of all the measurements per time interval. The following subsection gives some insights into the dataset, as well as the data processing done for this research.

Dataset and Datastructures

BPI_Challenge_2019 is a well-known published dataset in process mining (van Dongen 2019). The event data is a collection of economic processes across the whole year 2018, containing 41 different event types with their corresponding timestamps and standardized process meta data. As the dataset contains outlier events out of the scope of the year 2018, this experiment used a filtered set, that encompasses all events attributable to the year 2018. No further alterations were made, and the filtering was done using pm4py functionalities found in the xes_filter.py package. For the energy generation that corresponds to the event log, an EnergyEvent data structure was designed to add details to the process events that are not part of the original data set. To get a better understanding of the results, the frequency of each event type can be found in table 1. To ease the referral to specific groups of events, the different event types are grouped into classes.

EnergyEvent is a data structure that provides additional information for the energy signal generation. As the methodology works on fixed measurement intervals, the duration of specific events may have an influence on the energy allocation of the event across different intervals. To simulate this, the duration of the event was randomized, and the energy costs were distributed across different sections of the time series. As this must be expected in a real-world environment, but no duration data is present in the dataset, a random quantity will account for some of the distortions to be expected when using real measurements. An overview of the data structure can be found in figure 1.

The results of the conversion from the xes file can be saved using the pickle function of python. This way the binaries can be saved for further analysis without the need for repeated conversions. The framework is adapted to use standardized xes nomenclature and should be able to work with other process mining datasets with little adjustments. This enables the reader and future research to reuse the framework with updated event logs or more accurate basecost assumptions when applicable.

Table 1. *Frequencies and Group of each Event Type in the BPI challenge Dataset*

Event type	# Occurences	Grouping
'SRM: Created'	1625	Medium
'SRM: Complete'	1625	Medium
'SRM: Awaiting Approval'	1625	Medium
'SRM: Document Completed'	1625	Medium
'SRM: In Transfer to Execution Syst.'	1687	Medium
'SRM: Ordered'	1625	Medium
'SRM: Change was Transmitted'	1440	Medium
'Create Purchase Order Item'	251352	High
'Vendor creates invoice'	216700	High
'Record Goods Receipt'	305837	High
'Record Invoice Receipt'	218375	High
'Clear Invoice'	176755	High
'Record Service Entry Sheet'	164657	High
'Cancel Goods Receipt'	3047	Medium
'Vendor creates debit memo'	6213	Medium
'Cancel Invoice Receipt'	6768	Medium
'Remove Payment Block'	54216	High
'SRM: Deleted'	185	Low
'Change Price'	12189	High
'Delete Purchase Order Item'	8698	Medium
'SRM: Transaction Completed'	8	Low
'Change Quantity'	20924	High
'Change Delivery Indicator'	3172	Medium
'Change Final Invoice Indicator'	11	Low
'SRM: Incomplete'	6	Low
'SRM: Held'	6	Low
'Receive Order Confirmation'	32027	High
'Cancel Subsequent Invoice'	463	Low
'Reactivate Purchase Order Item'	535	Low
'Update Order Confirmation'	242	Low
'Block Purchase Order Item'	486	Low
'Change Approval for Purchase Order'	6961	Medium
'Release Purchase Order'	1610	Medium
'Record Subsequent Invoice'	151	Low
'Set Payment Block'	123	Low
'Create Purchase Requisition Item'	46585	High
'Change Storage Location'	40	Low
'Change Currency'	35	Low
'Change payment term'	7	Low
'Change Rejection Indicator'	2	Low
'Release Purchase Requisition'	467	Low

Figure 1. *EnergyEvent Datastructure*

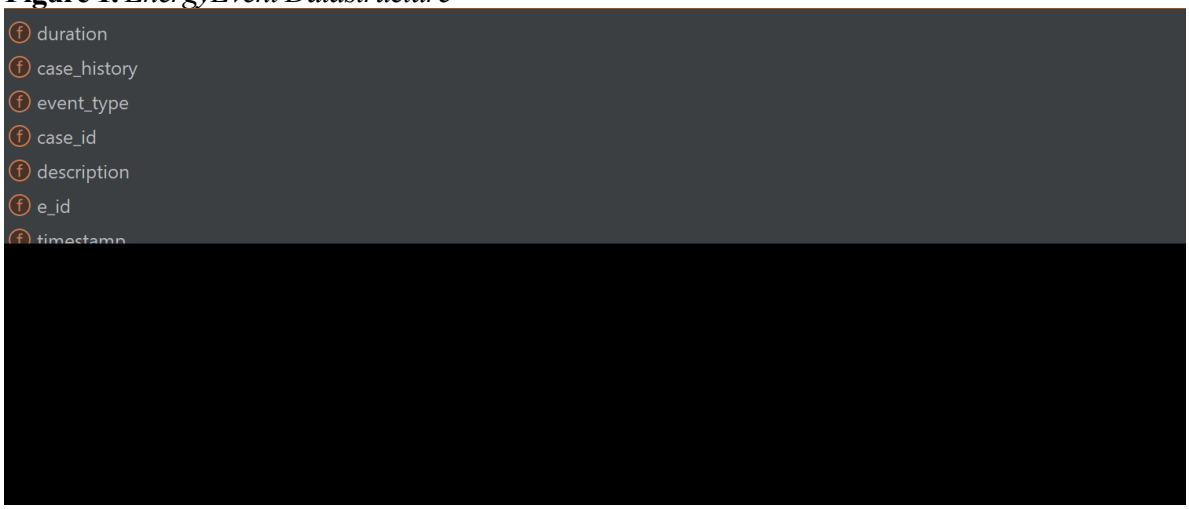

Signal Generation

The energy signals that should simulate a correlating energy signature to the given dataset is created using the EventObject data structure. The code can be found in the jupyter notebook in the repository (Lehner 2025). The idea is to inject already known event costs to a signal comprised of a noise signal that is modulated by a sinus wave in order to simulate empirically shown day and night energy consumption differences (Gupta 2022). As the energy consumption of a commercial endeavor can vary drastically between industries, implementations and products, a representative value for a generic application cannot be chosen confidently. To account for this, the research introduces variations in the signal generation to encompass the influence of the order of magnitude in different factors and are described in detail in the next section. A sample energy signal of the total and event costs can be seen in figure 2.

Figure 2. *Comparison of the Event Costs and Total Energy Costs, Experiment with no Scaling and 30min Intervals*

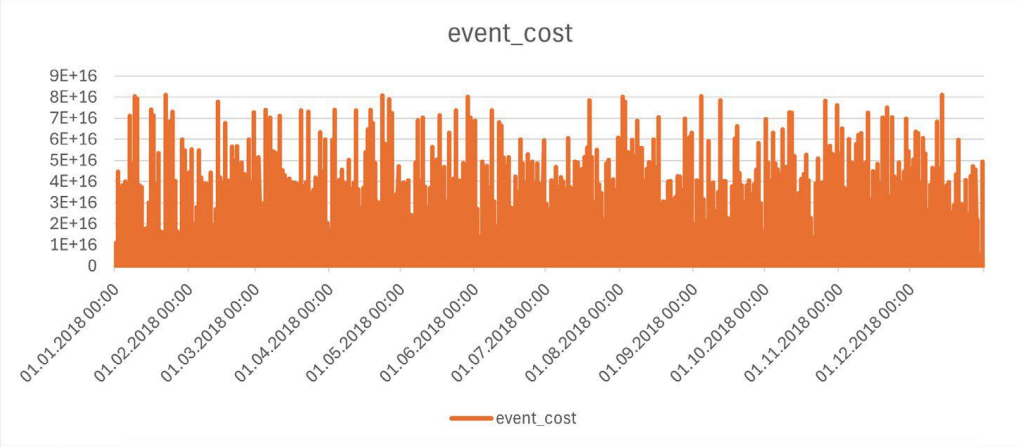

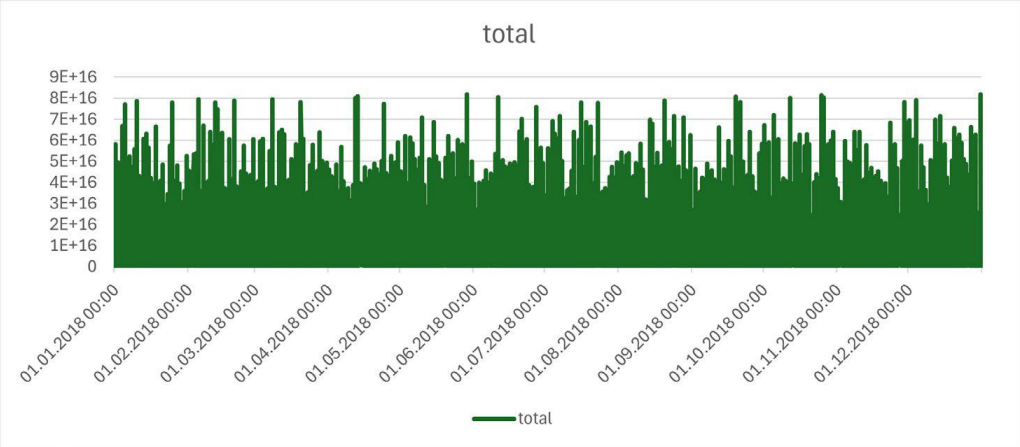

Signal Variations

To give a broad insight into the applicability of the method, the signals were generated with a wide range of parameter variations. Specifically, the noise added to the signal, the altitude of the sine wave that modulates the signal, as well as the event base costs that are given by design are scaled by two orders of magnitude. As the performance of the estimations should be reduced by real world distortions as well as the varying amounts of noise within a system, this spectrum should be a sufficient insight into the resilience of the method.

Implementation

event_object.py

This module defines the core data structure and processing logic for event instances derived from XES logs. The EventObject class encapsulates key attributes such as event identifiers, case associations, timestamps, and event-specific durations. It supports cost evaluation based on static base costs (__BASECOSTS__) and dynamic temporal penalties incorporating duration and delay penalties (__DURATION_SCALE__, __END_SCALE__). Additionally, it provides methods to determine subsequent events within the same case and compute total event-related costs.

The module includes:

1. A pipeline (process_xes_events) that parses XES event logs using PM4Py, transforms them into EventObject instances, and applies user-defined processing functions.
2. Utility for loading serialized event data via read_event_objects_from_pickle.

event_cost_eval.py

This module provides a statistical modeling framework for estimating and validating the energy cost associated with event types based on empirical usage data. Key functionalities include:

1. **estimate_energy_per_event**: Applies multiple linear regression to estimate energy consumption per event type using event frequency data across time intervals, with optional intercept control.
2. **analyze_energy_regression**: Extends the basic estimation by leveraging statsmodels to extract confidence intervals and p-values, enabling significance analysis of each event type's contribution.
3. **compare_estimated_vs_expected_costs**: Computes and reports absolute and relative deviations between regression-estimated costs and known base costs, supporting model validation.
4. **visualize_cost_comparison**: Generates bar plots comparing estimated and expected costs per event type, with annotated percent deviations for interpretability.
5. **estimate_and_compare_costs**: An integrated workflow to estimate, compare, and visualize energy costs from interval-based event and consumption data.
6. **create_event_matrix**: Constructs a matrix representation of event occurrences per time interval from an input XES log, aligning with energy usage timestamps to support regression analysis.

The module emphasizes both analytical rigor and practical usability, facilitating transparent and quantitative cost validation of process events.

The core of the signal generation was implemented in a jupyter notebook.The codebase implements a synthetic energy consumption data generator for business process management scenarios. The system creates realistic energy consumption patterns by combining periodic signals, noise, and process-specific energy costs derived from event logs. The core components are listed as follows:

time series foundation

The system begins by establishing a time series framework using pandas DateTimeIndex, creating regular intervals (15-minute default) for energy measurements throughout the specified period (2018).

periodic signal generation

The generate_sine_wave function creates a fundamental periodic pattern in energy consumption based on:

1. Daily cycles with configurable peak hours (default: 2 PM)
2. Amplitude variations (configurable)
3. Vertical shifts to establish baseline consumption

This models daily operational patterns in business environments where energy consumption follows predictable cycles.

noise integration

Random noise is applied via the noise_gen and apply_noise functions, simulating energy consumption unrelated to business processes (OS operations, background services, etc.). This adds realism by accounting for the variable, non-deterministic component of energy usage.

process-specific energy costs

The distribute_event_costs_series function:

1. Maps specific business process events to energy costs
2. Distributes these costs across time intervals based on event duration
3. Handles overlapping events and calculates proportional energy attribution

The system uses a detailed cost mapping dictionary (__BASECOSTS__) that assigns different energy weights to various business processes (e.g., "Record Goods Receipt": 99, "Create Purchase Order Item": 98).

experimental framework

The implementation includes a systematic approach to parameter exploration:

1. Noise scaling (0.1-10)
2. Base cost scaling (0.1-10)
3. Sine wave amplitude (1-1.5)
4. Sampling rate (30min)

The gen_experiment_parameters function generates combinations of these parameters, with each experiment fixing parameters at median values while exploring variations of a single parameter.

data transformation utilities

Post-generation utilities include:

1. convert_30min_to_1h_reset_index: Aggregates higher frequency data to lower resolution while preserving energy relationships
2. resize_sine_wave: Adjusts the amplitude of the periodic component without regenerating the entire dataset
3. for the analysis of this paper, not all utilities were used in order to not exceed content limits

methodology

The energy generation process combines these components sequentially:

1. Generate timestamp range at specified intervals
2. Apply periodic sine wave pattern with configurable parameters
3. Introducing random noise to simulate non-process energy consumption
4. Distribute process-specific energy costs from event logs
5. Calculate total energy consumption as the sum of these components

Each generated dataset is saved as a CSV file with naming conventions that encode the experimental parameters, facilitating subsequent analysis of how different factors influence energy patterns. By cloning the repository, all results can be calculated using the code provided and a glimpse into the main results are given in the next section.

Results

While giving some insights into the behavior of the methodology, it must be restated that the absolute values are of little interest and only give indication on whether the data collection and evaluation is meaningful given a concrete scenario. The synthetic energy signals are available in the repository as .csv files and contain separate columns for the noise part of the signal and the energy values infused by the event costs. Consider that when simply adding the base costs of the events within a timestamp interval will most likely not match the actual value of the signal, as the event costs have been allocated appropriately based on the start time of the event and the randomized duration in a linear fashion. (i.e. if the duration bleeds by half of the duration into the next interval also half of the costs are added to the next interval).

To evaluate if the methodology can be used in a specific application, this work provides a framework to get first insights, before any more elaborate implementations must be made. This chapter will provide a look into the general model performance, the well performing aspects and the problem areas.

General Model Performance

The performance of the linear regression model was evaluated using the analyze_energy_regression function of the code. Table 2 gives an overview of the r-squared, and the mean-percentage difference for all events of the dataset. As a main indicator of the overall performance the r-squared value gives good insight into the explanation-power of the model to predict overall energy. The values for the percentage difference can give insights into the performance when attributing costs to individual events, which is heavily influenced by the process structure.

Table 2. *Statistical Evaluation of Model Performance in each Experiment*

Scaling Parameters			R-squared	Mean Absolute % Difference
Cost	**Noise**	**Amplitude**		
0.1	0.1	1	0.7919	150.93
0.1	1	1	0.7914	146.74
0.1	10	1	0.7913	145.2
1	0,1	1	0.7948	298.5
1	1	1	0.7919	150.20
1	10	1	0.7913	146.67
10	0.1	1	0.6716	2770.89
10	1	1	0.7948	287.99
10	10	1	0.7919	150.59
1	0,1	1.5	0.7937	84.99
1	1	1.5	0.7916	148.24
1	10	1.5	0.7913	1738.64
10	0.1	1.5	0.7639	99.65
10	1	1.5	0.7937	85.23
10	10	1.5	0.7916	147.30

As a blank modelling approach this does not work that well, since process chains and dependencies cannot be accounted for in a least squares estimation model. Figure 3 shows the resulting estimations in comparison to the real costs of the experiment with the cost-/ noise-/ and amplitude parameters each set to 1. As visible from the illustration, the estimations vary widely for the different event types. With the frequency of the types in mind it shows that higher frequency events are estimated more accurately than low frequency events. This is likely due to the higher chance of separating clear signal data from varying noise during each of the occurrences. However, the estimations show even better results for event types that better fulfill the assumptions, which are discussed in detail in the next section. This is mainly independence due to being first in a process chain, and not closely followed by events afterwards.

Figure 3. *Estimation Result of Experiment Setting (1,1,1) and a 30-minute Interval*

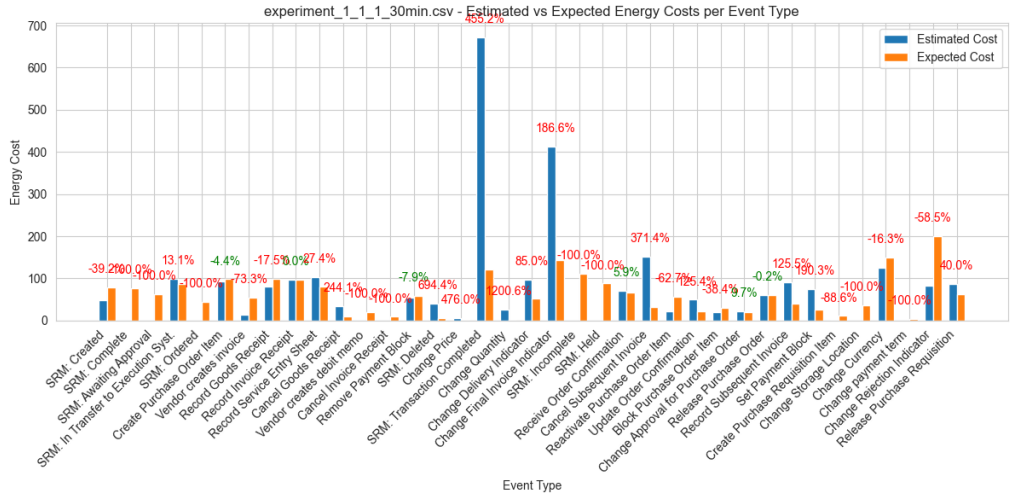

Zoom on better Performing Events

When looking at the specifically well performing event types the picture changes quickly and gives some details on how to improve the methodology. In figure 4 the results of the best performing events of the same parameters can be seen. With comparison to table 2 most of the consistently well-performing events are of high frequency. When comparing the different experiment runs, low frequency event types are estimated quite accurately, however this is likely due to random variance.

Figure 4. *Estimation Results of Experiment Setting (1,1,1) and a 30-minute Interval. Best Performing Estimations only*

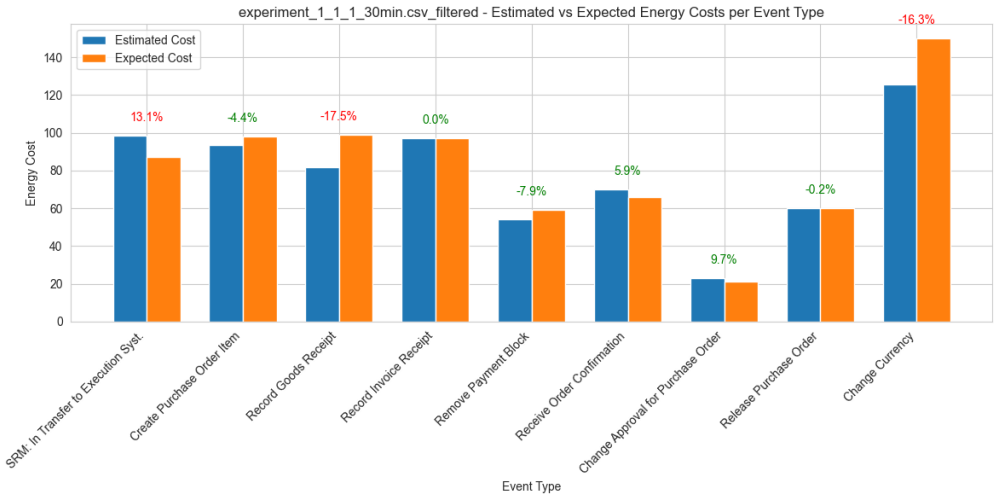

Problem Areas of Performance

The main areas of performance drop occur when looking at process chains that happen in some rapid succession. In the case of most of the SRM events, this is especially obvious as the cost of the whole process chain was summed up into the last event of the process chain SRM: transaction completed. This explains most of the huge spike of the costs in figure 2. However, as the model also does not account for all the process-induced energy costs from the signal, additional errors in that spike must be expected. To alleviate this discrepancy between the signal and the estimations, the correlations between different events must be considered. Different ways to address this are discussed in the next section.

Discussion

The evaluation methodology makes basic assumptions on the nature of how energy consumption behaves with respect to events in the log. The model relies on several assumptions regarding the system and its energy consumption behavior:

1. **Linearity**: The relationship between the individual event-related energy costs and the total energy cost is assumed to be approximately linear.
2. **No Multicollinearity**: The predictor variables (i.e., the energy costs of individual blockchain events) should not be highly correlated with each other. For instance, if event types such as validation and storage are strongly interdependent, this may lead to multicollinearity issues.
3. **Homoscedasticity**: The variance of the error terms should remain constant across all levels of the predictors.

4. **Normal Distribution of Errors**: The residuals, defined as the differences between observed and predicted total energy costs, should be normally distributed.

Most of the assumptions are present in the synthetic energy data per design, which probably gives an overestimation of the effectiveness of the method. This is possibly counterbalanced by the multiple orders of magnitude represented in the dataset, as a difference of 10^4 in energy consumption will mean that a meaningful increase in energy efficiency of the event costs is not impacting the total energy consumption of the operation. The decision, whether the proposed methodology is applicable to a potential process, must take a lot of previous knowledge into account, so that the above-mentioned assumptions hold to a meaningful extent. Further process mining techniques can be used to single out process variants or process paths that more clearly fit the assumption of no multicollinearity is met. Circular or strongly correlated process structures can be suspected to have some correlation in their energy signature and therefore parts of the costs will be underestimated by the bias coefficient. A way to address this drawback would be a restrictive modeling approach towards only independent variables and switching to other methodologies when looking at highly dependent event variables.

To estimate the real amount of multicollinearity within a real process, future work must be completed providing both datapoints1, an extensive event log and the corresponding energy consumption measurements. To provide a baseline of known event costs, the process must be modular in such a way that events can be process-independent of previous steps and the amount of energy needed should be independent of previous steps. These constant energy consumption measurements then can be used as a ground truth to evaluate the methodology in an application. Other than a simplifying approach, a statistical learning algorithm or feature extraction can be used to learn cost features from real time data. Depending on the feasibility of each of the next research projects, either method can lead to great improvements. Further economic computation trends, like off-site computation and cloud computing, will make data collection even more difficult. However, hardware to monitor and record energy consumption become affordable and often also included in regular commercial products. As a potential upside, providers of computing services that would like to separate energy costs to distinct clients could benefit from the application of an event-based energy model. This way a billable energy footprint could be attributed to a single process owned by the client. In return this consumption rate can then be incorporated into the energy balance calculation of the economic chain down the line. If this is a feasible way of accounting for energy costs must be shown with real data.

The data set used in this experiment maps all economic events of the enterprise, however it does not map to a realistic event collection when looking into computation costs. To analyze and possibly improve energy efficiency, the design and decisions which datapoints are recorded should be made using the biggest contributors to energy consumption in IT. The procurement of new IT products and the usage. Since a

[1]Combined energy measurement of all contributing process devices, as well as the process event data.

general determination which side of the consumption fields dominate (Hilty et al. 2007) a closer look at improving energy efficiency within processes is.

Conclusions

In conclusion this research is a step to provide reasonable indicators that with some modifications an event-based energy modelling system can be implemented in order to give insight into:

1. Process specific energy costs
2. Possibilities to model modifications in the process
3. Partly generate energy footprints for different process end products
4. Further usage of already collected energy data

However, a blank usage of this methodology is unfit to provide reliable values for the purpose of determining event costs. This can possibly be achieved when providing improvements to the methodology that ensures either a stricter adherence to the assumptions of linear regression models for each and every event type under consideration, or correlation information using process mining techniques to augment the existing data sources.

While at this point it cannot be estimated if a calculation can compare to real measurements, but similar approaches on stock exchange data had R^2 scores of about 0.96 (Majumder et al. 2022) which gives some reason to be optimistic. With the inclusion of real measurements in the energy of some processes, also other methods open up. These include, but are not limited to, learning algorithms and feature extractions to create a reliable modelling framework.

Acknowledgments

Many thanks for continuous research guidance are owed to Prof. Dr. Dr. Harald Kosch of the University of Passau, Prof. Dr. Rainer Groß of the Technische Universität Nürnberg, Dr. Thomas Götz of Atos/Eviden and Ms. Alexandra Knupe of Atos.

References

Delgado A, et al. (2023) Adding the sustainability dimension in process mining discovery algorithms evaluation. *Lecture Notes in Business Information Processing* 490: Business Process Management Forum.

Fritsch A (2024) Sustainability analysis patterns for process mining and process modelling approaches. *Lecture Notes in Business Information Processing* 533: ICPM. Springer.

Gelenbe E (2023) *Electricity Consumption by ICT: Facts, Trends, and Measurements.* Ubiquity, Article 1, August.

Gupta R, Antony A, Walia A, Dhingra N, Tathagat T, Varma P (2022) Examining the variation in daily and peak electricity use. University of Bath.

Hilty LM, Coroama V, Ossés de Eicker M (2007) The role of ICT in energy consumption. *ICT-ENSURE: European ICT Environmental Report*, 30.

Lehner M (2025) Event-based energy modelling – Repository for the BPI Challenge research. GitHub. https://github.com/Free2ndThought/event_based_energy_modellin g_bpi2018.git (accessed 30 June 2025).

Ma S, et al. (2020) Data-driven sustainable intelligent manufacturing based on demand response for energy-intensive industries. *Journal of Cleaner Production* 274.

Majumder A, Rahman MM, Biswas AA, Zulfiker MS, Basak S (2022) Stock market prediction: A time series analysis. In: *Smart Systems: Innovations in Computing* (Smart Innovation, Systems and Technologies).

Tsalis T, Avramidou A, Nikolaou IE (2017) A social LCA framework to assess the corporate social profile of companies: Insights from a case study. *Journal of Cleaner Production* 164: 1665–1676. Elsevier.

van Kempen N, Kwon HJ, Nguyen DT, Berger ED (2024) It's not easy being green: On the energy efficiency of programming languages. *arXiv* (October 2024). https://arxiv.org/html/2410.05460v1 (accessed 30 June 2025).

van Dongen BF (2019) Dataset BPI Challenge 2019. *4TU.Centre for Research Data.* http://icpmconference.org/2019/wp-content/uploads/sites/6/2019/02/BPIChallenge2019CSV.zip